Proceedings of the 21st International Ship and Offshore Structures Congress (ISSC 2022) – Xiaozhi Wang and Neil Pegg (Eds.)

Volume 1

COMMITTEE III.1
ULTIMATE STRENGTH

COMMITTEE MANDATE

Concern for the collapse behaviour of ships and offshore structures and their structural components under ultimate conditions. Uncertainties in strength assessment shall be highlighted. Attention shall be given to the influence of response to load combinations including accidents; fabrication imperfections; life-cycle effects; and user approach. Consideration shall be given to the practical application of methods.

AUTHORS/COMMITTEE MEMBERS

Chairman: Paul E. Hess
Chen An
Lars Brubak
Xiao Chen
Jinn Tong Chiu
Jurek Czujko
Ionel Darie
Guoqing Feng
Marco Gaiotti
Beom Seon Jang
Adnan Kefal
Sukron Makmun
Jonas Ringsberg
Jani Romanoff
Saad Saad-Eldeen
Ingrid Schipperen
Kristjan Tabri
Yikun Wang
Daisuke Yanagihara

KEYWORDS

Ultimate strength; Load-carrying capacity; Uncertainty; Ship Structures; Ships; Offshore; Ultimate limit states; Buckling; collapse; Fabrication-Induced Initial Imperfections; In-service damage and degradation

CONTENTS

1. INTRODUCTION

Determining the ultimate strength of ship and offshore structures involves the ability to predict and measure component, sub-system, and system structural maximum capacity beyond which the capacity diminishes. The purpose of this committee is to present a summary of recent work published after the time period covered by the 2018 committee that addresses these goals within the guidance of the Committee Mandate. Effective consideration of these factors requires definition of terms and description of the use of ultimate strength calculations and measurements prior to directly addressing the objectives set forth in the Mandate.

1.1 Definitions

The ultimate strength of a structure is defined as the maximum load carrying capability beyond which the load carrying capacity reduces. This may be viewed as the definition of failure for ultimate strength of any structure. This committee mainly focused on compressive buckling failure mechanisms vs tensile failure that would lead to fracture, which is addressed in Technical Committee III.2.

The majority of marine structures are a type of thin-walled structure, where the maximum load carrying capability of one component might be reached prior to the system reaching its ultimate limit. Defining the boundaries of the structure whose strength is being assessed is important both to support the analysis process, but also to communicate this information for use in decision-making. For example, a stiffener-plate combination that reaches ultimate strength would not necessarily coincide with collapse of an entire grillage or hull girder cross-section. Both of these failure modes are used in limit state equations to support decision-making, but representing very different assessments of structural performance, reliability, or risk.

1.2 Report Structure

The report is organized into 7 Chapters and an Appendix, with the primary technical chapters being Chapters 2 through 6, covering fundamentals, materials and life-cycle effects, and ship and offshore structures, culminating in a unique benchmark in Chapter 6 and the Appendix.

Chapter 2 covers Fundamentals, introducing aleatory and epistemic uncertainty quantification and effects, elements of strength prediction tools with a focus on high fidelity numerical modeling and reduced order modeling, and experimentation.

Material and life-cycle effects are addressed in Chapter 3, highlighting issues related to degradation such as corrosion and cracking, consideration of distortion, damage or repair effects, and residual stresses resulting from the manufacturing process.

Chapters 4 and 5 focus on the ultimate strength aspects particular to ships and offshore structures respectively. Each describe relevant load cases, structural elements, structural systems, and associated rules and regulations. For the structural elements and systems, research resulting in new analytical strength prediction models is introduced along with application of numerical modeling and experimental testing.

Chapter 6 provides the strength benchmark report for which the committee and additional invited participants considered the ‘blind’ prediction of a grillage collapse test using increasing levels of information, though not the as-tested strength nor failure progression. As will be described on the Benchmark Chapter, the grillage was tested by the Naval Surface Warfare Center, Carderock Division, USA, and the results of the test were withheld until the predictions were collected from all contributors at the different phases of the work. The benchmark is introduced in Chapter 6, then expanded on in the Appendix, and further described in a paper by Ringsberg et al. (2021).

2. FUNDAMENTALS

2.1 Uncertainty quantification

When determining the ultimate strength of a structure or component, whether by test or analysis, several uncertainties exist. Such uncertainties can be identified in material properties, component or structural geometries, loads, initial deformation, initial and current defects, analyses methodology, and boundary conditions in tests and in modelling, measurements, and user modelling choices. Some of these uncertainties are aleatory in nature, for example the material characteristics, which show a stochastic distribution. Uncertainties for those parameters can be diminished by additional testing or included in the analyses by the use of a stochastic approach. Others, such as numerical modelling, are epistemic, due to current lack of knowledge or data of the physical model or system, resulting in uncertainties less easily handled and quantified.

2.1.1 Effects of uncertainties

It is important to know which of the uncertainties have the largest influence on the prediction of the ultimate strength of a component or structure. In the 2012 ISSC report on Ultimate Strength (Paik, et al., 2012), benchmark analyses were done on unstiffened plates, stiffened panels and hull girders using different analytical and numerical techniques. Although the effect is not quantified, it is stated that the often-used buckling mode imperfection leads to a lower ultimate strength than a hungry horse look. That same observation is also mentioned in the work of Cui and Wang (Cui and Wang, 2020). They also stress the uncertainty in corrosion damage distributions. Pitting corrosion influences the strength substantially, especially when the corrosion is in the vicinity of the opening of a panel. Accurate determination of the initial deformations and corrosion is thus important. Yu et al (2018) studied the location and geometric uncertainties of cracks on the ultimate strength of a stiffened panel under compressive loading. Ultimate strength finite element analyses of 970 cases of through thickness, static, crack variations defined by parameters such as length (85-425 mm in 5 equidistant steps), location (distance from centre 0-1 in 9 non-equidistant steps) and orientation (0,30, 45, 60 a 90 degrees), were performed. Although that was not the purpose of this paper, such a parameter variation study could be used to determine which parameters should be determined or known most accurately to decrease the uncertainty in ultimate strength predictions.

2.1.2 Epistemic uncertainty quantification

As stated, the aleatory uncertainties could probably be diminished by additional testing or inclusion of stochastic distributions for the parameters. Attention for the remainder of this section will be on epistemic uncertainties and methodologies to better understand its effects. In principle these methodologies are application independent. As such, attention is not only paid to methodologies developed from a ship or offshore perspective, but also by looking at information from other application areas. The ISSC 2012 committee states that modelling technique can have a significant contribution to the uncertainty of the result (Paik, et al., 2012). This is confirmed by many other authors. An example of such epistemic uncertainty is shown in Goa and Shi (2018), who compare the results of a non-linear FE analyses with Smith's method for a container vessel. They show that the ultimate strength in hogging show a good consistency. However, the ultimate bending strength in sagging is underestimated when using Smith's method. Gao and Shi state that this is contributed to the inelastic buckling of the deck, but the ISSC members are not sure if this conclusion is due to a bad design or is correct to some extend in general.

Nahshon et. al. (2018) describe a methodology to quantify the uncertainty for high-fidelity simulations with large parameter spaces. When using high-fidelity computations for the large number of analyses needed to quantify the uncertainties, the computational costs are normally

very high. The authors use a simplified model, which is still physics-based, to scan the parameter space and determine a limited amount of parameter combinations that need to be analysed using the high-fidelity model. Although the study is focused on a stiffened plate ultimate strength, the methodology can be applied to a broader scope. Oberkampf et al (2002) also have developed a general framework to identify errors and uncertainties in solving partial differential equations (PDE). The authors distinguish between six different phases in the setting up and solving of the PDE, conceptual modelling, mathematical modelling, discretization and algorithm selection, computer programming, solving and representation. In each of these phases, uncertainties, either aleatory (stochastic) or epistemic (lack of knowledge) can be distinguished. From the framework, relations can be visualised and assumptions are made clear. Also, the framework shows how uncertainties, of both families, contribute to the analysis result. By variation of the identified uncertainties, the uncertainty in the final result can be quantified and uncertainties can be ranked. Liang and Mahadevan (2011) provide a methodology that enables the ranking of uncertainties in computational modelling. The methodology takes into account the combination and interaction of errors and uncertainties. A distinction is made between model form errors (is the set of equations or the type of model used correct for this analysis) and the solution approximation errors (were the equations solved correctly). The latter is divided into input error, discretisation error and (if applicable) surrogate model prediction error. Methods to determine the sensitivity of the solution approximation errors are given, which can be used for ranking of the uncertainties. Attention is given to the fact that even the error and uncertainty quantification methodology itself has an error, since only a limited number of FE evaluations are normally done. The information could be used as a generic approach to resampling. The model form errors are handled by validation of model predictions against experimental data. Of course, the latter validation does not take into account any uncertainties coming from the experimental data.

In Sugiyama (2004) a practical approach is taken into the determination of the uncertainties in the dynamic response of an arch bridge due to earthquake loading. Several researchers and engineers were asked to perform the structural response analysis. The scatter in the results for different result parameters was used to determine the uncertainty in modelling. By also studying the effect of several choices made by the researchers, for example the formulation used for damping, on the variations found, the importance of the different choices made in numerical analyses could be ranked. Also, Castaldo et al (2018) cover the uncertainties related to numerical modelling (epistemic uncertainties). Although they mainly focus on the determination of partial safety factors, which are related to ultimate limit states assessments and as such not directly relevant to this chapter, they start the process by determining the uncertainties in the modelling. They took a benchmark set of 21 different concrete structural members, which were tested by other authors and reported in literature. The tests represented different topology of a concrete structure and showed different failure modes. Each test was analysed using 3 different FE packages and 3 different assumptions for the material behaviour. By doing such a broad assessment of numerical models an idea on the uncertainties of numerical modelling can be obtained. However, it should be noted that the authors only looked at the numerically determined ultimate strength. This is deemed insufficient. Ultimate loading capacity close to the experimental results were obtained for some of the benchmark studies but with different failure behaviour than seen in the experiments. Therefore, it is recommended by the authors of this ISSC report to take into account more than just ultimate strength values for the determination of the uncertainties in numerical modelling.

An example of this can be seen in Wang et al (2019b) regarding the experimental and numerical investigation of the ultimate longitudinal strength of an ultra large container vessel. They compare the test results of a scaled ultra large container vessel in a hogging test condition with a

numerical analysis of this test, taking into account the (changing) location of the neutral axis, the comparison of the ultimate strength and the order and collapse behaviour of the different members in the structure. It is seen that the position of the horizontal neutral axis is well captured by the model as is the initial linear part of the force deformation curve. When plasticity and collapse of members occur, the deviation between numerical model and test results increases to about 8% in the final collapse load. The difference is mainly contributed to the absence of initial deformations and residual stresses in the model and the modelling inaccuracies of the boundary conditions. The actual collapse mode is very similar between model and test.

The methodology described above is deemed to be a good, fairly simple method to quantify the level of uncertainty due to modelling. For analysis of large structures, such as full ship analyses, it might be a computationally expensive methodology. However, compared to the costs of actual ships the costs of good modelling and analysis are low especially when such good practice engineering contributes to increased safety.

2.2 Tools

Tools for both science and engineering related to the ultimate strength assessment of ships and offshore structures have evolved significantly over recent years. An excellent review is presented by Sumi (2018) on the developments of this work over 100 years. Today the experimental methods at various length-scales as well as the simulations tools based on numerical computational methods and analytical equations are better, more comprehensive and more integrated than ever before. The experimental work is still carried out to a large extent in laboratory scale by using similarity rules especially at the hull girder, panel and component levels (e.g. Khargani and Guedes Soares, 2018, Kim et al., 2018a, Zhang et al., 2018., Chen et al., 2019b, Wang and Wang, 2019a, Wang et al., 2019b, 2020), but the extent of instrumentation can be much more extensive than before due to development of for example Digital Image Correlations. As another example, today with help of digital twins we can keep up with the state of the structure (e.g. actual dimensions, distortions, damages) throughout the design, building and operational stages and therefore better estimate the ultimate strength with different tools and different levels of sophistication depending on time and accuracy available for the assessment (Hulkkonen et al., 2017, 2019, Fujikubo, 2019). We can also via digital twins bring operational data and experience back to researchers, rule-makers and engineers when better tools need to be developed, and also help to identify critical sea states in terms of hull girder capacity by using real time weather data, load calculations and strength assessments. However, the end result, the digital twin, can contain numerous simplifications in the decision-making tools that are becoming extensively invisible to the end-users. Therefore, it is crucial to understand the limitations of the tools used in decision making. State of the Art reviews on both industrial and academic possibilities of digital twins are given for example by Fujikubo (2019) and Hulkkonen et al., (2017, 2019) which review extensive research efforts done in the Far-East and Europe on digital twins.

In ultimate strength assessment the starting point is the load application to the ship hull. The load can result from rigid or flexible body simulations (e.g. strip and panel methods, Computational Fluid Dynamics, Fluid Structure Interaction) and measurements (model- and full-scale) where the discretisation is typically different from the discretisation used in strength assessments (e.g. FEA, Smith's method). This applies to both time and space. Therefore, at this stage often simplifications are made at the interface between the load and the strength tools/models. Recent experiments from Iijima and Fujikubo (2018) of Very Large Floating Structures (VLFS) remove this simplification in model-scale experiments and the corresponding FEA. Tools used for the ultimate strength assessments can be split into experimentation, numerical

simulations or analytical calculations. The corresponding models contain different simplifications that can be at the level of geometry, materials and solution technique. This was discussed in excellent manner in the 2018 ISSC III.2 report on Fatigue and Fracture (Garbatov et al., 2018), which benchmarked initially-deformed slender deck plates and the influence of different modelling simplifications to the strength assessment. The actual geometry of the produced panels was optically scanned with very high accuracy and this data was transferred directly to the corresponding Finite Element model (based on Shell elements). Then different levels of simplifications were carried for the actual shape. The simplifications included setting equivalency to the maximum initial deflection, but varying the actual shape from that measured to those represented by trigonometric functions of different forms. These trigonometric functions are often used as mathematical descriptions of the shape in the ultimate strength assessment due to their capability to produce closed-form solutions. With the actual shape measured with very high accuracy, both the non-linear global panel level and local weld level responses were captured with very high accuracy. When simplifications were made in the shape, the accuracy in the global response decreased more slowly than the local response. This is also demonstrated later in this report in the benchmark Ringsberg et al., (2021). This is an important factor in panels where geometrical and material non-linearities get coupled and for example interact with temperature effects and strain rates. In such cases, the recent experiments by Paik et al. (2020a) and Körgesaar et al., (2016, 2017, 2018a,b) show that in the ultimate strength assessment highly localised stresses can act as failure initiation points for overall collapse. As the failure progresses in the structure, the coupling between non-linear geometry, material and load redistribution can be highly complex and occur very rapidly. In these experiments it was observed that even though the experiment was planned quasi-static and response expected to be also quasi-static, at the failure point catastrophic failure occurred. The rapid interactions observed are currently at the limits or beyond our experimental and computational capabilities due to the spatial and temporal discretization requirements.

In Finite Element context the full solid element models can be considered as the most accurate ones, but often we cannot use them due to computational and time restrictions except to calibrate the shell element models for example to ductile fracture simulations (see e.g. Nam et al., 2018). This is due to the fact that the level of simplifications is the lowest in solid element models when it comes to the structural geometries or modelling assumptions, followed by continuum shell elements (several nodes over the thickness), single-layer shell elements (single node over the thickness) and beams. Still as the investigation from Romanoff et al., (2019) shows, some phenomena related to localized deformations in heat affected zones of welded structure are very difficult to assess even with solid element mesh due to strain localization (de Borst et al., 1991,1993). On the other hand, due to the lack of simplifications, the size of the computational models is also the highest. In ultimate strength assessments of slender structures, shell elements, with a single node over the thickness, are still superior in performance when the combination of computational cost and accuracy is considered. Therefore, we reduce models to shell element models, and often even further to shell models with beam elements used for the stiffeners (see for details chapter 2.2.1). These dimension reductions reduce the computational costs, but also the accuracy. The reason is the fact that with these dimension reductions we make assumptions. These assumptions define explicitly the strain field within each element (e.g. First order Shear Deformation Theory) that can be overly restrictive in ultimate strength assessments. The stresses are computed based on constitutive relations that can be linear or non-linear, isotropic or anisotropic. These constitutive descriptions often become increasingly inaccurate as we approach to the point of ductile fracture in the material, however their impact to energy associated with the deformation can be marginal. Also, the assumptions have influences on the geometrical descriptions and for example we cannot model properly the shapes of welds. Therefore, the welds themselves are often neglected but their impact to residual stresses

and initial imperfections are induced to models. Many of these limitations are acceptable in today's structural designs, but as we look to the future, we must be well aware of the influence of these idealisations to the ultimate strength. This is why the experimental work is valuable as it allows us to truly test our finite element models.

An additional simplification is to use the so-called Equivalent Single Layer (ESL) theories for beams, plates, and shells that have both analytical solutions and finite elements in commercial FE software packages. In these theories, the entire structural behaviour is described by the displacement degrees of freedom of the reference layer of the structure; the layer is a line in a beam or a plane in a plate/shell. This reference layer is the mathematical connection between the geometrical structural model of the ship and the mathematical ESL element. The displacements and the section forces and moments are computed in this plane and estimated elsewhere based on the ESL mathematical assumptions. Examples of these models include the Smith's method at the hull girder level where significant research has been done in ship structures community over the last decades and still today extensions are made based on comparison to full 3D-FEA. For instance, as showed by Tatsumi et al. (2019) in large container ships, the global curvature can interact with the local panel level curvature and have significant effect on the predicted ultimate strength. This means that the analytical models need to be reformulated to include this type of observed new effects occurring due to new ship concepts. In secondary and tertiary levels one can find both fully-analytical tools (e.g. Ozdemir et al., 2018, Yu et al. 2018c), semi-analytical (e.g. Manco et al., 2018, Yang et al., 2019) and Finite Element versions (e.g. Reinaldo Goncalves et al., 2016, Romanoff et al., 2019) which require similar corrections when new designs are introduced and for example the validity of closed-form design rules are tested (e.g. Narure et al, 2019). These have been developed based on classical continuum mechanics assumptions where fundamentally the two-consecutive length-scales are infinitely far apart. In ship structures, this assumption is often questionable. Therefore, we should look at the recent research in solid mechanics community which has focused on the so-called non-classical continuum mechanics where this assumption has been relaxed (Srinivasa and Reddy, 2017). Also, the corresponding beam, plate and shell elements have been developed. The needs and possible applications of these theories to ship structures was discussed by Romanoff et al. (2019).

In next subsections, we review the developments on reduced order models, 3D-Finite Element modelling and experimental work in details in comparison to the overview of the tools given here.

2.2.1 Reduced order and analytical models

Many mathematical models of physical phenomena can pose challenges when used in numerical simulations, due to the complexity problem and physical size. For ultimate strength analysis, reduced order models are commonly used to reduce the complexity of the problem and to obtain computationally efficient tools that can be used in design. Reduced order models are useful in cases where it is unfeasible to perform numerical simulations for the complete full order model. This can be due to limitations in available information and/or computational resources due to large model size, long real-time simulations, or many cases to be analysed (e.g. parameter studies, optimisation, several load cases, etc.).

Figure 1 illustrates examples for physical complex problems that are simplified with reduced order models. This is typically done by reducing the complexity of mathematical models in numerical simulations. Dependent on the problem, there are several ways to reduce mathematical models of physical phenomena:

- Reduced physical size of the problem (with appropriate boundary conditions)

- Reduced degrees of freedom (e.g. using sub-elements, assumed displacements, projection-based reduction, etc.)
- Reduced complex description of a physical problem based on assumptions and simplifications using physical insight (e.g. from analytical or empirical solutions)
- Machine learning, big data, etc.

In many cases, combinations of various methods mentioned above are used for a physical problem to obtain a computational efficient model, ref. Figure 1.

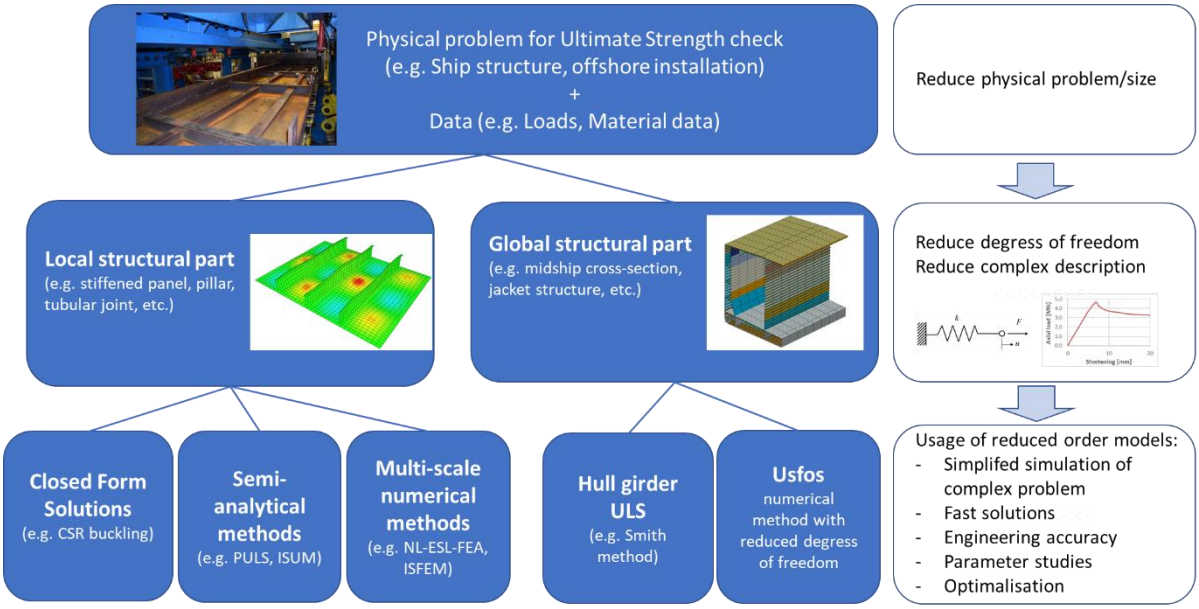

Figure 1: Illustration and examples of reduced order models for physical problems

There are several methods to reduce the number of degrees of freedom, either by using a mathematical approach with projection-based reduction or by using physical insight. Projection-based reduction relies on the projection of either the model equations or the solution onto a basis of reduced dimensionality compared to the original solution space. In comparison, physical insight can be used to reduce the degrees of freedom for instance by assuming displacements. For example, for a buckling problem of a plate or a beam, it is very usual to utilize a buckling pattern that is typically an up-and-down pattern, and then it is usual to assume harmonic functions for the displacements. This assumption is for instance used in PULS (DNVGL 2018), USFOS and most of the closed form methods. It has been also used in equivalent, homogenized, shell elements with material and/or geometrical non-linearity accounted in non-linear equivalent stiffness properties that evolve as local buckling or plasticity progresses (e.g. Reinaldo Goncalves et al., 2016; Korgesaar et al., 2016; Putranto et al., 2021).

The requirements of a reduced order model to be applicable for a physical problem, can be:

- A small approximation error compared to the full order model (in the context of energy, displacements, strains, stresses, stress resultants)
- Conservation of the properties and characteristics of the full order model
- Computationally efficient
- User-friendly and robust modelling techniques

In many cases, reduced order models are calibrated against known solutions or against more advanced numerical simulations such as finite element analysis, CFD, etc. Typically, the academic communities are aiming for the most accurate solutions, while in the engineering communities and in design, it is more common to be on the conservative side with a 'good enough' solution (engineering accuracy). This paradigm is a fruitful source for further method development of the models to balance between accuracy and computational resources.

In design of ship and offshore structures, it is necessary to have computationally efficient tools to validate the structural integrity, and reduced order models are commonly used for ultimate limit strength analysis both for structural analysis (action effects) and the load application (actions). Some examples for reduced order models are:

- Local buckling models of structural elements: Closed form methods for CSR (2019), PULS (DNVGL 2018), ISUM (e.g. Ueda et al. 1994), etc and numerical methods such as 2-scale equivalent shell element formulations (e.g. e.g. Reinaldo Goncalves et al., 2016; Korgesaar et al., 2016; Putranto et al., 2021) and ISFEM (e.g. Paik and Hughes, 2010).
- Global capacity models with reduced degrees of freedom using sub-elements: Multi-step method (Smith 1977), USFOS (Søreide et al. 1988), etc.
- Hydrodynamic models: DNVGL Shipload, Cabos et al. (2006), etc.

There is a long tradition for reduced order models within practical design of ship and offshore structure, and there exist many different models with different level of complexity even within the same discipline. For instance, for ship structures there exist many different approaches or closed form methods to check the local strength of stiffened panels. However, in the last decade, there has been a continuous work in international association of classification societies (IACS) to harmonize the rules for local buckling models. In a first phase, a Closed Form Method (CFM) for local buckling check was developed for Common Structural Rules (CSR) for Bulk Carrier and Oil Tankers. As a continuation, it has been decided that a harmonized buckling methodology should be further developed and implemented into CSR and all relevant Unified Requirements Strength of Ships (URS) resolutions IACS (2019, 2015a-d, 2017). In this development, some improvements will be done related to the stiffeners buckling computation.

- global elastic stiffener buckling
- torsional stiffeners buckling
- U-type stiffeners fitted on hatch covers.

More details on this is given in Section 4.4.

2.2.2 Numerical Prediction

Analysis of hull girder longitudinal collapse via Finite Element models is perhaps the most commonly approved approach for accurate prediction of the ultimate strength. The ultimate strength is reached when the hull girder cannot withstand the external (bending) loads. Hence, the longitudinal collapse can be defined as the collapse of a sufficient number of longitudinally relevant principal members (i.e. stiffener-plate combinations, plates, hard corners) to cause a large decrease in hull module's bending stiffness. For the longitudinal collapse the predominant load is hull girder bending (sagging and/or hogging) and the principal response is hull girder flexure, which can be expressed in terms of hull girder local curvature as also exploited in reduced order models such as Smith's method. Thus, often a numerical assessment of ultimate strength by FEA aims to establish a bending moment-curvature relationship, while it can also

deal with more relaxed description of the failure in flexure (i.e. curvature does not have to remain constant in the cross section under bending).

A numerical model should be established in a way that the accuracy of the outcome is in line with the aim of the analysis. A distinction has to be made, whether the ultimate strength is assessed (i) in an early design phase, when detailed three-dimensional finite element modelling is not available or practical, or (ii) in a final design level or during service life, when the topology is fully established including possibly the as-produced initial deformations and residual stresses. Furthermore, in the case of an optimization process, where large number of designs is considered, semi-analytical or reduced order methods offer advantages over the full 3D-finite element analysis. This section focuses on non-linear finite element method (NLFEM), while the reduced order methods were discussed earlier.

NLFEM offers a tool for numerical assessments of the final ship design as the influence of structural details can be accounted for. Numerical predictions should support multiple failure modes and their interactions, while giving precise predictions of collapse and post-collapse behavior of the structural members and assemblies involved, particularly those under compression. Thereby, the performance of numerical assessments is affected by the idealization of geometry, material and loads. Furthermore, solution techniques can also influence the outcome if not executed properly. The main influencers are summarized in Figure 2.

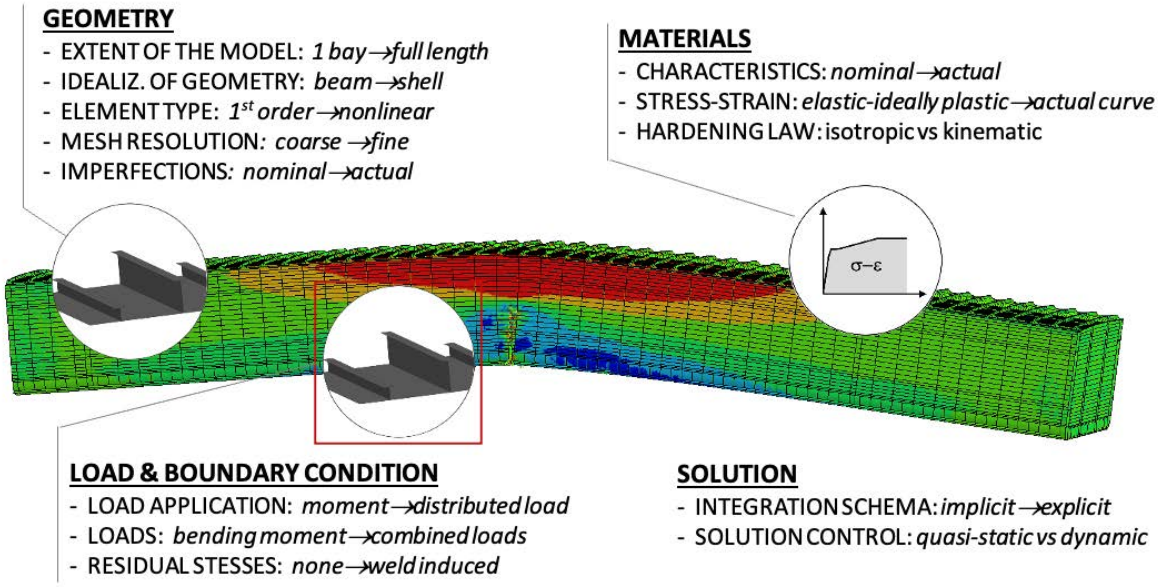

Figure 2: Different aspects in numerical modelling and solution

While early numerical assessments of ultimate strength used relatively short models, only one frame spacing or 1-bay, increasing computational power has made it possible to analyze several tank lengths (Tatsumi and Fujikubo, 2020), or even the whole ship model (Xu et al, 2019). A larger model has clear advantages. While in very short models the pure bending moment is imposed through model boundaries, in larger models the actual pressure distribution (Tatsumi and Fujikubo, 2020) and several different load combinations can be applied (Matsumoto et al, 2016). A full model also allows to consider the effect of transverse bulkheads on the actual bending curvature. Tatsumi & Fujikubo (2020) studied the effect of boundary conditions for ½+1+½ cargo hold model, i.e. the boundary conditions were applied at half the cargo hold length from the studied section. Two types of boundary conditions were studied: end planes of the model were assumed either rigid or simply supported with implied kinematic constraints.

It was found that the effect of analyzed boundary conditions on the ultimate strength of the critical section was not significant. Xu and Guedes Soares (2020) investigated numerically the effect of experimental boundary conditions on the collapse strength of stiffened panels, where four configurations of the boundary conditions were considered. Based on the performed analysis it was suggested that both translation and rotation degrees of freedom of the loaded edges should be constrained to facilitate the collapse of the central span before the others.

Especially in the compression zone, the structural elements should be modelled in a level allowing for a proper buckling/collapse shape to be developed. Thus, it is suggested to model the structural elements using shell elements. At least 5 elements are suggested across the web height and 2 across the width of the flange. Smaller elements such as stiffeners can be modelled as a combination of shells and offset beams, especially when modelling the region outside the buckling zone. Element formulations must allow for material and geometric nonlinearity and large displacements and rotations. If post-buckling behaviour is of interest, large strain formulation is required. Effect of initial imperfections on the ultimate strength is discussed among others in (Wang et al, 2018a) and Vu Van et al (2018).

For the ultimate strength assessment, the model can be loaded by applying pure bending moment vie the end plates or by loading the model with local pressure that results more accurate local loads, shear force and bending moment distribution. Matsumoto et al (2016) and Tatsumi & Fujikubo (2020) studied the influence of local loads on the bending of the double bottom of a container ship. It was shown that the ultimate hogging strength of container ships is significantly reduced by upward local loads acting on outer bottom plates.

Ultimate strength assessment can be performed either using an implicit or explicit approach. Implicit analysis is better suited for smaller models as the calculation to make an inverse of the stiffness matrix takes a long time in the implicit FEM (Yao and Fujikubo, 2016). However, as the calculation capacity increases, the implicit approach becomes feasible also for larger models. Explicit analyses have successfully been used to analyze the models of the whole ship hull (Tabri et al, 2020)

In terms of local panel level modelling, Shi et al. (2019c) performed a series of finite element analysis of cracked stiffened plates subjected to axial compression; the model is verified based on experimental results. The influence of varying orientation, length, and crack location on the residual compressive strength is studied. It was concluded that the effective cross section of the cracked stiffened plate plays a key role in the assessment of the residual ultimate strength. Also, the initial weld induced plate distortions have a significant effect on the residual ultimate strength including the measured data by tests and the buckling-type one. Li et al. (2019a) studied numerically the effect of welding residual stress and steel grade on the ultimate strength of stiffened plates under uniaxial compressive load. Nineteen stiffened plates built with three types of stiffeners with various column slenderness ratios provided in the ISSC2000 VI.2 (Yao, et al., 2000) benchmark calculations avoid time-varying analysis are employed in the present study. Various types of stiffeners as well as column slenderness and different shipbuilding steel grades are considered. The commercial finite element code ABAQUS is applied to simulate the collapse behavior of the stiffened plates and verified against the benchmark calculations. A simplified model for the distribution of welding induced stress is adopted, and this model bears a difference from the actual residual stress distribution. Using the non-linear FEM commercial software ANSYS and the approach stipulated by the Common Structural Rules, Woloszyk et al. (2018) assessed numerically the ultimate strength of severe corroded stiffened plates, taking into account the effect of different governing factors such as corrosion degradation level, material properties, initial imperfections and boundary conditions. The numerical results were compared with the published experimental results and the calculations made based on the CSR

approach and empirical formula, showing that the FE analysis are quite accurate for predicting the ultimate strength of corroded plates, conditionally to the changes of the mechanical properties as a result of corrosion degradation.

2.3 Experimentation

The role of the experimentation in tools is on one hand to validate the computations and on the other hand to explore the phenomenon associated with the ultimate strength of the structures. The experimentation is important so that the structural idealizations and their impact on the actual performance of the structure are identified. This also motivated the benchmark investigation presented later in the report. We approach the problem here at the levels of small scale tests on plates and stiffened panels, larger scale tests on panels and grillages and finally on scaled models on the hull girders.

The main purpose such experiments is to test models which are designed to reflect the possible failure modes under different loading conditions to calculate the ultimate strength capacity of such structural components in intact or damaged condition. Also, to analyze both local and global response of the structure and to study carefully the trend of each specimen in all regimes; pre-buckling, post-buckling and post-collapse.

The experiments may be performed using universal testing machines or loading frames, which may be load or displacement controlled. The setup of each experiment may differ according to the simulated boundary and loading condition. Several instruments may be used to track the structural response as displacement gauges and strain gauges which may be mechanical (multi use) or single use ones.

2.3.1 Small-scale tests (plates and stiffened plates)

The welded stiffened plate is widely used in naval architecture and offshore engineering as basic structural members. Therefore both local and global behavior has to be studied carefully and this can be done easily using experimental; full or scaled models and such scale models may be scaled using dimensional theory. One type of such plates is the wash plate, which may be subjected to different types of loads as well as damage scenarios. The effect of different opening sizes as well as opening location on the ultimate strength of such plates may be investigated through conducting a series of experimental compressive tests.

A series of experimental tests for intact/corroded plates, stiffened plates and stiffened panels with and without openings which may be used as wash plates, have been performed by Saad-Eldeen et al. (2018), Saad-Eldeen et al. (2019) and Saad-Eldeen et al. (2020). The analysis presented here are continuation of a long-term study dealing with steel structures with openings and subjected to different degradation and deterioration scenarios. The testing machine used in the experiment is a universal machine as shown in Fig. 1, of 250 kN hydraulic jack and the tests are carried out using load control with a rate of 0.5 kN/s. The specimen has been mounted between two stiff supporting clips, using bolt connections. The used supports impose conditions of constrained lateral displacement and rotation within the depth of the support of 20 mm. A displacement gauge was mounted to the tested specimens to record the lateral displacement, and the local strain was measured by a mechanical strain gauge, see Figure 3.

Figure 3: Experimental test setup, plate with one opening (left),
stiffened plate with multiple openings (right)

Saad-Eldeen et al. (2018) investigated experimentally the influence of different opening sizes and shapes, different steel materials and structural configurations on the ultimate strength of steel plates. Based on the experimental results, it was concluded that the asymmetric allocation of an opening may affect the global and local responses and reduces the strain energy of the stiffened panels. For high tensile steel unstiffened plates with different circular opening sizes, as the opening size increases, the strain energy density decreases regardless of the steel grade of the material and the opening shape. By decreasing the residual breadth ratio, both global shortening strain and local strain decrease nonlinearly. Also, the results show that in spite the ratio between the yield stress of high tensile steel and mild steel materials is 2.9, the ratio of the ultimate load carrying capacity as well as the ultimate stress at any residual breadth ratio is different and may be fitted with a power function.

Saad-Eldeen et al. (2019) carried out a series of experimental buckling collapse tests on steel plates with multiple openings of different degrees of openings, with the same test set up shown in Figure 3. The effect of real corrosion wastage as well as initial imperfections is also investigated. A nonlinear relationship between the axial compressive force and the remaining volume is developed, which may be expressed by an exponential function. It was noticed that in a buckling analysis, the remaining volume is a better representative parameter for compressive strength capacity of plates with multiple openings than the remaining cross-sectional area. Also, the number of openings is an additional parameter that affects both response and capacity of plates with multiple openings, where the higher number of openings shows better compressive capacity than the lower number with the same degree of openings. Therefore, from a design point of view for a plate with multiple openings, the higher number of openings is a better design option than the lower number, because the higher number creates a small length between every two consecutive openings, which directly increase the stiffness due to its short length.

Saad-Eldeen et al. (2020) performed a series of compressive tests on high tensile steel stiffened plates with multiple openings. The openings were created with different degree of openings and numbers to investigate its effect on the ultimate load carrying capacity. A failure assessment diagram of for high tensile steel stiffened plates, SP-HTS and mild steel plates, with multiple openings was developed based on the lower confidence level of the 95% confidence interval, which is in a benefit to the design stages of stiffened plates with openings. Based on the experimental results, several failure modes are observed during the buckling tests as stiffener tension-induced failure, plate-induced failure and the overall failure of the stiffened plate. It

may be stated that if the final deformed shape follows the initial imperfection shape, the resultant ultimate capacity is lower than the one with an opposite final deformed shape.

Xu and Guedes Soares (2021) performed seven stiffened panels with different configurations and subjected to in-plane longitudinal compression. The initial imperfections were recorded before the test and also, strain gauges were mounted on both plate and stiffener to measure the strain during the test. It was stated that lack of constraint at the unloaded free edges has less effect on the buckling of stiffened panels with large geometrical dimensions. Also, the effect of boundary condition on the collapse mode as well as the ultimate strength have been addressed.

In the ship and offshore engineering context, sandwich panels are often used in advanced marine vessels and offshore energy exploration structures such as offshore wind turbine blades.

Kai et al. (2020) investigated the ultimate tensile strength of sandwich composite L-joints for ship structures. The L-joint consists of two base sandwich panels, two longitudinal stiffeners , and one transverse stiffener. Skin material of the L-joint is 3 mm thick GFRP, which is made up of orthogonal plain-woven cloth and epoxy resin. The core material is Polyvinyl Chloride (PVC). Experiments of the L-joints are conducted on the test machine shown in Figure 4. During the experiments, the two ends of the L-joint are clapped by premade steel fixtures. The lower end is latched to the test bench, and the upper end is latched to the actuator. The applied load is controlled through the displacement of the actuator, which is set at the speed of 2 mm/min upwards.

Figure 4: A sandwich composite L-Joint for ship structures under tension load.
[Kai et al. 2020]

2.3.2 Large-scale tests (panels and grillages)

Large-scale ultimate strength experiments are rather limited in the literature. Paik et al. (2020a) used a specially designed test rig as shown in Figure 5 to apply axial compressive loads to collapse a steel stiffened plate structure. The loads were provided by two hydraulic actuators which were fixed on a reaction wall. Each loading actuator can carry up to 1,000 tons in compression for a maximum of 2,000 tons in total. The 'rigid-body' jig helped achieve the application of a uniformly distributed compressive loading and uniform displacement over the loaded edge, which assigned fixed boundary conditions except for the moving direction of the actuators. The other end of the test structure was fixed by a reaction wall. A personal computer

controlled the synchronizing of the two actuators so that the uniform loads were applied over the loaded edge, see Figure 6.

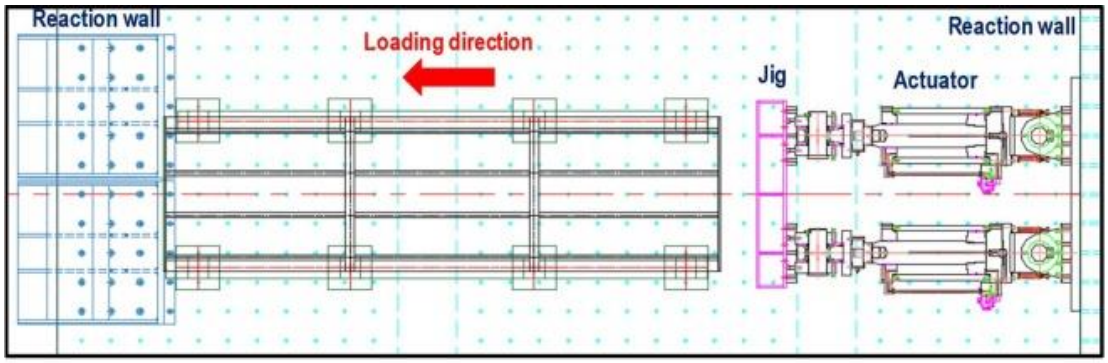

(a) Plan view of the test set-up

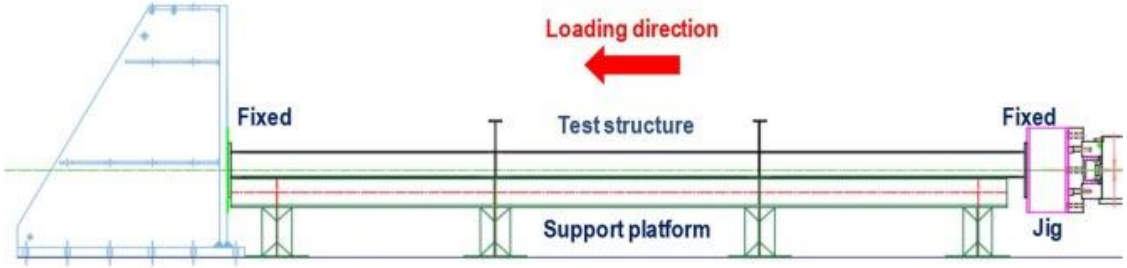

(b) Profile view of the test set-up

Figure 5: Layout of a specially designed test rig to collapse a steel stiffened plate structure with the two hydraulic loading actuators and the reaction wall. Paik et al. (2020a)

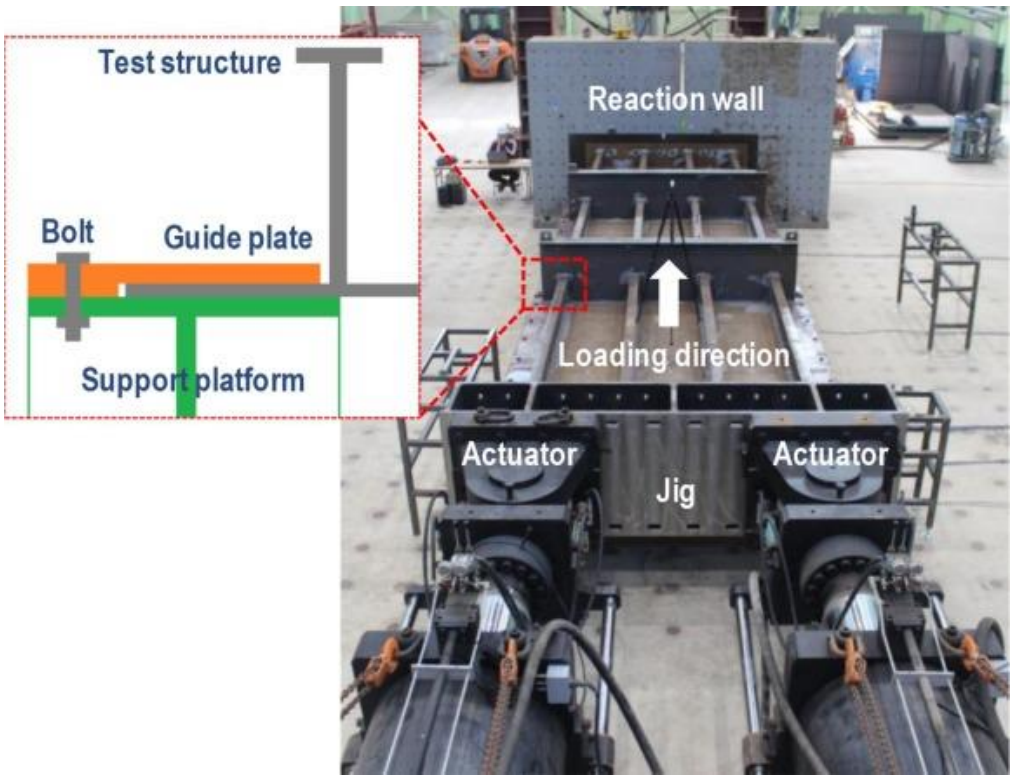

Figure 6: A specially designed test rig to collapse a steel stiffened plate structure under cyclic axial-compressive loading, Paik et al. (2020a)

Cui and Wang (2020) carried out collapse testes on stiffened plates with central opening and artificial pitting corrosion (through thickness), subjected to uniaxial compressive load, according to the experimental set up shown in Figure 7. It was stated that for the same volume of corrosion pits, the post-collapse as well as the ultimate strength may differ, especially within the extent of opening. Also, the out of plane deformation of the supporting members plays the most important role in the strength capacity assessment.

Figure 7: Experimental layout [Cui and Wang (2020)]

To experimentally examine buckling strength of sandwich shells used in large-scale offshore wind turbine blade structures, a recently developed subcomponent test setup has been proposed by Chen et al. (2019b) as shown in Figure 8. Attention has been made to avoid undesired premature failure at the specimen's boundaries. Both ends of the specimen are reinforced internally by gluing in a layer of plywood. The specimen is then glued to the steel plates of the test rig. Further, plywood is applied externally to clamp the specimen to the test rig. Epoxy adhesive is also used to fill the gaps between the specimen and the plywood clamp. The epoxy adhesive was cured using heating pads. Over lamination using wet hand lay-up is applied to reinforce local materials near the clamped boundaries. These boundary treatment ensured the structural failure in the desired test region.

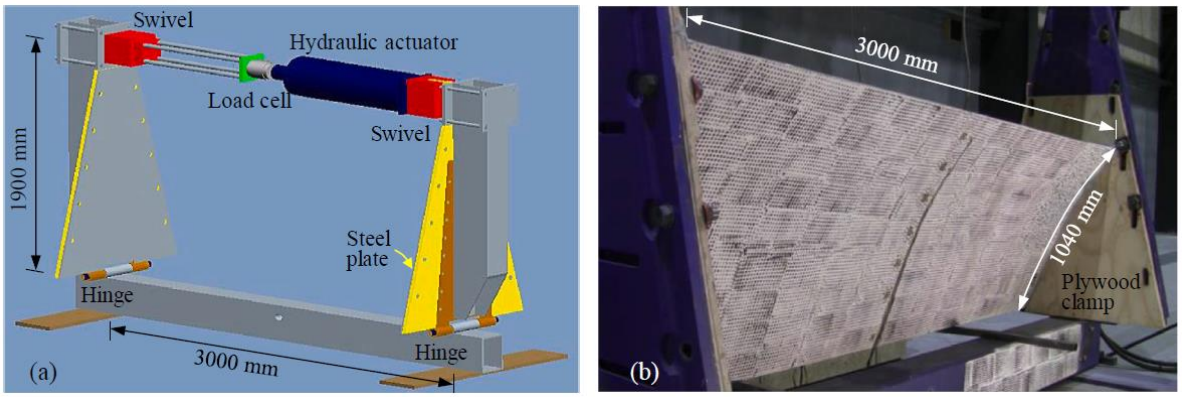

Figure 8: A recent developed experimental setup to apply compressive loads to a sandwich shell used in large-scale offshore wind turbine blade structures. (a) A test rig applies compressive loads to the specimen using a hydraulic actuator with a loading capacity of 500 kN. (b) the sandwich shell structure is mounted in the test rig through steel plates that are hinged at the bottom of the test rig. Speckle patterns are painted on the specimen surface for digital image correlation (DIC) measurement. Chen et al. (2019b)

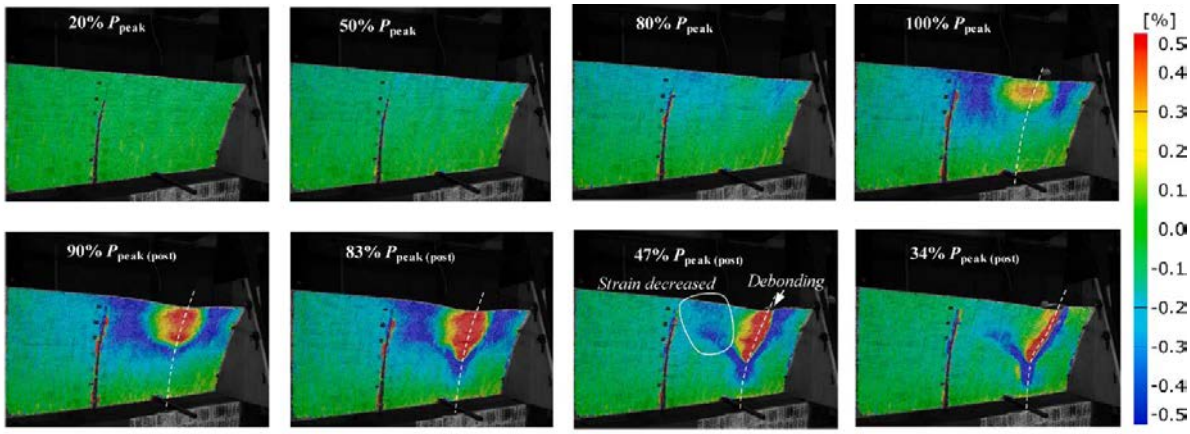

Figure 9: Longitudinal strain distributions measured by DIC show buckling and failure process of the sandwich shell structures during compressive static loading. Note that the structural failure occurs in the desired region away from the boundaries, Chen et al. (2019b).

2.3.3 Hull Girder level tests

Ultimate strength tests on traditional hull girders such as tankers and bulk-carriers have been extensively studied over several decades (see for example: Dowling, 1973; Gordo and Guedes Soares, 2004 and 2015; Shi and Wang, 2012) in order to validate the reduced order models and the finite element-based simulations. In passenger ship there are large and long superstructures typically extending over the entire length of the hull girder. These advanced hull girders also have side shell recess and many window openings making the cross-sectional behavior of the hull girder extremely complex, especially if the ultimate strength is concerned; see also the benchmark on ultimate strength simulations of passenger ship from ISSC 2006 (Yao, et al., 2006). However, experimental contributions to this topic have been lacking until recently. The recent experimental paper from Shi and Gao (2021) investigated the collapse behavior of scaled steel ship model with superstructures (See Figure 10). Based on the numerical and experimental findings the superstructure effectiveness was analyzed. The authors also investigated the combined action of bending moment and shear force and proposed a formula to account their combined action at the hull girder level. Similar investigations have been carried out in different ship types over the period of this committee. These will be reviewed in details in the Section 4.3.

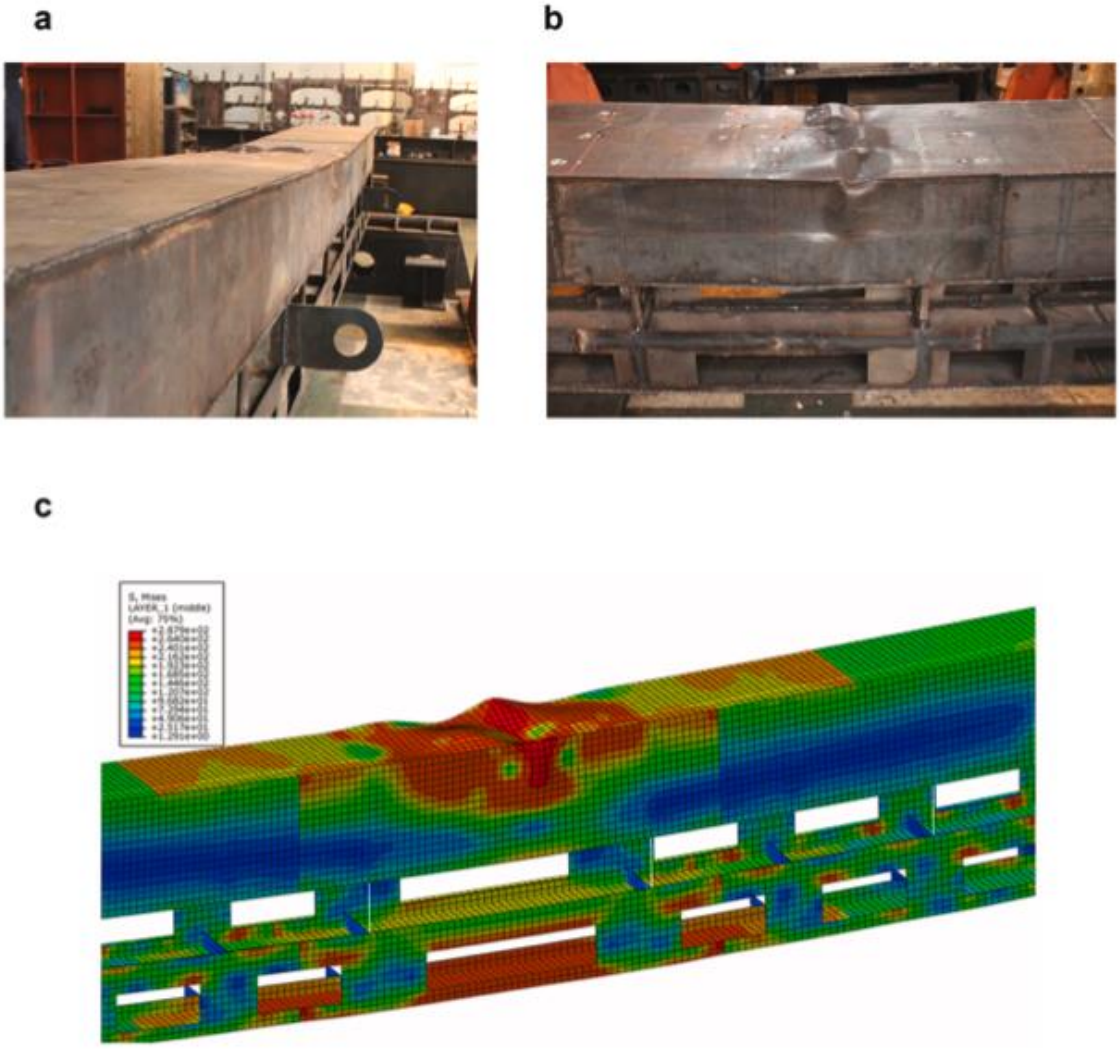

Figure 10: Comparison between failure modes derived experimentally and numerically to passenger ship with long superstructure for scaled models, Shi and Gao (2021).

2.4 Concluding remarks

2.4.1 Conclusions

The determination of the ultimate strength of ship and offshore structure is still highly affected by uncertanties.

- The aleatory uncertainties can be diminished by additional testing or inclusion of stochastic distributions for the parameters.
- On the other hand, epistemic uncertainties often require a large number of time consuming analyses to be quantified, hence literature work has focused on providing methodologies that enables the ranking of uncertainties in computational modelling based on the sensitivity of the solution.

In the context of FE analysis, solid elements are considered the most accurate, but often clash with computational efforts. Hence, shell models still represent a widely accepted compromise, but we must be well aware of the influence of these idealizations on the ultimate strength. This is why the experimental work is valuable as it allows us to truly test our numerical models.

Keeping an eye on the advantages of computational tools, it is worth noting that, as the calculation capacity increases, the models ranging over the three-hold hull model have been successfully modelled using implicit approach.

Experiment work is still carried out in laboratory scale by using similarity rules especially at the hull girder, panel and component levels. Technologies like Digital Image Correlations are providing important advantages in the acquisition of data. Moreover, with the help of digital twins in the future, we will be able to keep up with the state of the structure (e.g. actual dimensions, distortions, damages) throughout the design, building and operational stages.

As the failure progresses in the structure, the coupling between non-linear geometry, material and load redistribution can be highly complex and occur very rapidly. In this context, even quasi-static tests may lead to sudden catastrophic failure. The rapid interactions are currently at the limits or beyond current experimental and computational capabilities.

In the case of an optimization process, where a large number of designs is considered, semi-analytical or reduced order methods offer advantages over the finite element analysis. For ultimate strength analysis, reduced order models are commonly used to reduce the complexity of the problem in the design stage and accommodate limited information. Reduced order models are still useful in cases where it is unfeasible to perform numerical simulations for the complete full order model. This can be due to limitations in computational resources for instance due to large model size, long real-time simulations, or many cases to be analyzed.

There is a long tradition of the use of reduced order models within design of ship and offshore structure, and there exist many different models, with different level of complexity even within the same discipline. However, in the last decade, there has been a continuous work in International Association of Classification Societies (IACS) to harmonize the rules for local buckling models. As a continuation, it has been decided that a harmonized buckling methodology should be further developed and implemented into CSR and all relevant Unified Requirements Strength of Ships (URS) resolutions (IACS 2019, 2015a d, 2017).

2.4.2 Recommendations for future work

The following recommendations are given for future work:

- When quantifying epistemic uncertanties in numerical modelling via experimental/numerical comparison, it is recommended to take into account more than just the ultimate strength value, but to consider in the validation also the failure modes and the overall collapse behavior.
- Numerical predictions should support multiple failure modes and their interactions, while giving precise predictions of collapse and post-collapse behaviour of the structural members and assemblies involved. Especially in the compression zone, the structural elements should be modelled to allow proper buckling/collapse shape to be developed.
- Shell elements currently represent a good modelling compromise, but as we look to the future, advances in computational power may lead to the development and use of larger scale models using solid elements.
- Significant literature works showed that simplifications in the shape (e.g. due to imperfections and corrosion) leads to significant loss of accuracy at local scale, rather than global. In such cases, the recent experiments showed that in the ultimate strength assessment highly localised stresses can act as failure initiation points for overall

collapse. For this reason, efforts should be devoted to expand our knowledge about the effect of real corrosion wastage and imperfections, also on the experimental side.

3. INFLUENCE FACTORS OF MATERIALS AND LIFE-CYCLE MANAGEMENT

The fast growing offshore wind farms in Europe now have wind turbines approaching their design lifetime of 20 to 25 years. Assessing the remaining strength of these structures and extending their service lifetime are among the most imminent challenges (Aabo et al., 2018). Indeed, smart structural health monitoring and digital twins have become popular topics enabling safer operations and longer service lives of suchlike structures. This chapter reviews the most recent literature from the perspective of materials and life-cycle management affects on ultimate strength prediction, with focus on metallic and non-metallic material performance and degradation, new materials, and new operational environments.

Two areas of interest were found in the recent research. The first is the work done on the temperature effect. This is particularly of interest in view of cryogenic fuel tanks. Erofeev et al (2019) studied the hydrogen impact on the initiation and propagation of welded cold cracks in low-alloy steels. They show with experiments that the welding of low-alloy steels at low temperatures reduces the critical brittleness temperature by 40-50 °C and hence the amount of energy needed for crack growth. Harshini et al (2019) describe tests done on stainless steel 316L using liquid CO2 for cooling (at 0, -25, and -50 °C) and a furnace at temperatures of 750, 825 and 900 °C. Different strain rates were also considered. It was found that a temperature increase leads to a decrease in strength and increase in failure strain both by approximately a factor of 2. The strain rate effect at low temperatures is far less than that in ambient environments. More strain hardening is seen instead of a plastic plateau. Xu et al. (2018b) considered extreme temperature change between -60 ℃ to 80 ℃ and investigated the ultimate strength of stiffened panels under longitudinal compression experiencing such temperature shift. The material properties were obtained by tensile tests under various temperatures and were used in nonlinear FEA.

The second focal point is on new materials. Hosseini et al (2019) studied high strength low alloy (HSLA) steels. The aim was to increase the amount of Cu, Ni and to some extent C in order to increase the yield strength while maintaining toughness. It was seen that if a proper selection was made for the temperatures of rolling, austenisation and aging, a HSLA 100 with increased Cu and Ni can possess higher mechanical properties with only a small toughness reduction. Gao et al (2019) developed a new ultra-high strength steel with balanced strength and toughness. The authors created an experimental steel by nanoscale beta-NiAL and M2C precipitates. The strength and toughness of the experimental steel are comparable to the known ultra-high strength steels (strength up to 2000 MPa), with a 50% reduction in costs. Ultra-strong nickel aluminum bronze alloys were created according to Ma et al (2019a) by continuous heavy hot-rolling at different temperatures. The process led to a grain refinement and dislocation strengthening. Using a combination of rolling temperatures resulted in a higher ultimate strength material (around 800 MPa) while maintaining a fair ductility (14.5%).

Instead of the traditional production techniques, Additive Manufacturing (AM) has become increasingly popular, allowing more organic designs with less lead time. Bajaj et al (2020) looked at the microstructure of AM stainless steels and their mechanical properties. In general, the microstructure of the AM steels is finer by an order of magnitude than that from conventional processes. The strength and corrosion resistance are normally in line with or even exceeding the conventional stainless steels, however, the ductility and fatigue resistance can be lagging behind. Surface treatment can improve these properties. Although not targeted for maritime and offshore, Buchanan and Gardner (2019) provide a good overview of AM metals.

3.1 Corrosion

Corrosion is one of the major degradation forms found on ships and offshore structures. Although extensive research has been carried out by corrosion scientists and engineers to understand the fundamental mechanisms, it is difficult to accurately predict and quantify corrosion damage throughout assets' service lives. This is primarily due to the multi-variant nature of corrosion, often shown as 'random' in terms of the damage shape, size, location, corrosion rate and severity. The way these random characteristics are simulated in experimental and/or numerical models may have significant effect on the structural analysis.

Traditional ultimate strength assessments are based on idealized corrosion features such as uniform thickness reduction and cylindrical pits (Saad-Eldeen et al., 2019; Feng et al., 2020a). In some studies, the corrosion-effect was simplified by testing corroded specimens (Saad-Eldeen et al., 2019, Ringsberg et al., 2018 and Woloszyk et al., 2018) and using reduced tensile properties. Although this approach greatly reduces the complexity of modelling corrosion, it needs to be noted that such tensile properties should only be considered as 'equivalents' to incorporate the effects of surface roughness and micro-cracks. The actual steel's mechanical behavior may not be affected by corrosion, especially in marine environments.

Woloszyk et al. (2018) used FEA stipulated by the Common Structural Rules to study the ultimate strength of stiffened plates subject to general corrosion modeled as uniform thickness reductions. Different factors governing the structural behavior, such as corrosion degradation level, material properties, initial imperfections and boundary conditions were considered. The numerically estimated ultimate strength was demonstrated to be very close to those observed during the experimental test. This led to an approach of using an equivalent thickness for a relatively fast and practical ultimate strength assessment for this type of structures.

Yeter et al. (2019) conducted FEA studies of jacket offshore wind turbine support structures assuming a uniform thickness reduction to simulate general corrosion. Adopting a model containing two loading steps, namely elastic dead-load step and elastic-plastic environment load step, the ultimate strength of three types of jacket support structures was investigated, with thickness reduction located on the leg components in the supported module just above the mean still water level. The ultimate strength was found to decrease proportionally with the reduced thickness, leading to up to 50% strength loss for a 50% thickness loss from the tubular structure immediately below the platform (original thickness = 24 mm). It was concluded that the integrity of the first supporting module just below the platform was the most critical in determining the remaining ultimate strength of the entire structure.

Regarding localised corrosion, steel tubular members with idealised pitting were studied by Ahn et al. (2018) and Wang & Shenoi (2019d) using both experimental and numerical methods. Both studies used cylindrical "pits" that were machined on the tubular samples, varying size, intensity and distribution pattern. Samples were subject to uniaxial compressive loads on both end of the tube. FEA parametric studies were conducted after validation against experiments.

Ahn et al. (2018) reported that the ultimate strength of the tube decreased proportionally with the equivalent cross-sectional area ratio and damage volume ratio. Wang and Shenoi (2019d) found that random pitting distributions resulted in larger strength reduction compared to regular pits with a local buckling failure mode. With a focus on offshore applications, Wang et al (2019c) studied the effect of pitting defects on the buckling strength of a thick-wall cylinder under axial compression. Uniform and random pitting effects were tested and analysed using FEA. When pits were located close to the end of the pipe, the buckling load decreased more significantly compared to pipes with pits close to mid-span. The collapse mode of pitted pipes was found different from uniformly corroded ones.

Empirical formulas were proposed by Li et al. (2018a), Piscopo & Scamardella (2018) and Shi et al. (2018) to predict the ultimate strength reduction of stiffened panels subject to localized attack, accounting for the degree of pitting, pitting locations, geometrical imperfections and welding residual stresses. Specifically, Shi et al. (2018) used reduced plate slenderness and column slenderness ratios to estimate the corrosion effect. All of these formulae were developed based on FEA with idealized pitting features. Cui et al. (2019a) focused the bi-axial ultimate strength of a typical bottom stiffened panel in container ship under both uniform and non-uniform localized pitting corrosion and performed a series of nonlinear FE analyses. Stochastic modelling was applied to express the growth of corrosion and probabilistic characteristics of the ultimate strength reduction.

New methods incorporating electrochemistry and advanced data analytics also emerged in recent years. Abdussamie et al. (2018) studied corroded plates using an adaptive neuro-fuzzy inference system method, a tool combining both neutral network and fuzzy logic. This was to predict the ultimate strength of plates with pitting corrosion subject to uniaxial in-plane compress loads. The authors used the database from Ok et al. (2007) and investigated the efficiency of different membership functions. The maximum error was 2.8% compared to Ok et al.'s FEA results. However, the application scope of this method is unclear.

Wang et al. (2018b; 2019e) and Ilman et al. (2020; 2022) developed a new methodology to link the corrosion experimental data and ultimate strength analysis for stiffened plates and panels using FEA. This was based on the measurement of carbon steel corrosion in seawater and subject to active tensile loading, simulating the mechano-electrochemically induced corrosion (interplay between mechanical stresses and corrosion). This enabled the model to capture the dynamic change in corrosion characteristics with time and location. Bench-shaped features were obtained, which closely resembled corrosion patterns observed in reality. Additionally, a failure mode change was observed compared to models with uniform thickness reduction.

Ma et al. (2019b) analysed extreme cyclic loading and pitting for the high strength steel NV-D36 commonly used in offshore platforms. Different degrees of pitting damage were generated by laboratory electrochemical accelerated corrosion. Seven typical cyclic loading programs were designed based on the real extreme cyclic loads that offshore platform may be subjected to. The cyclic loads were applied to the specimens to obtain the hysteretic properties of healthy and pitting specimen. Under cyclic loading, the pitting damage caused local volume loss and local stress concentration, which resulted in degradation of stiffness and strength of steel. Generalised yield strength and generalised Young's modulus of the steel specimens were gradually degraded with the deepening of pitting damage. The cyclic hardening coefficient linearly degenerated with the pitting volume loss rate, and the degree of degradation was almost irrelevant to the cyclic loading program. The cyclic hardening exponent was almost unaffected by pitting damage.

3.2 Non-metallic materials

For composite materials, research into mechanical behaviour after ageing is seen to be a current area of interest. Ding et al (2019) studied the effect of ageing of sandwich composites using a vinyl-ester glass composite with a closed cell PVC core. Specimens were exposed to different temperature cycles and salt concentrations in water (submerged) or salt-fog spraying. Tension, compression and shear strength were tested. The submerged specimens showed a higher water absorption than the specimens subjected to vapour. For the hygrothermal exposed specimen, the solar radiation exposed specimen showed far less weight increase than the specimen subjected to high and low temperatures. Mechanical properties were not changing excessively due to the exposure. All failure patterns were the same as for the non-aged specimen, mainly in the core. As such it is concluded that the PVC core is not much affected by the exposures. Fiore et

al (2019) studied the effect of sodium bicarbonate treatment on the aging resistance of natural fibres (epoxy based flax or jute fibre reinforced composites) in a marine environment. Sodium bicarbonate treatment is an eco-friendly chemical treatment. Natural fibres are becoming more interesting because they are cheap, easy to process and renewable. However, on the downside they show large differences in mechanical properties (influence by harvest, climate, location, weather etc). The properties are lower than synthetic fibres and show high moisture absorption and weak compatibility for several matrices. Fibre pre-treatment can improve the mechanical behaviour and the durability. In the paper the authors studied the effect of soaking flax and jute fabrics in sodium bicarbonate solution for 5 days at room temperatures. Tensile, flexural and impact test with salt-fog spray aging (ASTM B117) were performed. In general, it can be stated that for flax fibres the aging resistance improves, whereas for jute fibres the pre-treatment has a light decreasing effect on the durability. However, jute does show a large increase in impact energy after aging due to the increase in deflection at failure. Jesthi and Nayak (2019) investigated the mechanical properties and morphology of seawater aged (hybrid) carbon and glass epoxy composite. The effect of stacking sequence of the carbon and glass layers was studied with respect to seawater exposure on the tensile, flexural and impact strength based on ASTM D570-98 aging. The water absorption of the hybrid samples is less than for the full glass or carbon versions. This is thought to be caused by uneven swelling or thermal expansion of the fibres. Tensile and flexural strength reduction is the same as for mono-fibre specimen. For the impact damaged case, the strength reduction of the hybrid materials can be even less than for plain glass and all hybrids perform better than the carbon specimens.

Dinesh et al (2020) studied the use of naturel and synthetic hybrid composites for marine application. They manufactured samples using either Kevlar fibres with coir fibres in an epoxy matrix. The Kevlar fibre is an eggshell powder reinforced epoxy matrix or a kevlar coir fibre combination in an eggshell powder reinforced epoxy matrix. Tests including tensile, impact and water absorption tests were performed. Both water absorption behaviour and impact characteristics were the best for the second sample. The tensile strength was the highest for the third sample with both coir fibre and eggshell. The authors recommended these materials for maritime applications. A similar study was undertaken by Bhoopathi and Ramesh (2020) who looked at the influence of eggshell powder on hemp fibre epoxy laminates. They also found that water absorption and impact strength improved by the use of eggshell powder. However, tensile and shear strength decreased with increasing eggshell powder volume.

Elanchezhian et al (2018) provide a review on the use of metal matrix composites for marine applications. The composite consists of a grade 5 titanium with Kevlar and carbon fibres. A summary of several experimental studies on mechanical properties is given.

3.3 Fabrication

3.3.1 Welding

For metallic structure, the fabrication methods can greatly affect the material properties and hence the actual strength capacities. For example, the material properties of offshore pipelines may be greatly affected by the welding type, namely, seamless (only welded in hoop direction) or longitudinal/spiral welded seams (produced by U-ing, O-ing and expanding). The latter was shown to induce anisotropic mechanical properties, with up to 30% reduction in compression yield stress (Cai et al., 2017). This will result in large variations in the pipe's ultimate strength.

Research into the effect of welding-induced imperfections on the ultimate strength of ships has been carried out for decades. Recent development includes more sophisticated modelling for both small- and large-scale structures. Both the buckling mode geometric deflection and simplified residual stresses were modelled in Xia et al.'s FEA work (2018) to investigate their

effect on the ultimate strength of steel plates. As expected, the transverse residual stresses had less effect on the longitudinal ultimate strength compared to the longitudinal residual stresses. Moreover, the combined effect of the two imperfections cannot be taken as simple linear superposition. The initial deflection magnitude plays a dominant role in ultimate strength reduction. The authors also studied the combined effect of cracks, which will be discussed in Section 3.4.1.

The influence of three levels of welding-induced initial geometric imperfections on the dynamic ultimate strength of stiffened panels were investigated by Yang et al. (2018) using FEA. Both uniaxial compression and lateral pressure were considered in the models. This was also compared with static ultimate strength analysis. It was found that the larger initial imperfection resulted in smaller dynamic ultimate strength; and suggested that accurate imperfection shape was important. However, there was no in-depth explanations in the ultimate strength difference induced by the two imperfection shapes. On a similar structure (a stiffened plate), Chen and Guedes Soares (2018a) studied the residual stress effect generated from a thermo-elasto-plastic FEA. A simplified model was reported to be capable of effectively representing the residual stress distribution in steel-plated structures in a wide range of engineering applications. In addition, the widths of the tension zones had a quasi-linear behaviour against the plate slenderness ratio. Chen et al. (2019a) investigated the sensitivity of imperfections on the buckling and post buckling of stiffened panels made of aluminum alloys, based on which a design optimization was performed. In addition to traditional stiffened panel configurations, the authors proposed new panels containing different types of sub-stiffeners, as shown in Figure 11. The first eigenvalue buckling mode was used as the initial imperfection. The FEA results indicated that the sub-stiffeners improved the stability and ultimate strength of the panel by up to 36% without increasing the overall weight of the structure.

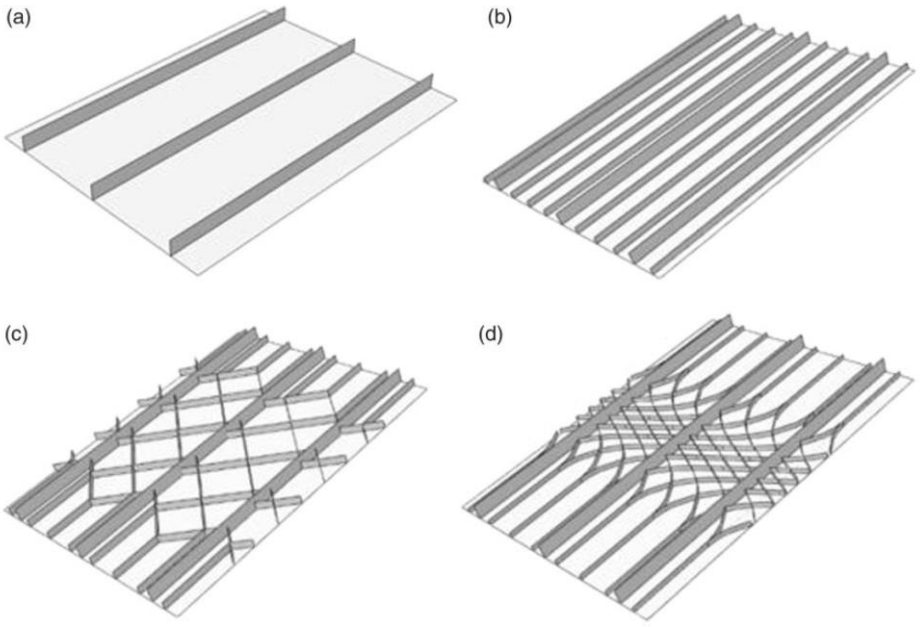

Figure 11: Investigated sub-stiffener panels: (a) traditional panel; (b) prismatic sub-stiffened panel; (c) grid sub-stiffened panel; (d) curvilinear variable stiffened panel (Chen et al., 2019a)

The effect of initial geometric imperfections on the ultimate strength of ultra large container ship (ULCS) structures were investigated by Wang et al. (2018a). Featuring large deck openings and low torsional rigidity, the assessment of container ships under load combinations comprising of vertical bending moment, horizontal bending moment and torsion is vital in the structural design stage. The study was based on a series of nonlinear FEA of a transverse mid-ship section of an ULCS using dynamic explicit solver. The initial imperfections were assumed to be following the "thin horse" mode for panels and flexural buckling/tripping mode for stiffeners. The deflection magnitude ranged from 0 to 30 mm, based on which a new closed form formula was proposed, describing the ultimate strength interaction relationship under combined three load components. It was also concluded that the assumed initial imperfection had more significant influence on the horizontal bending moment compared to the other two loading scenarios. However, it is not clear how the modelling was validated.

3.3.2 Non-welded connections

When composite materials, or a combination of composites and metals, are used in ship structures, connections between different parts are made by bonding, bolting or a combination of both. Bonded connections are beneficial when connecting metallic and non-metallic (fibre reinforced composite) parts. The adhesive creates a smoother stress field than a bolted connection. In the latter, stress concentrations occur in the region of the bolt. However, since the failure of adhesively bonded joints can be very brittle and the behaviour after aging is relatively unknown, the use of adhesively bonded joints, especially for primary structures, is still very limited. Nevertheless, in recent years many projects and research have been done into adhesively bonded joints. The Qualify project (https://www.qualify-euproject.nl/) specifically looks at the bonded connection between a steel hull and a composite superstructure. In Saleh et al (2020) the water absorption and material properties after aging of a methyl acrylate based (MMA) adhesive are determined. Also the combined effect of water uptake and temperature is studied. Bulk adhesive specimens were placed for 14 weeks in a salt-spray (5% salinity) chamber at a 50% humidity at 35°C. The tensile strength at failure (as well as the modulus) decreased by about 20%. Next to the bulk material the effect of aging on mode I (salt-spraying) and mode II (immersed) fracture behaviour of the steel adhesive interface was also studied. No significant effect on the mode I values was found, however, for the mode II behaviour the effect is significant with a decrease in mode II fracture energy of nearly 60% after 5 days of exposure. The unaged samples showed cohesive failure, whereas the aged specimen showed adhesive failure.

It is known that the bond line thickness has an effect on the strength and failure characteristic of the joint. A lot of research has been done in the past on this effect of thickness. However, most of that research was done for automotive or aerospace applications, in which the bond lines are maximum 1 mm thick. For applications in maritime and offshore structures, much thicker bond lines are normally taken due to the geometrical variations in the joining parts. In the report of Saleh et. al. (2020) it was also shown that the thickness of the bond line has a clear effect on the shear strength of the joint. With a decrease in strength at increasing bond line thickness. Bond lines up to 13 mm are studied and a decrease in shear strength of about 20% were seen when increasing the bond line from 3 to 13 mm. A very large decrease of the failure strain was also found of more than a factor 2. A similar effect was seen in the work of Mestre Rodriquez (2018) and Mestre Rodriquez et. al. (2019). The authors studied double lap steel composite joints with either an epoxy (bond line 1,3,5,8, and 10 mm) or a urethane acrylate (bond line 1, 3, and 5 mm) adhesive. Both adhesives showed a clear decrease in shear strength of about 50% as well as a significant decrease in failure strain.

Since only limited experience is available on bonded connections, the Ramsses project (www.ramsses-project.eu) is of interest (Hagenbeek 2020). Within this EU project a demonstrator is designed and built to test to failure bonded connections between a composite hull and a composite deck. Kharghani and Soares (2018) looked into the strength of hybrid steel composite balcony overhangs for cruise ships. They tested and analysed a joint in which the composite panel is actually attached between two steel plates only by using the resin material (so no additional adhesive), Even though several drops in load occur already at an early stage due to probably internal debonding initiation, the ultimate strength of the joint is significant. Numerical modelling of the joint was however challenging, since the debonding was not predicted in the numerical analyses. Gaiotti et. al. (2018) did tests and analyses on a combined bolted/bonded connection between a steel deck and a composite side shell plating. Again failure takes place in stages, starting by localized failure probably due to defects or delaminations. Also they conclude that accurate analyses of the failure is challenging, if not impossible due to these local effects.

3.4 Effect of mechanical damage

Ship structures are often designed to serve for 20 to 25 years, whereas offshore structures are expected to operate for much longer period in some of the most harsh environments. This leads to inevitable mechanical damage to the structure, including dents, cracks and marine fouling.

3.4.1 Stable cracks

Research on the effect of stable cracks on the ultimate strength of ship structures is mainly focused on transverse and longitudinal directions. The studied parameters mainly include crack dimension, location, plate thickness and plate aspect ratio. FEA is the most adopted method for such analysis. Limited work is available on the ultimate strength of cracked offshore pipes subject to external pressure or bending moments (Cai et al., 2017). It needs to be noted that the crack initiation and propagation are outside the scope of the review in this section, as it is reported that buckling usually occurs prior to crack propagation for thin plates (Hu et al., 2018; Shi et al., 2019).

For small-scale structures, semi-circle cracks were modelled on a plate by Xia et al. (2018) using FEA, varying the length and location however without crack growth. The effect of initial imperfections (both geometric and residual stresses) and slenderness ratio were also included. Based on numerical results, it was revealed that cracks would change the effect of residual stress on the ultimate strength of the plate, depending on the crack's location and length. This led to cases where a higher ultimate strength was obtained compared to models without cracks. This was believed to be due to the breaking effect of the crack on the residual stress redistribution, which is highly dependent on the crack location, i.e., in compressive or tensile zone. The authors remarked the results may not be generalised. However, the methodology could be used to investigate other type of materials and/or structures. Feng et al. (2020b) combined idealized pitting with through-thickness crack damage on a plate in their FEA modelling. It was found that the influences of longitudinal crack and corrosion on the ultimate strength can be linearly superimposed. Welding-induce residual stresses were not considered in this study.

The ultimate strength of stiffened plates/panels with cracks under longitudinal compressive loading was studied by Yu et al. (2018) and Shi et al. (2019) using FEA. Experimental data were also provided by Shi et al. (2019) as validation. The ultimate strength was found to decrease with increase in crack size in center-cracked and edge-cracked models, which was manifested by the initial geometric imperfections. The effective cross section of the cracked stiffened plate plays a key role in the assessment of the residual ultimate strength. Based on the numerical results, an empirical formula as a function of crack length, orientation angle and

location, was proposed to predict the ultimate strength of cracked stiffened panels under longitudinal compressive loading (Yu et al., 2018).

In terms of large-scale structures, Hu et al. (2018) investigated the residual ultimate strength of large opening box girders with crack damage under individually or combined torsion and bending loads. A range of FEA were carried out varying the crack length, location, and orientation angle. Only the buckling mode geometric imperfections were included in the model. It was found that the transverse crack (length and location) had more detrimental effect on the ultimate torsional and bending strength compared to longitudinal cracks. Based on the individually loading cases, two of the most dangerous crack damage situations were adopted, leading to an interaction formula proposed for predicting the ultimate strength of large opening box girders with cracks under combined loads. The validity of this formula was verified by crack damage cases of varying crack length. However, it is not clear whether it is applicable to other types of hull/box girders.

Babazadeh and Khedmati (2018) presented a detailed review on the effects of different crack parameters such as crack length, crack location, crack orientation and gap size, plate thickness, aspect ratio, boundary conditions on the ultimate strength of ship hull elements introducing some existing research work on the cracked structural elements. Moreover, they suggested a new plastic collapse mechanism, i.e., buckling localization near a crack. A semi-analytical formulation was later derived to estimate post ultimate strength behavior of cracked plates (Babazadeh and Khedmati, 2019).

3.4.2 Other types of damage

Tekgoz et al. (2018) analyzed the effect of structural damage and associated neutral axis translation and rotation on the ultimate strength of a container ship hull subject to asymmetrical bending loading. The assessment was performed by FEA and formulations based on the Common Structural Rules. Sideshell damage had a significant effect on the ultimate sagging bending moment of the container ship section, with up to 20% strength reduction. The neutral axis rotation of the damage hull had more pronounced effect on the hogging than the sagging bending moment, when the damage was located on the side plating and stiffeners.

The aim of the study in Parunov et al. (2018) was to assess the ultimate strength of the double hull oil tanker damaged in collision. Collision damage was simplified as a 'rectangular box', assuming to start from the main deck downwards. Nonlinear FEA with explicit dynamic integration method implemented in LS-Dyna was adopted. This approach enabled for the first time a systematic investigation of the ultimate strength under combined horizontal and vertical bending moments. Ultimate strength interaction diagrams were developed allowing for rapid assessment of the damaged oil tanker. Collision damage was also studied by Ringsberg et al. (2018) using explicit FEA. Corrosion was also considered in terms of uniform reduction of thickness (CSR corrosion margin for oil tankers and 20% gross scantling for RoPax vessels), increased friction coefficient on corroded surfaces (from 0.3 to 0.5) and change of material properties (Young's modulus, static yield strength, ultimate tensile strength and hardening coefficient). Specifically, the material property change was based on the work by Garbatov et al. (2016). The ultimate strength of the struck ship was calculated using the Smith's method. It was found that the ultimate strength was largely dependent on the corrosion margin, material models, damage opening, damage location and shapes.

Regarding offshore structures, damage including gouges and notches on the ultimate strength of offshore pipelines were reviewed by Cai et al. (2017). The damage could be induced by contacting with sharp objects such as anchor and fishing board. It was reported that different shapes of the damage did not affect the ultimate strength greatly (Cai et al., 2017). Dents, a

form of plastic deformation, may trigger local buckling with the effect of plain dents (a dent with smooth curvature variation) being the main focus in the literature. The strength capacity of offshore pipelines under external pressure is critically dependent on the maximum ovalisation of the dent (Cai et al., 2017).

In addition, Zhang et al. (2019a) studied the collapse behavior of stiffened panels exposed to fire and calculated the residual ultimate strength applying thermal-elastic-plastic FE analyses with the temperature-depended material parameters for the stiffened panel under two different heating modes, namely stiffener heating and panel heating. It was found that the difference of the heating mode caused the difference of the collapse mode.

3.5 Maintenance and repair

Upon periodical ship survey a remedial action may be required for inspected damage. This repair strategy may involve coating, welding, crop and renew sections. For thickness wastage on metallic structures, there is a growing interest in researching composite patch repair, i.e., bonding a composite stack (often CFRP) on top of the damaged area. Quinn et al. (2019) studied how structural approval procedure works for marine structures made from polymer composites that would generally need to be SOLAS compliant. They also highlighted a case study on the corrosion repair of FPSO using the ColdShieldTM technology developed by Coldpad. Accelerated thermal and mechanical ageing tests suggest a 10-year design life for such repair and could be extended with appropriate inspection. The work was built on existing 'classical' bonded composite solutions from the European FP7 Co-Patch project to qualify and certify a new solution based on small-scale and full-scale testing and modelling. The advantage of such method includes the possibility of on-site repair (no dry-docking) and no hot work needed.

An alternative to composite patch repair is the use of composite stiffeners, the so-called Strengthening-by-Stiffening method. In Anyfantis (2019), a series of design assessment of shear panels repaired using this method were conducted numerically. The assessment was based on the elastic buckling under pure shear to determine the optimised configuration of composite stiffeners. The stiffeners act as means for strengthening the plating against buckling. It was concluded that the length and bending stiffness of the stiffeners had significant effect on the buckling strength, whereas the effect of orientation angle was minimum. An extension of this work to nonlinear buckling strength would be of interest for a more realistic structural condition.

Among various repair and/or retrofit methods for corroded offshore steel structures, underwater wet welding has been recognized as a cost-efficient technique. According to Chen et al., 2010, fillet weld joints made by underwater wet welding had higher ultimate strength than their counterparts made in air. The strength increase ranged from 7% to 41% depending on different base steels and the load directions to the weld line. The load-carrying capacity of corrosion-damaged offshore pipe piles repaired by underwater welded patch plates was investigated by (Chen et al., 2011). A weld model was proposed to simulate the strength and ductility of underwater wet fillet weld joints in a structural scale. Both global buckling strength and local weldment failure were predicted in this model. This study also proposed a repair method using underwater wet fillet weld joints by specifying when and how to consider the stiffness of weld joints in repairing corrosion-damaged offshore pipe piles under compression.

3.6 Life-cycle management

3.6.1 Hull-form structures

Life cycle management of hull form structural performances is often based on reliability analysis and probabilistic modelling of the material degradation (mainly corrosion). It enables the consideration of long-term service scenario into the design/optimization stage. It could also

lead to optimized repair strategy and potential service life extension. Work in this area ranges from structural components to hull girders.

Choung et al. (2019) quantified the structural availability of stiffener buckling strength. Structural availability is defined as the probability that a structural element under loads is fully functional at any specific time for a specific time interval. It has the potential to deal with the features of operation and the maintenance of structures, as well as structural integrity, in a quantitative manner. In the study the stiffener was located on the bottom plate of an AFRAMAX double-hull oil tanker. The structural degradation over time was modelled as a specific time function using statistical corrosion models in the literature. The structural availability decreased gradually over time with corrosion degradation. Using a numerical method such as a Monte Carlo simulation enabled the quantification of the time-dependent availability, providing the failure mode can be defined as a time function.

Van et al. (2018) analyzed the ultimate bending moment capacity of a capesize bulk carrier and a handymax bulk carrier under the influences of initial imperfections and corrosion wastage over time. The corrosion rate estimation model for bulk carriers was introduced according to the literature. Repair periods were calculated for each bulk carrier subject to different levels of corrosion and initial imperfections. It needs to be noted that this study was based on a deterministic approach. In comparison, Garbatov et al. (2018) developed a risk-based framework for a multipurpose ship based on ultimate strength assessment and life cycle cost (design, build and maintenance). Structural degradation over time was considered in terms of general corrosion using the exponential model developed by the authors in their previous research. The probability of progressive collapse of the ship hull was calculated using the first order reliability method. It was suggested that the developed framework could be used in the early stage of design with limited data, while allowing for a more economical design considering future maintenance plans. However, both the coating life and the transition time were fixed to be 5 and 7 years, respectively. The accurate prediction of these two values is critical to determine the onset and severity of corrosion. Similarly, in the study by Gong et al. (2019), a risk-based maintenance decision-making framework was proposed for ships to address the optimal drydocking inspection. The corrosion rate of plating and stiffeners followed a Weibull distribution with different mean and COV values at different structural locations. It was found that the cost of structural renewal had little contribution to the lifecycle cost regardless of the corrosion extent. With more accurate input of the maintenance cost, the model could be refined. Liu et al. (2019) presented a framework for a synthesized life-cycle risk analysis of an aged high-speed naval vessel's performance considering reliability, cost, and availability. This framework revealed the implications of structural repair decisions in risk management of ships. It enables decision makers to choose optimal repair option with respect to different service life extension needs.

Georgiadis and Samuelides (2019) applied Bayesian updating for a statistical corrosion model from the literature and subsequently assessed the ultimate strength of a VLCC hull girder using the Smith method. The assessment was based on data collected at specific time instances over the service life of 25 years. Uncertainties associated with material properties, corrosion rate and coating life were included. It was found that the ultimate strength was most sensitive to material's yield strength, indicating the importance of accurate material modelling. The method needs validation from real inspections and was suggested to be applied for FPSO units for less variations in environmental conditions. Improvements could be made in the theoretical model of corrosion wastage prediction accounting for the non-linearity of annual corrosion rate diminution over time, giving a more realistic perspective of the phenomenon. Woloszyk and Garbatov (2019) assessed the reliability of a tanker ship hull structure subjected to vertical bending

moment and corrosion degradation. The progressive collapse and ultimate load carrying capacity were estimated, based on experimentally tested scaled box-shaped-specimens. A sensitivity analysis concerning the stochastic variables, included in the ultimate limit state function, was performed aimed at identifying the partial safety factors.

Another aspect of life-cycle degradation is to consider multiple cycles of bending of the hull girder with magnitudes close to the ultimate strength. In other words, when a ship is subject to a series of extreme waves, each load may be below the ultimate strength of the structure. However, a combination of alternating load cycles may weaken the capacity (Li et al., 2019d). Unlike the ultimate strength analysis under monotonic load, the cyclic hardening and Bauschinger effects were included in FEA plate models (Li et al., 2019d) and hull girder models (Li et al., 2020) considering multiple load cycles. It should be noted that the inertia effect was eliminated and hence the analysis was static even though a dynamic solver was used. Significant reduction (~40%) in the residual ultimate strength of the hull girder was found with an increasing number of loading cycles. However, this reduction will eventually stop when the cycle number exceeds a certain value.

In Li et al. (2019e), a structural reliability analysis model based on a Bayesian belief network (BBN) is proposed for the hull girder collapse risk after accidents. BBN is used to represent the random states of variable risk events after accidents, and SRA is used to evaluate the failure probability of hull girders for each possible accident condition.

In order to asses for a rapid hull girder strength calculations of double hull oil tankers after collisions, Faisal et al. (2016) and Youssef at al. (2017) developed a method to predict the hull girder residual strength of double-hull oil tankers by considering probabilistic collision damage scenarios, based on the historical ship collision database, studying four different as-built double-hull oil tankers to formulate the collision damage reduction ratio of the vertical hull girder moment of inertia and ultimate bending moment, identified in the form of diagrams.

3.6.2 Platforms and other offshore structures

The life cycle prognosis of offshore structures is based on linking between design, and inspection, monitoring, maintenance and repair (IMMR) (Moan, 2018). Based on risk and reliability design methods, experience and information from operation and inspection of individual structure could contribute to risk control and the IMMR plan throughout the structure's life cycle (Moan, 2018).

Marine fouling poses issues to offshore platforms by increasing drag and structural weight. It can also accelerate the corrosion process and threaten the platform's structural integrity. Mohd et al. (2019) investigated the effect of time-dependent fouling and corrosion on a fixed platform in Malaysian waters. The ultimate bending capacity was assessed using pushover analysis based on an FEA model of the platform. Corrosion was simulated as a uniform thickness reduction using the model developed by Paik et al. (2003b), which shows a linear relationship between corrosion depth and time from 5 years onwards. The marine fouling over time was modelled in terms of thickness increase for different water depths. It was found that the marine fouling significantly increased the load on the structures, leading to 38% reduction in the reserve strength ratio (RSR) after 5 years in service. The corrosion condition will further reduce the RSR by 7% annually and shorten the platforms life from 29 years to 50 years.

A series of sensitivity analyses was conducted by Zeinoddini et al. (2017), whereby the marine fouling was also one of the variables under investigation. The study focused on six aged platforms (40 years old) operating in the Persian Gulf. The ultimate strength and the RSR with respect to the 100-year environmental loading were calculated from push-over analysis. Spe-

cifically, the environmental load was determined based on API RP 2A-2.3. Cracks and perforated plates were also included in the modelling. However, details regarding these defects were not provided. The variable marine fouling was assumed to follow a lognormal distribution, with a mean of 75 mm, a median of 50 mm and the coefficient of variance of 0.5. It was found that both the ultimate strength and RSR were more sensitive to variables that related to the load, including the marine fouling, compared to the strength related variables. Tornado diagrams were provided to quantify the variable sensitives.

3.7 Summary

This section indicates that recent research on the lifecycle and degradation effects is mainly focused on carbon steel structural components and ship/hull form structures. Nonlinear FEA and the Smith's method are the most used approaches for assessing the ultimate strength. Many of the studies only considered the geometric imperfections induced by welding, as it has been suggested to be more influential to the strength capacity compared to the welding-induced residual stresses. However, there is little focus on the effect of welding defects, which could be due to their greater importance in fatigue/fracture compared to the buckling behavior.

Corrosion, together with other types of damage and material degradation, are age old issues considered in ultimate strength analysis for ships; and are still actively investigated. Methodologies of how to incorporate such damage to a structure model is relatively well-established. The biggest challenge is how to better predict the degradation and the associated uncertainties throughout the structure's service life. There is an increasing interest in adding corrosion fundamentals in structural analysis. It is also essential to have new database of thickness measurements from ship surveys in the open literature to allow advanced data analytics such as machine learning to facilitate a better damage prognosis. This will have profound impact on developing optimized design/maintenance and full digital twin models. The recognition and incorporation of uncertainties has started early in offshore industry from design stage to maintenance and repair. This is realized by adoption of risk and reliability methods to make rational decisions. Over the last three years, continuous advancement in researching the effect life cycle and degradation can be seen, focusing on corrosion, marine fouling and the capability of updating prediction models based on in-service data collection. Future research is needed to better predict/quantify the material degradation processes, especially when new materials are increasingly used for offshore construction; and to better incorporate the human element (from fabrication to operation) into the analysis.

4. SHIPS

Chapter 4 focuses on the ultimate strength of ships that are not fixed in place but are meant to transit between ports. The ultimate strength of a ship at the system level is important to safety considerations of the vessel in that collapse may lead to sinking or capsize. The ultimate strength of the ship structural elements are often precursors to a broader structural system failure that may result in loss of the ship.

This chapter begins with examination of load types such as wave, collision, and explosive in 4.1. Then, strength of structural elements is addressed in 4.2 such as stiffened panels and grillages. After that, the section 4.3 considers structural systems such as hull girder strength. Finally, recent advancements in rules and guidelines that govern design and analysis for ultimate strength are presented in 4.4.

4.1 Loads

In this section, the loads related to the collapse behaviors of ship structures and their structural components under ultimate conditions are discussed. Moreover, they are classified into the

following items: still water and wave-induced loads, ice load, collision and grounding loads, fatigue and corrosion, explosion loads and loads of climate change and safe design.

4.1.1 Wave-induced loads

Recently, the trend for further development and enhancement of numerical methods continued for predicting accurate wave loads. The three-dimensional time-domain nonlinear hydro elastic approaches are used to estimate the ship's wave load, which is mainly utilized to calculate the ship's ultimate wave bending and torsional moments. For instance, Chen et al. (2019d) used the Rankine source method to analyze the nonlinear hydro elastic response of a container ship in regular oblique waves. Moreover, Jiao et al. (2019) developed a three-dimensional time-domain nonlinear hydro elasticity theory where the nonlinearities are arisen from incident wave forces, hydrostatic restoring forces, and slamming loads.

New research focuses on the challenging CFD-FEA coupling method by comparing the predictions with strip method, three-dimensional panel method, and towing tank test. For example, Takami et al. (2018) developed a numerical simulation method for predicting global and local hydro elastic response of a ship based on CFD and FEA coupling. Takami et al. (2020) further used the first-order reliability method for coupled CFD and FEA, by which the most probable wave episodes leading to given VBMs are identified under a given short-term sea state.

4.1.2 Ice loads

Due to global warming, the numerical simulation methods have been increasingly developed to evaluate ship performance on ice and under ice load in recent years. Ding et al. (2019b) calculated the maximum yield stress and buckling factor by applying ice load to the structure model and compared them with the allowable value according to IACS PC rule. The bow and mid-ship of a polar ship was used in the case study. Zhou et al. (2018) presented a new tool to simulate ice-structure interaction in six degrees-of-freedom in time domain. The horizontal motion of ice rubble and distribution of ice rubble at each panel are calculated to derive the ice accumulation force. Ice bending and crushing failures are considered for icebreaking.

4.1.3 Collision and grounding loads

Loads on ship damaged by accidents are still areas of concern in ship design and operation. In general, damages due to collision and grounding are most frequently observed; therefore, various research studies focused on these types of damage scenarios. To give an example, Tabri et al. (2020) presented a method for the assessment of residual strength of a ship hull damaged in a grounding accident. The strength assessment is based on a coupled beam method that allows time-efficient analysis. As a case study the method was applied to a double hull tanker. In addition, Zhang et al. (2019b) used the analytical approach and finite element analyses to study model-scale and full-scale collision tests in detail. An analytical method for ship collision damage assessments was validated with numerous experiments and one full-scale collision accident data.

4.1.4 Fatigue and Corrosion

The service life of the ship is related to the fatigue and corrosion design. It mostly requires the assessment of a lifetime vertical bending moment histogram for a ship. The lifetime bending moment histogram summarizes the ranges of bending moment magnitudes and their corresponding number of cycles expected during the ship’s service life. These bending moments include those due to changes in wave height and slam induced whipping. The assessment of the loading sequence on fatigue crack growth of cracked details is essential when the ship hull is subjected to random wave-induced loading during the service time (Huang et al., 2018). Recently, Tekgoz et al. (2020) provided an overview of the ultimate strength assessment of

ageing and damaged ship structures in the entire ship hull structures subjected to corrosion degradation, fatigue cracking, and mechanical damage caused by accidental loading or impact.

4.1.5 Explosion loads

The warship deformation mechanism of underwater explosion is very important for the assessment of warship survivability. Underwater explosion and its highly nonlinear effect on nearby structures are more complicated. Fluid-structure coupling analysis is generally used, and transient fluid-structure interaction is always a challenge in ship structure analysis. To address this challenge, Kong et al. (2021) studied the long-distance underwater explosion, the dynamic buckling of the hull's main deck grillage completely collapsed. This dynamic buckling is mainly due to the dynamic moment of the hull when the hull moves suddenly under the action of explosive impact load. Moreover, Gan et al. (2019) conducted the experiment in a water pool of underwater explosion, the numerical calculation is carried out through the coupled Eulerian-Lagrangian algorithm, and plastic hinge of the hull girder under explosion bubble collapse are studied.

4.1.6 Loads of climate change and safe design

The Fifth Assessment Report of the Intergovernmental Panel on Climate Change (IPCC) uses four scenarios for future greenhouse gas concentrations in the atmosphere called Representative Concentration Pathways (RCP). The predicted changes in the ocean wave climate and its impact on ship safety design with particular attention to related uncertainties is an important issue. Bitner-Gregersen et al. (2018) addressed projected changes of wave climate in the North Atlantic and their impact on the safe design of ships, with a particular focus given on associated uncertainties. The paper discussed how structural design of ships can be upgraded to account for climate change and rogue waves without necessarily leading to significant economic consequences. The past and projected future wave climates of selected locations in the North Atlantic and North Norwegian Sea were considered by Guo et al. (2019). The hull girder ultimate strength governs sagging and hogging failures, which is one of the most critical failure modes for a ship hull, and a linear model for bending moment in extreme weather with a nonlinear correction factor was adopted in the analysis.

4.2 Structural Elements

A ship structure mainly consists of many monolithic and stiffened panels. Accordingly, structural assessment of plates, stiffened panels/grillages, column, joints (e.g., weld lines) is a great importance for ultimate strength of ships. Therefore, this section discusses the recent research and developments on the ultimate strength of the unstiffened and stiffened panels as structural elements in ship structures.

4.2.1 Stiffened panels

Many researchers have derived the simple formulas to estimate the ultimate strength of stiffened panels under in-plane compression, most of which were formulated as a function of a plate slenderness ratio and column (stiffener) slenderness ratio.

Ao et al. (2019) investigated the ultimate strength of stiffened panels under longitudinal thrust. A few existing empirical formulas to express the ultimate strength were selected and their validities were investigated comparing with FE results. The formula proposed by Zhang et al. (2009) was focused as the most appropriate one which is an equation of two dominant parameters, namely the plate slenderness ratio and the column slenderness ratio and was modified adjusting the coefficients. The error band of the modified formula is narrowed from ±15% to ±5%. The original equation from Zhang, et al (2009) is:

$$\frac{\sigma_u}{\sigma_Y} = \frac{1}{\beta^{\alpha}} \frac{1}{\sqrt{1+\lambda^{\eta}}}, \qquad \alpha = 0.28, \qquad \eta = 3.2$$

where λ is the column slenderness of stiffened panel, and β is the panel slenderness. In the modified equation from Ao, et al. (2019), α and η are given as:

$$\frac{\sigma_u}{\sigma_Y} = \frac{1}{\beta^{\alpha}} \frac{1}{\sqrt{1+\lambda^{\eta}}}$$

$$\alpha = 0.3014 e^{-\left(\frac{\sigma_Y - 619.7}{471.9}\right)^2} - \left(0.03604\left(\frac{b}{h_w}\right)^2 - 0.2976\left(\frac{b}{h_w}\right) + 0.5208\right)$$

$$\eta = \left(0.2539\left(\frac{b}{h_w}\right)^2 + 0.005958\left(\frac{b}{h_w}\right) + 2.7\right) e^{-\left(\frac{\sigma_Y - 605}{445}\right)^2}$$

As depicted in Fig. 12, Xu et al. (2018a) performed FEM analyses for the stiffened panel subjected to in-plane compression and lateral pressure. It was clarified that the lateral pressure increases the in-plane ultimate strength in some cases with small stiffeners although the pressure decreases the strength in most cases. Based on the FEM results, the empirical expressions were derived for the ultimate strength assessment using the plate and column slenderness ratios and the lateral pressure expressed by water head. Through the comparison between the FEM and previous test results and other formulas, it was confirmed that the developed formulae are useful for predicting the load carry capacity of stiffened panels.

Moreover, Ozdemir et al. (2018) proposed a new approximate method based on analytical formulas to estimate the ultimate strength of stiffened panels. Analytical solutions based on Elastic Large Deflection Analysis (ELDA) were derived assuming deflection functions to express both the local and overall buckling shapes. The ultimate strength was estimated as initial yield strength using the stress calculated by the analytical solutions. The estimations and the nonlinear FEA results were compared, and a very good agreement was confirmed for all collapse scenarios investigated.

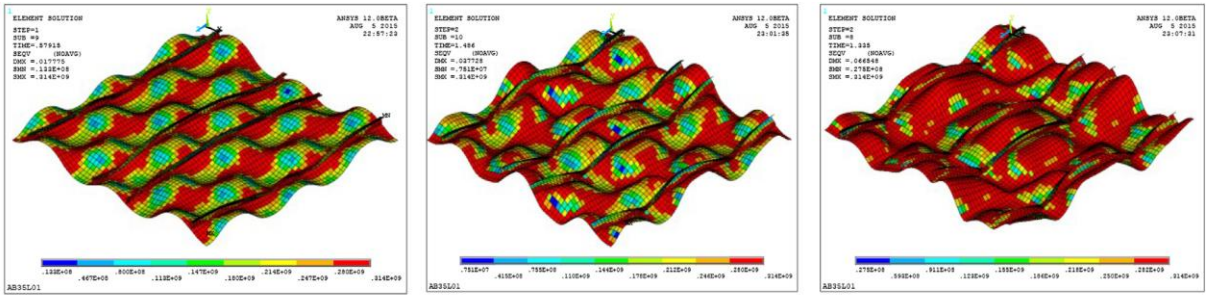

(a) q=0 (b) q=0.1 MPa (c) q=0.2 MPa

Figure 12: Collapse shapes of the stiffened panels with different lateral pressure (plate: 2550×850×33mm; Angle stiffener: 150×90×9/12mm) (Xu et al., 2018a).

Furthermore, Komoriyama et al. (2018a) proposed a new method to estimate the ultimate strength of stiffened panels under biaxial compression mainly in transverse direction. Since the stiffened panels collapse with the local panel buckling mode in this case, the estimation method was composed of the formula for the unstiffened panel under transverse compression and the effects of biaxial compression, stiffeners and von Mises yield condition were added. The method was compared with an existing method and formulae used in the CSR-OT, CSR-BC,

and CSR-H, it was confirmed that the proposed formula has sufficient accuracy and high availability.

4.2.2 Curved panels

Curved panels and curved stiffened panels are applied to a bilge corner in ship structures. Although it was found that the curvature of the curved panel has the effect to enhance the buckling strength, the ultimate strength and collapse behavior of these curved panels are not clarified compared with flat panels and flat stiffened panels.

Park et al. (2018) carried out nonlinear FE analyses for cylindrically curved plates under axial compression and lateral pressure to clarify and examine the fundamental behavior. The effects of curvature, initial deflection, slenderness and aspect ratio and boundary conditions were discussed. The panel slenderness ratio was modified so that the effect of the curvature could be considered and a formula to estimate the ultimate strength was proposed using the slenderness ratio. Moreover, a similar investigation for stiffened curved plates was also conducted as shown in Fig. 13.

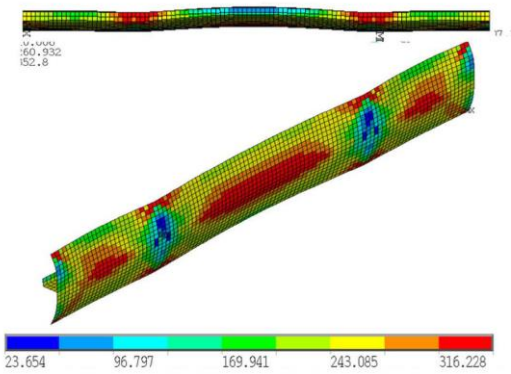

Figure 13: Collapse mode and distribution of equivalent stress of curved stiffened panels under combined axial compression and lateral pressure (Park et al., 2019).

Cui and Wang (2019b) assumed that a bilge stiffened panel in ship hull was subjected axial compression due to vertical bending of the hull and lateral pressure and performed nonlinear FE analyses for the curved stiffened panels with various geometric parameters and structural scantlings. Closed-form ultimate strength prediction formulas were proposed for curved stiffened plates applying the panel slenderness ratio considering the effect the curvature and the column slenderness ratio. From the comparison with the FE results, it was confirmed that the proposed formula has sufficient accuracy.

Ljubinkovic et al. (2020) conducted collapse tests of curved stiffened steel panels under axial compression and simulated the collapse behavior of the test models by nonlinear FE analysis. Moreover, they investigated the post-buckling behavior and ultimate strength of simply supported cylindrically curved steel panels subjected to a pure shear load through nonlinear FE analyses varying the geometrical parameters, such as curvature and aspect ratio (Ljubinkovic et al., 2019) and provided empirical formulas for the ultimate shear reduction factor.

Manco et al. (2018) analysed curved panels under uniaxial compression and developed a semi-analytical model for the post-buckling behavior based on ELDA. The results calculated by the proposed model were in good agreement with the FEA results. Additionally, the closed form formula for the prediction was also derived by reduction of deflection coefficients.

4.2.3 Complicated loading

Panel and stiffened panel as structural components of a ship structure are subjected to not only static and monotonic loading but also complicated loading such as dynamic or cyclic. For example, Yang et al. (2018) performed nonlinear and dynamic FE analyses for ship bottom stiffened panels under uniaxial compression and investigated the dynamic ultimate strength. The influences of the magnitude of initial deflection, loading speed (strain rate), lateral pressure and boundary conditions of the edges of the FE model on the dynamic ultimate strength of the stiffened panels were discussed. In the results, it was clarified that the effect of the lateral pressure on the dynamic ultimate strength is small although the other terms do affect the strength.

The dynamic ultimate strength of rectangular simply supported panels under in-plane half-sinusoidal impact loading was investigated by Yang et al., 2019. A simple and reasonably accurate empirical formula was derived. The ultimate strength by the proposed formula was compared with the dynamic FE results of three existing ship hull plates and the applicability of the proposed formula was verified.

Komoriyama et al. (2018b) carried out the cyclic compression loading experiments with two stiffened panel specimens as illustrated in Fig. 14. The first specimen was subjected to in-plane and cyclic compressive load under displacement control with increase of its average level. The second specimen was subjected to the cyclic load limited to a level lower than the calculated ultimate strength. It was found that the cyclic compressive loading increased the accumulated buckling deformation and decreased the ultimate strength.

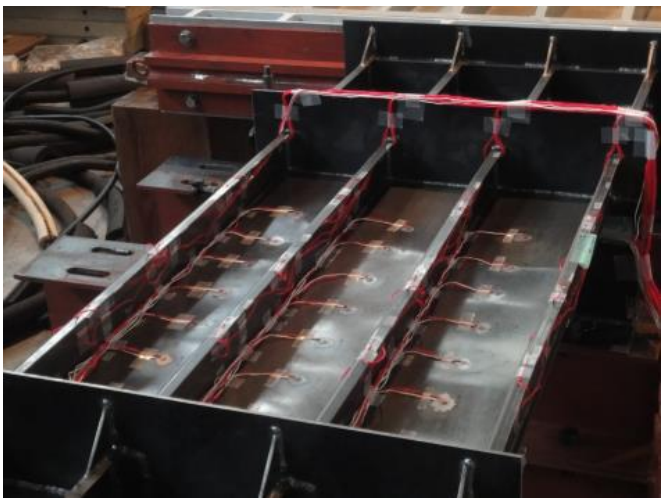

Figure 14: Collapse test of stiffened panel under cyclic compressive loading (Komoriyama et al., 2018b).

4.2.4 Validation of estimation formula

As mentioned above, many new formulas were developed to estimate the ultimate strength of the structural elements. Although the validity of these formulas was discussed through the comparison with nonlinear FE results, the comparison between the formulas was hardly performed.

Kim et al. (2018) reviewed the research on the estimation of the ultimate strength of stiffened panels under longitudinal compression and introduced various empirical formulas using plate slenderness ratio and column (stiffener) slenderness ratio. The estimated ultimate strengths by the design formulas such as Euler, Johnson-Ostenfeld and Perry-Robertson, the introduced empirical formulas, and the analytical method software, ALPS/ULSAP (2019) were compared

with the nonlinear FE results for total of 10,500 cases of stiffened panels. The empirical formulas provide more proper ultimate strength than the design formulas, but the ALPS/ULSAP provides most accurate ultimate strength.

Note that the estimation formulas introduced in the reviewed papers were not validated for the structural elements with common dimensions and the applicability cannot be compared. It is recommended that these are investigated through a benchmark study.

4.3 Structural Systems

In this section, hull girder, intact and damaged residual strength, superstructure inclusion, and their effect on ultimate strength of ship is discussed to review the recent advances in the structural systems of ships.

4.3.1 Intact hull girder

In the past decades, well-assessed analytical and numerical methods have been developed to estimate the hull girder ultimate strength. Discrepancies between results are often found. Clear guidelines on governing factors are of key importance for reliable estimation of ultimate strength.

Van and Yang (2017) and Van et al. (2018) recently conducted a historical review associated with the ultimate hull girder strength, then compared and discussed results of thirteen traditional methods for predicting the ultimate bending moment of ship hull girders, considering a set of six different cross sections. It was found that Viner's method, Qi and Cui's method, and IACS-CSR method underestimate the ultimate hull girder strength in several cases, while Mansour and Faulkner's method, Faulkner and Sadden's method, Valsgaard and Steen's method, and stress distribution method overestimate the ultimate bending moments of several hull girders. The authors also concluded that it is of key importance to improve the methods to consider the initial geometric imperfections and residual stresses, and the age-related damage (such as corrosion wastage, fatigue cracks, and local dents).

Xu et al. (2017) discussed a reliable and suitable FE modelling strategy within the explicit dynamic method, which could keep the balance of the acceptable accurate results and computation resources. Several influential factors on the collapse behaviors of hull girder were discussed including boundary conditions, Refinement of finite element model, element types, loading methods and loading time. The results of a Suezmax oil tanker and Reckling models are compared with that by the other analytical methods or experimental results. The main findings of this relevant study were:

- FE models adopting beam elements cannot consider the initial sideways deflections and tripping buckling for stiffeners, thus giving excessive torsional stiffness, which may overestimate the ultimate strength of hull girder. Hence, it is recommended to adopt the shell element for both plate and stiffener.
- The imposed moment method at the end of hull girder might overestimate the ultimate longitudinal strength. The imposed rotation angle method is more similar with the actual loading process of progressive collapse of the vessel voyaging under severe sea condition. When the loading time assessed by the actual period of wave is used in the explicit dynamic analysis, the solution time might be very long; and a too short loading time may lead to overestimating the result due to inertia effect. A proper loading time is advised as 0.25 s for the full-scale hull girder.

Zhang et al. (2017) proposed an analytical model to estimate the longitudinal strength of ship hulls in composite materials under buckling, material failure and ultimate collapse based on the ultimate strain of fiber reinforced plates and stiffeners, with a simplified analytical method.

Shi et al. (2019b) compared the rule requirements of ultimate strength in CSR-H and CSR-OT/CSR-BC based on five typical Bulk Carriers and four typical Oil Tankers. The hull girder ultimate strength is mainly analyzed by Smith's method in rule requirements due to fast and stable calculation of results, although nonlinear finite element method was also adopted to explain the critical influence factors of structural elements. The actual ship evaluation results can be used to inform the new CSR-H ship design.

4.3.2 Superstructure inclusion

Shi and Gao (2019a) proposed a simplified modelling method of whole ship structures to calculate the hull girder ultimate strength by nonlinear FE analysis, analyzing in detail the variation characteristics of superstructure's effectiveness from elastic state to limit state for a cruise ship. Owing to non-continuous structures, such as window openings and side shell recess above lifesaving deck, effectiveness of the superstructure on longitudinal strength of cruise ships is difficult to determine. The conclusions obtained in this paper provided a reference for assessment of hull girder ultimate strength in cruise ship design.

4.3.3 Load combination

Research on the effects of combined loading on ultimate strength of hull girders have mainly covered two topics in the period covered by the present report. Namely the effect of dynamic response of hull girder (i.e., whipping) combined vertical and horizontal bending moment, torsional moment, and combination of bending and torsion.

Ultra large container ships feature large deck openings causing low torsional rigidity. In rough sea, when the ship sails at an oblique heading, the horizontal and torsional moments may lead to significant stresses, which combine to axial stresses when the vertical bending moment is included. In such cases, hull girder ultimate strength assessment of container ships under load combinations is necessary in the design stage. Bending torsion interaction on ultra large container ships was debated by Cui et al. (2019c). Wang et al. (2018a) conducted a series of nonlinear finite element analyses aimed at proposing a formulation to assess the ultimate strength capacity of the hull girder vertical moment, torsional moment and horizontal bending moment. The same authors (Wang et al., 2019a) proposed an experimental setup, of a scaled model, for the experimental evaluation of hull girder ultimate strength of large container ships under combined bending/torsional moments, based on the outcome of nonlinear finite element analysis.

Takami and Ijima (2019) developed and validated a numerical method based on a two-way coupled computational fluid dynamics and finite-element analysis. Hence, an investigation was made into the effect of the hydro-elastic component in the double bottom moment on the total DBM and the hull girder ultimate strength. It was found that the wave-induced and hydro-elastic components respective proportions are 11% and 7% of the total DBM, and the DBM component reduces the ultimate strength by about 11%. Similarly, Jiao et al. (2019) developed a three-dimensional time-domain nonlinear hydroelasticity theory, where the included nonlinearities are those arising from incident wave force, hydrostatic restoring force and slamming loads. The hull girder structure was simplified as a slender Timoshenko beam, fully coupled with the hydrodynamic model in a time domain. The hull girder ultimate strength is assessed by both the improved rule approach and direct calculation.

Corak et al. (2018) studied the ultimate vertical bending moment capacity of hull girder of container ships with respect to the stochastic modelling of the loads, consisting of static still-water bending moments (SWBMs), low-frequency rigid body vertical wave bending moments and high-frequency whipping bending moments. Such study may be useful for classification societies in further development of recently introduced IACS Unified Requirements for longitudinal strength of container ships.

4.3.4 Multi-hull

Xu et al. (2019) presented an experiment on the ultimate strength of an inland catamaran subjected to a vertical bending moment, comparing the result with a finite element model. A large-scale specimen was designed employing the scaling laws and linear finite element static analysis. During the experiment, the load-displacement and strain data, overall and local structural collapse are recorded. Good agreement was found between experimental results and numerical predictions and conclusions on the improvement of the ship ultimate longitudinal strength was also presented.

Liu et al. (2018) presented an experiment aimed at examining the ultimate strength of a one-eighth scaled SWATH (Small Waterplane Area Twin Hull) ship model subjected to transverse loads. The transverse ultimate strength was found critical due to large stress concentrations in the narrow struts and haunches. The ultimate strength of the actual SWATH ship was evaluated according to scaling laws, and the ship safety margin analyzed.

4.3.5 Progression sequence of failure

For a long time, ultimate strength of ship hull girder has been considered under monotonically increasing bending moment. Under extreme ocean wave conditions, the hull girder is more likely to withstand extreme cyclic-bending moments under which the ultimate bearing capacity of the hull girder may be dominated by cyclic buckling failure, extreme low-cycle fatigue failure or the coupling of the two. In the study conducted by Cui and Yang (2018a), the ultimate strength and failure characteristics of five steel box girder models were studied under two different kinds of cyclic-bending moments (repeated sagging and alternating sagging/hogging). The two box girder models subjected to alternate sagging/hogging bending moments fractured apparently due to the extremely low-cycle fatigue. The rest of the three models exposed to cyclic sagging bending moments collapsed by cyclic buckling accompanied by accumulated plastic deformation. The experiment shows that the extreme cyclic-bending moments will significantly reduce the ultimate bearing capacity and fatigue limit of ship girder, and lead to disaster. Along with the increasing of loading cycles, the ultimate bending moment strength keeps decreasing. To assess the actual ultimate capacity, the complex in-service history of the hull structures must be considered, including cyclic loading, and unloading. The same authors (Cui and Yang 2018b) also used these experiments to verify a numerical model based on the traditional Smith's method, by introducing the cyclic stress-strain curves of basic structural elements to a simplified calculation program.

Li and Benson (2019c) reevaluated the use of shakedown limit state in the assessment of longitudinal strength of ship hull girders, which was originally proposed by Jones (1975). Six cyclic finite element analyses were conducted, and an energy-based limit state characterization proposed. Authors concluded that the future development of structural assessment of ship hull girders under longitudinal bending can be placed on assessing the overall behavior and accumulative loss of resistance capacity during a given loading scenario. Also, a systematic investigation of the hull girder and structural components under large loading and unloading is needed. In addition, Yamada (2019) studied the dynamic collapse mechanism of hull girder of container ships in hogging with nonlinear dynamic FEM models, finding that ultimate strength as well as collapse mode is significantly dependent on load time duration of hogging moment.

4.4 Rules and guidelines

This section focuses on current practice specific to ships, recent developments, rules and regulations posed by IMO, IACS, Class, National standards, safety factors, and limit state definition for ships' ultimate strength.

4.4.1 General

Design of ships has been under continuous development in the last decades to be fit for the present demands such as increased size and cargo capacity, specialized vessel types for different purposes, etc. In the shipyard industry, the focus is on weight optimization to save steel and to be more environment friendly. This requires that the rules are applicable on many different designs with respect to different structural arrangements, steel qualities such as high tensile steel, loading conditions, etc. The application of direct calculation approach using finite element analysis, has also gained increasing attention which can be used for special cases that is not covered fully by explicit design rules.

Rules and guidelines such as classification rules provide the framework to achieve a safety level in the design and construction of ships. A particular aspect of these rules is that they address the required level of safety by defining a limit state. This limit state contains definition of both resistance of the structure (capacity) and loads (demand) which is usually a predicted extreme load case. Recently, the procedures for dimensioning the hull structure are changing due to the modern computers that are used in automatic routines for scantling calculation based on the classification rules. The current industry practice for preliminary hull structural design is illustrated in Fig 15. In the design of ships, the resistance of the structure is checked on different levels. Acceptable safety levels are typically achieved by checking the ship structure on two levels:

- Ultimate strength of the hull girder
- Local buckling strength for individual members

The ultimate hull girder strength check ensures that the global strength of the ship is strong enough to sustain the external loads without a total collapse of the ship, and this check gives an indication on the corresponding safety margins. The local buckling check ensures that local elements are strong enough to prevent local damages or progressive collapse of larger structural parts.

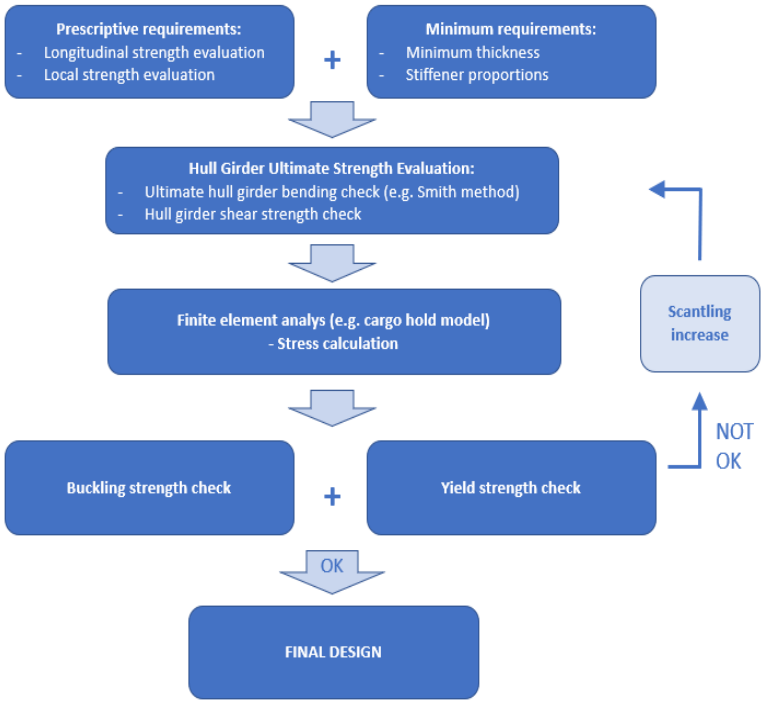

Figure 15: Illustration of the current industry practice for structural design.

4.4.2 Ultimate hull girder strength check

The ultimate hull girder capacity under longitudinal bending is one of the most essential strength measures for a ship. This measure is traditionally referred to as the ultimate hull girder strength of the ship which is a measure of the hull capacity under longitudinal bending conditions. In the previous ISSC 2018 III.1 report (Czujko, et al., 2018), there was a lot of focus on the ultimate hull girder strength check, and only the essential aspects of this strength check are presented here for the completeness of the report.

For a ship structure, the global strength with respect to hull girder bending is typically checked using a Smith approach (Smith 1977) which is a method where a hull section is subdivided into several individual load carrying structural members (e.g., stiffened plates, girders). The total hull girder strength is found in an incremental procedure by increasing the external loads until the maximum point is reached. In this approach, it is assumed that each individual member will be subjected to strains that increase linearly with the distance from the neutral axis by assuming that plane sections remain plane. The reserve strength of a damage ship hull can also be validated using the Smith approach. For such cases, the reduced hull girder strength can be estimated conservatively by removing individual members that are damaged. This will give an indication about the safety margins against total collapse of the vessel. More details on the ultimate hull girder strength check can be found in the ISSC 2018 III.1 report (Czujko, et al., 2018).

4.4.3 Local buckling check

For ship structures, local buckling checks are performed for stiffened panels, pillars etc. for many different load combinations of in-plane loads, bending moments, and lateral pressure. Typically, loads on local level are computed from linear finite element stress analysis (i.e., direct strength analysis) of a larger structural part (e.g., cargo hold model) or by loads from prescriptive requirements.

There exist many methods for local buckling check of strength members in ship structures, dependent on the type of vessel, structural element, etc., and each class society has their own rule sets for strength calculations. In IACS Unified Requirements URS-11 (IACS 2015a) there is a buckling procedure for non-CSR vessels, but this set of buckling assessment is based on a rather old buckling philosophy where local elastic plate buckling is not accepted. In addition, most of the class societies has reservations in place to use their own buckling assessment requirements.

More recently, the buckling procedure in Common Structural Rules (CSR) for Bulk Carriers and Oil Tankers (IACS 2018) was developed which is a buckling method based on ultimate strength principles where elastic plate buckling is accepted. This method is widely accepted by most of the Class Societies. Further, the same buckling procedure was adopted by the IACS Unified Requirements for containers vessels URS-S11A (IACS 2015b) which was established after some major structural failures of large containerships in recent years.

4.4.4 Recent development for IACS for local buckling check

In the last decades, there has been a focus in IACS to harmonize the buckling methods, and one first step was the harmonization of Common Structural Rules for Bulk Carriers and Oil Tankers (IACS 2018). As a next step, there is an ongoing work to harmonize all the different IACS Resolutions on ultimate strength calculations to accommodate comments from the industry that there are different buckling methodologies in CSR, UR S11, S11A, S21, S21A and S17 (IACS 2019, 2015a-d, 2017). For this work, IACS has established a project team with expert members from different class societies.

The harmonization of the buckling methodology will provide consistency among all the documents on buckling and simplify the design process. The goal is to have a URS buckling methodology without reservations from most of the class societies. This will be relevant for all ship types and all the class societies that follow the buckling philosophy in IACS.

In the harmonization of the buckling methodology, the procedure from CSR buckling (IACS 2018) will be used with some modifications and improvements for some special cases where unphysical behavior in the formulations has been observed. Feedbacks from shipyards, designers and class societies indicate that the present buckling methodology may give inaccurate results for plates with long/slender stiffeners or high stiffeners. Consequently, the buckling methodology will be improved for global elastic buckling and torsional buckling capacity. In addition, the methodology will also be improved for U-type stiffeners fitted on hatch covers considering feedback from designers, hatch cover makers, and class societies. In summary, the ongoing work is focusing on improvements of buckling formulations for:

- Global elastic buckling (i.e., out-of-plane buckling of a stiffened panel)
- Torsional buckling capacity (i.e., sideways tripping of stiffeners)
- U-type stiffeners fitted on hatch covers (i.e., stiffeners with a closed profile)

For the rule improvement regarding the formulas for global elastic buckling, it is proposed to use orthotropic plate theory to replace the original beam theory. In the original formulas with beam theory, global elastic buckling is accounted for by transforming all in-plane loads combinations (i.e., bi-axial and shear loads) into an equivalent lateral pressure. However, comparisons with finite element analysis and PULS (DNVGL 2018) showed that this was inaccurate for combined in-plane loads, and especially for transverse loads. Thus, it was decided to use orthotropic plate theory to compute the global elastic buckling load which is more like the philosophy in PULS for global elastic buckling.

To validate the improvements for the buckling formulation, a variety of stiffened plates and load combinations have been analyzed. For plates with dominant axial loads in the stiffener direction, the methodology in CSR (IACS 2018) gives almost the same results as for the improved formulation since the beam theory is relatively accurate for pure axial loads to represent global buckling of a stiffened panel. However, for plates with combined loads or dominant transverse loads normal to the stiffeners, the beam theory in the CSR (IACS 2018) is somewhat inaccurate.

Typical results are shown in Fig. 16 for plates with slender/long stiffeners subjected to transverse loads. These results present a comparison between results for CSR (IACS 2018) and the updated rules (IACS 2021). For these plates, the effect on the ultimate strength by varying the plate thickness and the stiffener spacing is investigated. A detailed description of the plate dimension and load combinations for each case is given in the technical background for CSR (IACS 2021). Examples on actual plates with slender/long stiffeners subjected to transverse loads can be side plates in LPG/LNG carriers or bulk carriers, vertically stiffened bulkheads in oil tanker, etc.

The results in Fig. 16 demonstrates that the trend on the buckling utilisation is different for CSR (IACS 2018) where the utilisation is increasing for increasing thickness, while the opposite is the case for PULS, FEM and CSR (IACS 2021). The same is found for increasing stiffener spacings, where the utilisation for CSR (IACS 2018) was decreased for increased stiffener spacing, while the opposite for the three other methods. For the FEM results, fully nonlinear analysis is performed, but the overall global elastic buckling load is computed using orthotropic shell elements which is taken as an upper limit of the plate capacity. This prevents global elastic

buckling which is a sound design principle in most rule sets for buckling capacity, since global buckling is a rather unstable response and will result in stress redistribution to supporting frames.

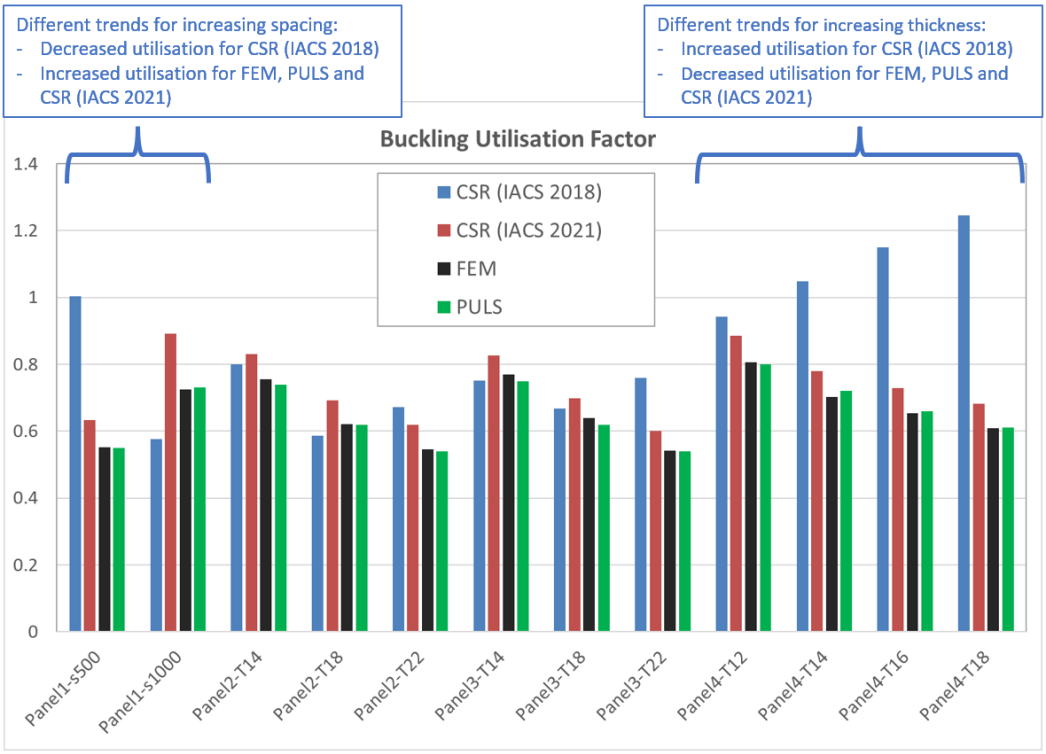

Figure: 16: Utilization factor for buckling of actual plates with slender/long stiffeners subjected to transverse loads.

The effect of increasing the stiffener length was also studied for plates subjected to transverse loads and results are shown in Fig. 17 where the length is increasing while all the other dimensions are kept fixed. For shorter stiffeners with aspect ratio less than eight, the critical buckling mode is plate buckling and then the agreement between all the methods is very good. However, for longer stiffeners, the utilisation for CSR (IACS 2018) is much larger compared to the others. The dashed black curve in the figure is the global elastic buckling (GEB) computed using FE with orthotropic shell elements and this is the upper limit (cut-off) of the capacity for the longer stiffeners.

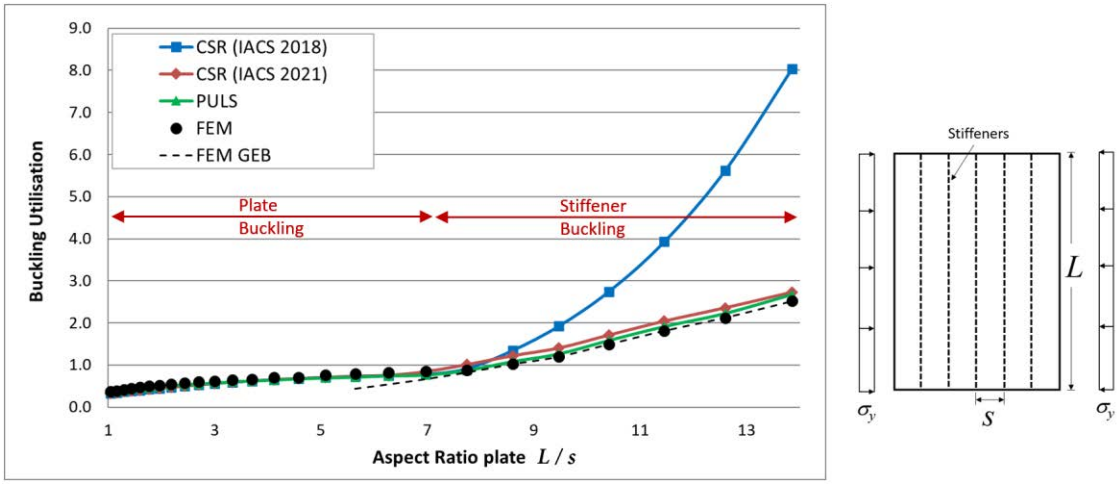

Figure 17: Effect of varying the aspect ratio for a stiffened panel with transverse load.

Regarding stiffener torsional buckling, a stress dependent expression was introduced in the modified formulations since the original formulas may be unphysical for weak stiffeners under torsional loads. In addition, the expression for elastic torsional buckling is improved since the original expression was somewhat optimistic. More details on this aspect can be found in the technical background for CSR (IACS 2021).

5. OFFSHORE STRUCTURES

Preserving sufficient ultimate strength is crucial to ensure the structural safety of offshore structures. The ultimate strength has been an active research topic over the last decades. With the rapid development of offshore energy, particularly renewable energy, offshore structures scale up in size continuously. In the meantime, non-traditional offshore structures such as large fishery farms and offshore thermal energy convertors are being built more in recent years. These changes demand updating previous knowledge gained from the traditional offshore oil and gas industry. This chapter is therefore focused on reviewing the recent literature in these areas. Recent advances and future research needs are presented regarding the ultimate strength of offshore structures. The latest changes in design standards and rules relevant to this topic are also summarized in this chapter.

5.1 Loads

The load effects on the ultimate strength of traditional offshore structures have been widely investigated. In this report, recent advances in relatively new structures such as offshore wind turbines, arctic offshore structures, and composite risers are summarized.

5.1.1 Load effects on offshore wind turbines

Offshore wind turbine support structures are subjected to a high level of stress as a result of operational, extreme, and accidental loads. It is important to carefully examine the ultimate strength of the structural components of offshore wind turbines including their foundation. Chen et al. (2015, 2016a, b) investigated the structural collapse of offshore wind turbines under typhoon impact in real-world cases, see Fig. 18. It is found that rotor blades and towers failed under extreme loads which were below the design wind speed of 70 m/s, highlighting the urgent need for more research on the ultimate strength of offshore wind turbines under extreme wind conditions. Although both steel towers and wind turbine blades are thin-walled structures that are susceptible to buckling under extreme load, the identified prevailing failure modes are yielding driven buckling of steel towers where weld joints are present and buckling driven collapse of composite rotor blades.

Do et al. (2018) performed experimental investigations and numerical predictions on the responses of dented stringer-stiffened cylinders subjected to hydrostatic pressure, see Fig. 19, and found that the effects of collision damages on the ultimate strength of stringer-stiffened cylinders under hydrostatic pressure were extremely low. Chen et al. (2018b) analyzed the ultimate bending performance and failure modes of grouted connections in offshore wind turbine support structures and found that moderate eccentricity had little effect on bending capacity, bending stiffness, ductility, and stress distributions of the specimens.

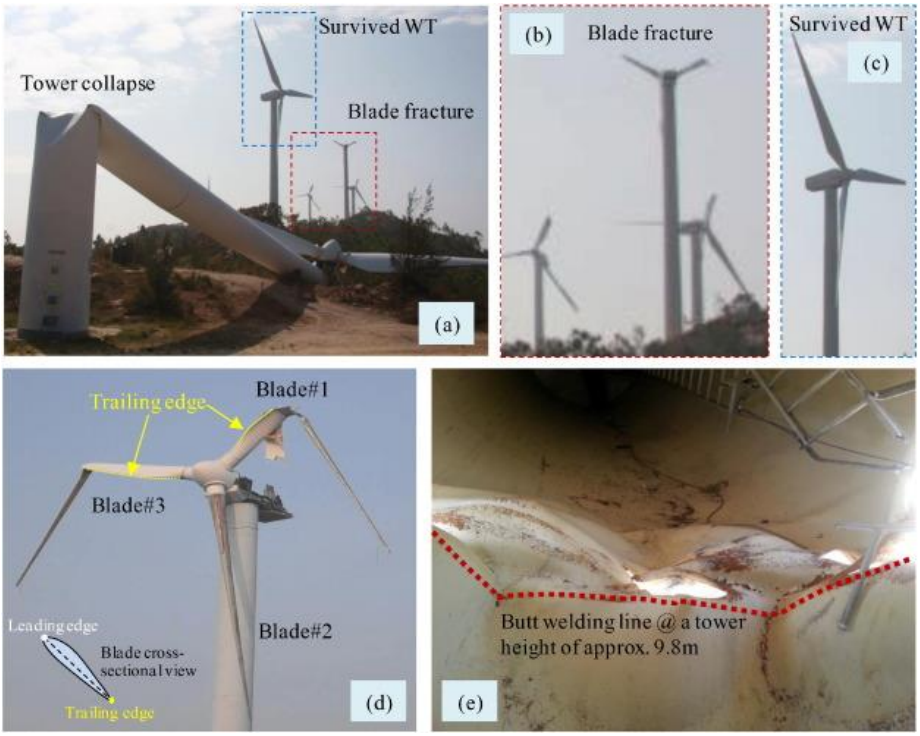

Figure 18: Structural failure of wind turbines due to extreme wind loads during a typhoon. The structures failed at a wind speed below the design value [Chen et al. 2016b].

(a) Structural failure in a coastal wind farm. (b) Blade fracture. (c) A survived wind turbine (d). Blade fracture. (e) Local buckling of the tower at shell wall thickness transition region with weld joints.

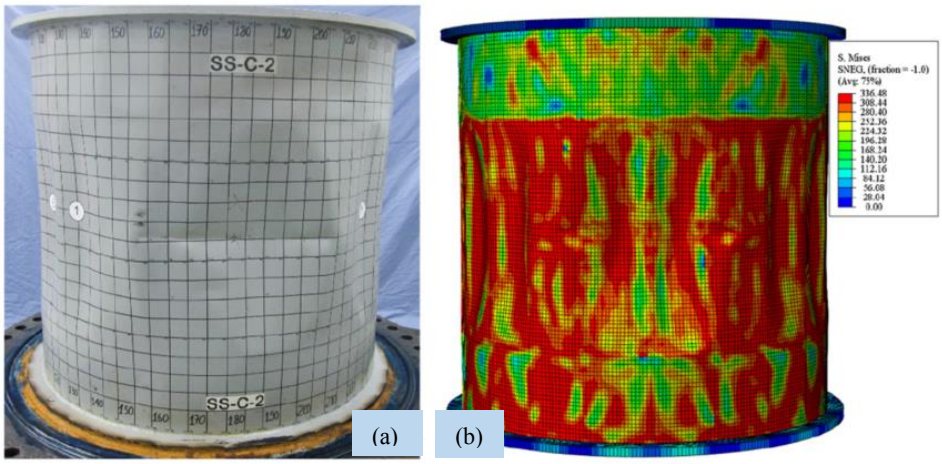

Figure 19: Experimental observation and numerical simulation of dented stringer-stiffened cylinders subjected to hydrostatic pressure [Do et al., 2018].

(a) Deformed shape of physical model: SS-C-2. (b) Predicted collapsed shape of the model.

Designing a floating offshore wind turbine system is a quite challenging task because of the complex environmental loading and complicated coupling effects. By merging the unsteady actuator line model into the in-house code, Cheng et al. (2019) established the fully coupled aero-hydrodynamic model for numerical simulation of floating offshore wind turbine, which is quite time-saving comparing with other conventional CFD tools and provides more accurate flow information over traditional blade element momentum (BEM) and potential flow theory.

Offshore wind turbines in hostile environments may be exposed to not only the wind and wave loadings but also the most violent seismic loadings, if they are bottom supported (e.g. jacket, tension leg). To alleviate the dynamic structural responses of the jacket supported offshore wind turbines due to the seismic loads associated with other operational loads, multiple tuned mass dampers (MTMD) can be installed at the top and base of the turbine tower corresponding to the mode shapes of the structure. Hussan et al. (2018) optimized the MTMD parameters based on response surface methodology and evaluated the multi-mode control strategy through investigating frequency response function, fast Fourier transforms, peak and lateral displacements of the tower, root mean square, shear, and moment of the uncontrolled and controlled structures. The results indicated that the multi-mode control strategy is prominent in suppressing the first two vibrational modes.

5.1.2 Ice load on arctic offshore structures

Sea ice poses hazards to ships and offshore structures that create challenges for designers. Riska and Bridges (2019) analyzed the limit state definitions adopted in the different offshore and ship standards with emphasis for those applicable to low temperatures and ice-covered regions, such as the Finnish Swedish Ice Class Rules, International Association of Classification Societies Polar Class Rules, and ISO 19906. The analysis indicated that there is a lot of variation between standards for offshore structures and ships, for example, the different definitions of the design air temperature can give very different design values.

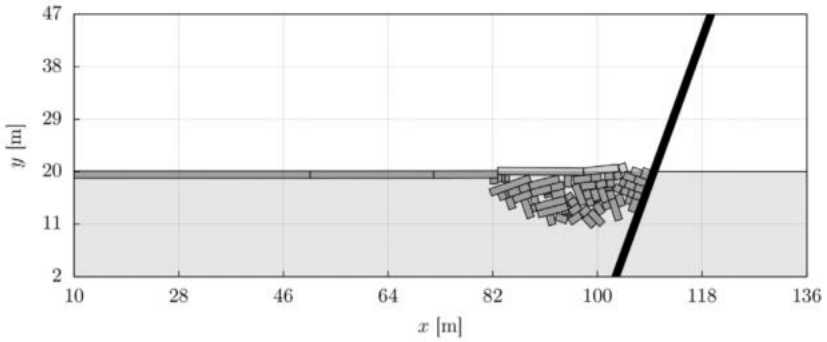

Figure 20: A snapshot from a simulation at a stage with the length of the pushed ice of 125 m, the thickness of 1.25 m and the plastic limit of 1 MPa [Ranta et al., 2018].

The Arctic is a sensitive environment and imposes stringent safety requirements for all marine operations. One of the key factors in developing safe Arctic operations is a reliable prediction of sea ice loads. By using a two-dimensional finite-discrete element method, Ranta et al. (2018) simulated the failure of level ice against an inclined structure and discussed the evolution of the ice-structure interaction process. In the simulations, an initially continuous ice sheet, modeled as a homogeneous floating beam, breaks into ice blocks as the ice sheet is pushed against an inclined structure with a constant velocity, as shown in Fig. 20. The results show that the thickness and the plastic limit of ice have a strong effect on the ice load.

5.1.3 Load on composite risers

A flexible riser is a key enabler for the oil and gas production in ultra-deep which transports production fluids between floating production systems and subsea wells. Excessive hydrostatic pressure may cause collapse failure of flexible risers, as shown in Fig. 21 (Fernando, 2015) and thus predicting the critical collapse pressure is of significant importance to their anti-collapse design. Li et al. (2018b) reviewed the recent advances on collapse prediction of flexible risers and highlighted the gaps in existing methods, such as the lack of an effective equivalent layer

method due to the neglect or incorrect consideration of contact issues of the carcass, imperfections generated from manufacture process, complex collapse behavior under combined external and bending loads, etc.

Figure 21: Collapse failure of a flexible riser caused by excessive hydrostatic pressure [Fernando, 2015].

Flow-induced vibration of multiple marine risers frequently occurs in deepwater applications and may result in serious structural failure due to fatigue damage accumulation. Compared with the case of a single cylinder, the oscillation characteristic and wake flow of multiple cylinders are much more complicated and have not been fully understood due to the interactions of a bundle of cylinders. Xu et al. (2018c) carried out a series of experimental tests to investigate FIV of two side-by-side flexible cylinders with a high aspect ratio (length to diameter, L/D = 350) in a towing tank, and found that the apparent proximity interference exists in cross-flow direction when the spacing is smaller 6.0 diameter.

5.2 Structural elements

This section presents the recent research and development on the ultimate strength for structural elements and connections in offshore structures.

5.2.1 Tubular joints

Many alternative stiffening methods such as rack/rib, joint can, ring, doubler plate, collar plate, and fiber-reinforced plastic have been adopted to increase the static strength of tubular joints as shown in Fig. 22 (Murugan et. al, 2019). Out of these methods, some methods are applied during the fabrication stage (e.g. rack/rib, joint can, ring, doubler plate), and some other methods which are applicable during both fabrication and operation stages (e.g. collar plate, Fiber-reinforced plastic).

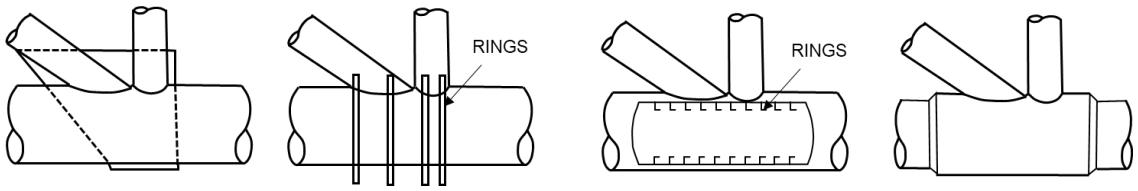

Figure 22: Types of stiffening mechanisms (Murugan et. al, 2019).

(a) Pass-through gusset (b) external ring stiffener (c) internal ring stiffener (d) joint can

Pass-through gusset plates were the first attempt for the stiffening joint, however, it can reduce the fatigue life due to the undesirable stress concentrations. To overcome the disadvantages of gusset plates, reinforcing joints with the external stiffeners were adopted and found to be the easiest way of local stiffening, but additional wave forces are inevitably generated (Shiyekar et al., 1983). Internal ring stiffeners were used in the 1970s and they showed an advantage of longer fatigue life and less corrosion (Raghava et.al 1989), but a disadvantage of reducing the

internal clear diameter of the chord. American Petroleum Institute (API) recommended a thicker chord section (Joint Can) in the vicinity of the intersection (API 2014). Both the collar plate reinforcement and doubler plate reinforcement are found to be efficient in distributing the axial brace load to a larger region of the chord. The thicker chord section nearer to the joint enhances the strength of the joints. The grooves usually increase the residual stress and as a result increases the strength (Murugan et. al, 2019).

Nassiraei et. al (2016) investigated the structural behavior of T/Y-joints reinforced with collar plates subjected to compressive loading at fire-induced elevated temperatures (Fig. 23(a)). A finite element (FE) model was developed and verified by the results of six experimental tests carried out in a previous study. At the next step, a total number of 360 FE analyses were performed to investigate the effect of elevated temperatures, dimensionless geometrical parameters and brace inclination angle on the initial stiffness, ultimate strength, and failure mechanisms. The joints were analyzed under axially compressive load and five different temperatures.

An innovative stiffened circular hollow section (CHS) X-joint has been used in offshore long-span transmission towers due to its higher bearing capacity in comparison with traditional CHS X-joint (Fig. 23(b)). A total of 480 joints are numerically modeled and corresponding load-displacement curves and ultimate bearing capacities are obtained by FE analysis by Chen et al. (2019c). Parametric sensitive study results show that the bearing capacities of corresponding unstiffened X-joint and chord rings could be used for predicting the strength of stiffened X-joints. In this survey, the stiffened joint is observed to provide strength enhancement up to 811% in comparison with the traditional unstiffened X-joint, which proves that the stiffening method employed herein is capable of improving the bearing capacity greatly.

Murugan et. al (2019) dealt with the effect of grooves on static strength and stiffness of tubular T joints of offshore jacket structures (Fig. 23(c)). Three-dimensional finite element analysis has been carried out to investigate the effect of grooves placed over thickened chord sections on the static strength of tubular T joints subjected to axial compressive load. The grooved configuration was found to increase the joint local stiffness by more than 250 percent.

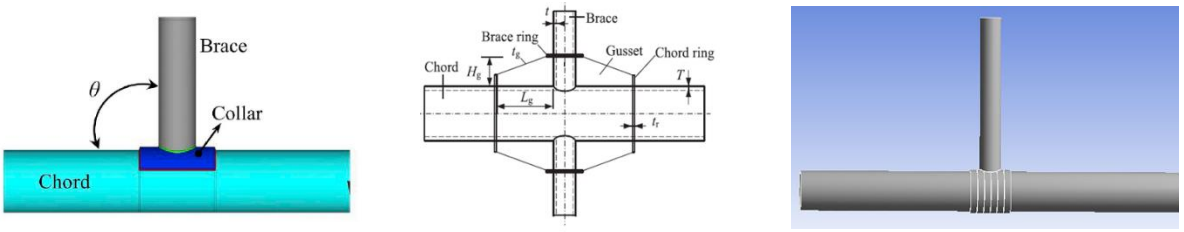

Figure 23: Various types of stiffened tubular joints.

(a) a joint with collar plate (b) circular hollow section X-joint (c) a joint with grooves

5.2.2 Tubular members

When it comes to a tubular member, recent researches have focused on the ultimate strength for a tubular member with some accidental damage such as perforation or collision. Vaz et. al (2018) investigated the strength capacity and design formulas for intact members subject to axial compressive forces. However, there are few studies on the behavior of perforated tubular members from offshore aged units and their remaining load capacity assessment. Perforation damage leads to deterioration of strength capacity and lifetime shortening of the structures. This study presented an experimental campaign and a numerical finite element model to obtain the ultimate strength of tubular structures with circular perforated damage subjected to axial compression.

When a tubular member is damaged by a lateral impact such as a collision by a supply vessel, a decision on whether to repair or replace the members needs to be made based upon the residual strength assessment of the tubes. Li et. al (2019b) investigated the relationship between the residual ultimate strength of the damaged circular tube by collision and the energy dissipation due to lateral impact. The influences of several parameters, such as the length, diameter and thickness of the tube and the impact energy, on the reduction of ultimate strength are investigated. Based on a series of numerical nonlinear FE analyses, a non-dimensional parameter was introduced to represent the degree of damage and a simplified formula has been derived to describe the relationship between axial compressive residual ultimate and lateral impact energy and tube parameters.

Zhu et.al (2018a,b) conducted dynamic experimental investigation on the behavior of fully clamped pipes with different diameter-to-thickness ratios and length-to-diameter ratio equal to 10 subjected to transverse impacts by 15-degree wedge-shaped striker. Based on the experimental investigations, Zhu et.al (2018b) performed a two-phase analysis, a wedge impact analysis for an intact tubular bracing member and an ultimate strength analysis for the damaged member under axial compression using ABAQUS. Then, a parametric study was conducted to investigate the effects of diameter, wall thickness, pipe length, damage depth, and the damage locations on the ultimate strength of tubular members and to propose an equation for predicting the ultimate strength of the damaged pipe.

Yu and Amdahl (2018b) provided a review of the state-of-the-art with respect to the response dynamics and mechanics of offshore tubular members subjected to mass impacts. The review covers various topics such as material modeling, ship impact loading, energy absorption, global and local responses of tubular structures, the residual strengths of damaged tubular members, and design considerations to mitigate against ship impacts. Ship collision assessments of such platforms should be carried out using dynamic analysis. During a collision, energy absorption in the platform occurs mainly through lateral deformation of the struck and adjacent members, buckling of compressed members and global motions of the platform.

5.2.3 Curved stiffened plate

It is known that curvature is expected to increase the buckling strength and the ultimate strength of a curved plate. The study by Park et al. (2018) aimed to clarify and examine the fundamental behavior of cylindrically curved plates under axial compression and lateral pressure via a series of elastoplastic large deflection analyses. The effects of curvature, initial deflection, slenderness and aspect ratio, boundary conditions and secondary buckling behavior are examined and a modified Faulkner's formula to predict the ultimate strength of the curved plate was proposed. Buckling modes of ring-stiffened cylindrical shells under external pressure can be categorized as follows: (1) the local buckling of the cylindrical shell between ring-stiffeners, (2) the buckling of the entire region of the cylindrical shell including ring-stiffeners, (3) the tripping buckling of the ring-stiffener, and (4) the local buckling of the web or the flange of ring-stiffeners. If the dimensions of ring-stiffeners increase, the overall buckling strength increases, whereas the tripping buckling strength decreases. The estimation formula is required to estimate the tripping buckling strength accurately. Shiomitsu et al. (2019) proposed an analytical formula for the tripping buckling strength of ring-stiffeners in stiffened cylindrical shells.

5.3 Structural Systems

More recently, important technological developments and new marine facilities used for offshore aquaculture, renewable energy exploitation, subsea mining, have attracted increased attention and they are addressed here from an ultimate strength point of view.

5.3.1 Offshore aquaculture platforms

Due to limited nearshore area and great impact on the local ecosystem, the aquaculture industry is trying to move the fish farms from nearshore to more exposed sea regions where waves and currents are stronger. The floating collar fish farm is the most commonly used concept nowadays. Each unit in a fish farm typically comprises a floating collar with two concentric tubes, a flexible net cage, a sinker tube and possible chains connecting the sinker tube and the floating collar. The system is moored with a complex mooring system with bridle lines, frame lines and anchor lines, supported by spar type buoys. Shen et al. (2018) investigated a realistic aquaculture fish farm system in both regular and irregular waves by numerical simulations and model tests. The physical model used in the experiments featured all the main components presented in a full-scale sea cage system (with single cage) commonly used in Norway, and the set-up of the experiment with the model test scale of 1:16 is shown in Fig. 24. The study suggested that the mooring loads in the anchor lines and in the bridle lines were not sensitive to the majority of the wave types. The most important parameter for the anchor loads is the flow reduction factor in the rear part of the net cage.

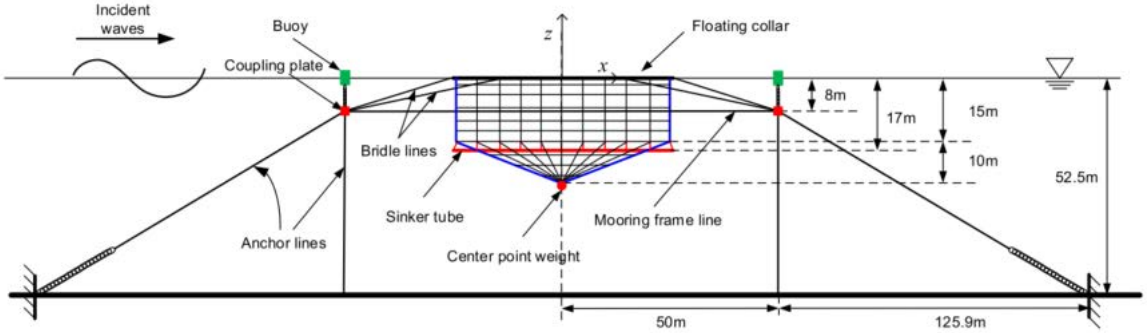

Figure 24: Set-up of the physical model experiments for a realistic fish farm. Two springs were inserted in the front two anchor lines. [Shen et al., 2018].

5.3.2 Ocean thermal energy conversion

Ocean Thermal Energy Conversion (OTEC) is a process of harvesting energy from the ocean by utilizing the temperature difference between surface warm water and deep cold water. The most challenging component of OTEC floating structure is the cold-water pipe, which is installed to transport the deep seawater to the board, as shown in Fig. 25. Adiputra and Utsunomiya (2019) studied the effects of internal flow on the stability of the pipe and performed the design analysis to select the pipe material, top joint configuration and bottom supporting system. The results yield conclusions that pinned connection at the top joint is preferable to decrease the applied stress, clump weight installation is necessary to reduce the motion displacement, and the fiber-reinforced plastic is the most suitable material among the examined materials.

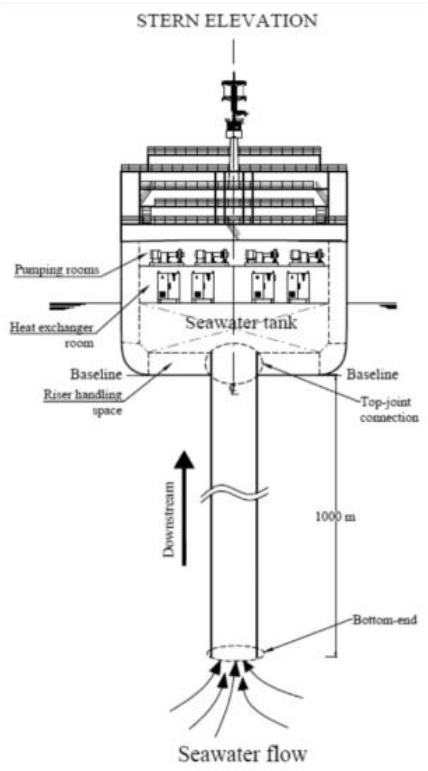

Figure 25: Sketch of cold-water pipe for OTEC system [Adiputra and Utsunomiya, 2019].

5.3.3 Offshore wind farms

The development of offshore wind energy is gaining tremendous momentum in recent years. More wind farms have been built in the sea where wind turbine structures are subject to unconventional loads and environmental conditions such as typhoons, hurricanes and tsunamis. The ultimate strength of each single offshore wind turbine is dependent not only on its own but also on the other wind turbines, particularly the ones upwind due to the wake effect, see Fig. 26.

Figure 26: A photograph of the offshore wind farm at Horns Rev 2 Denmark was taken by helicopter pilot Gitte Lundorff. The photo of the fog over the sea dramatically pictured the offshore wind farm wake – which requires large offshore wind farms to be designed against both ultimate strength and fatigue resistance on a system level.

The wake effect on energy production and fatigue loads of wind turbines has been studied considerably. The literature review found that there is a lack of study on how extreme wind conditions would affect the structural integrity of offshore wind turbine structures in large wind farms. Both steel towers and composite rotor blades are thin-walled structures susceptible to buckling when under extreme loads.

5.4 Rules and guidelines

The most recent class rules/guidelines/guides have only minor updates regarding the calculation of buckling and ultimate strength of offshore structures. Table 1 shows a list of rules/guidelines/standards from the various classes. Some highlights are summarized as follows:

5.4.1 ISO

In the current edition of ISO 19900, several updates have been made regarding the process for limit state verification. The procedures to validate the structure operations and its components with sufficient integrity have been clarified in the combination with provision for construction and operation with respect to all applicable design/assessment situations dependent on exposure level. A new definition and grouping of ULS criteria have been established in order to address the strength and stability of structures and structural components to avoid collapse in whole or in part. ULS in the current edition can be divided into two groups, i.e., ULS1: action effect in individual structural components exceeding resistance (in some cases reduce by deterioration), including loss of structural stability (e.g., buckling), and ULS2: loss of static equilibrium of the structure, or critical part of the structure, considered as a rigid body (e.g: overturning, sinking, or capsizing).

In addition, assessments of structural integrity management (SIM) of offshore structures with a quantitative method that uses explicit probabilities by ultimate strength method (USM) should be performed using static nonlinear analysis, dynamic nonlinear analysis and structural reliability analysis (ISO 19901-9: 2019). USM generally applies to structures where a static analysis adequately represents the structural response. For dynamically sensitive structures, dynamic, time domain, nonlinear analysis may be utilized. As for ISO 19901-3: 2015 no updates have been made since January 2015.

5.4.2 ABS

There are only minor updates and an ABS new Guide for classing floating offshore wind turbines (ABS FOWT). In general, buckling criteria is carried out by referring to the ABS Guide for Buckling and Ultimate Strength Assessment for Offshore structures (WSD or LRFD) or recognized standards (e.g: Buckling criteria API 2V and 2U). As a supplement to all ABS rules/guide of offshore structures ABS provide new Guidance Notes on Nonlinear Finite Element Analysis (NLFEA) of Marine and Offshore Structures for cases that are not covered by the ABS Rules and Guides, or for those involving novel structural designs and loading situations where NLFEA may provide a better insight into the adequacy of a proposed design. These Guidance Notes address the main technical aspects of using NLFEA and provide the best practices and general recommendations for achieving more reliable results when analyzing yielding and plastic deformations, buckling, ductile static fracture, etc.

5.4.3 LR

Buckling check in local structure is carried out using a prescriptive formula, for plate element, there is a table for the selection coefficients of buckling factors and reduction factors which depending on the configuration of the load direction and distribution, boundary conditions and structural geometry [LR 2020]. The buckling criteria only takes into account the effect of hull girder compressive stresses whereas the effects of other membrane stresses and lateral stresses

were ignored. In other structures buckling check is carried out in plate, stiffener and primary member subject to compression and shear stress. For primary members there is a correction for elastic critical buckling exceeding 50% of yield strength material [LR 2020].

Table 1: Classification Society Rules for Offshore Structural Strength

Class/Standard	Rules, Guide, or Guidance	Edition
ISO	ISO 19900 – General requirements for Offshore structures	July 2019
	ISO 19901-3 – Specific requirements for offshore structures – Part 3: Topside Structures	January 2015
	ISO 19901-3 – Specific requirements for offshore structures – Part 9: Structural Integrity Management	September 2019
ABS	Rules for Building and Classing Floating Production Installations (FPI)	January 2021
	Guide for Building and Classing Floating Offshore Liquefied Gas Terminals (FLGT)	August 2018
	Guide for Buckling and Ultimate Strength Assessment for Offshore Structures	August 2018
	Guide for Buckling and Ultimate Strength Assessment for Offshore Structures (LRFD)	July 2016
	Guide for Building and Classing Floating Offshore Wind Turbines (FOWT)	July 2020
	Guidance Notes on Nonlinear Finite Element Analysis of Marine and Offshore Structures	January 2021
LR	Rules and Regulations for the Classification of Offshore Units	July 2020
DNV GL	DNVGL-RP-0286, Coupled analysis of floating wind turbines	May 2019
	DNVGL-OS-C101, Design of offshore steel structures, general - LRFD method	July 2019
	DNVGL-OS-C102, Structural design of offshore ship-shaped units	July 2020
	DNVGL-OS-C103, Structural design of column stabilized units - LRFD method	July 2020
	DNVGL-OS-C104, Structural design of self-elevating units - LRFD method	July 2019
	DNVGL-OS-C105, Structural design of TLPs - LRFD method	July 2015
	DNVGL-OS-C106, Structural design of deep draught floating units - LRFD method	July 2015
	DNVGL-OS-C201, Structural design of offshore units - WSD method	July 2017
	DNVGL-RP-C208, Determination of Structural Capacity by Non-Linear Finite Element Analysis Methods	September 2019
RINA	Rules for the classification of floating offshore units at fixed locations and mobile offshore drilling units (MODU, FPSO, FSO, FSRU, FLNG)	January 2020
	Rules for the Classification of Steel Fixed Offshore Platforms (Fixed Platform)	August 2015
BV	Rules for Classification of Offshore Unit	February 2019
	Classification of column stabilized units	December 2016
	Rules for the classification of self-elevating units - jack-ups and lftboats	December 2016
	Rules for the classification of tension leg platforms (TLP)	July 2012
	Classification and certification of floating offshore wind turbines	January 2019
	Classification of floating gas units	May 2019

5.4.4 DNVGL

The hull girder's ultimate strength for ship shape offshore units/installations is assessed using the same procedure with HCSR Rules. Buckling calculation used Net scantlings concept and action stresses are generated from direct strength analysis. DNVGL specifies allowable buckling utilization factors for different design load scenarios. As for other structures (self-elevating, TLP, deep draught floating unit and etc.) buckling checks are provided in both load resistance factor design (LRFD) and the working stress design (WSD) format [DNVGL OS C101 2019, DNVGL OS C201 2017]. Structural analysis may be carried out as linear elastic, simplified rigid-plastic, or elastic-plastic analyses. Either first-order or second-order analyses may be applied. In all cases, the structural detailing with respect to strength and ductility requirement shall conform to the assumption made for the analysis. As a supplement of other ship or offshore structures rules, DNVGL provides design buckling and ultimate strength for various structure members such as plate, shell, bars and framework, spherical shells, tubular members, etc. in DNVGL RP C202 and DNVGL CG 0128.

DNVGL provides new recommended practice for coupled analysis of floating wind turbines related to extreme loads (ultimate limit state) that are generated primarily by extreme environmental impacts e.g. storm events with a recurrence period of 50 years. Furthermore, system failures such as loss of power or braking failures (e.g. due to rotor over speed) typically generate extreme loads similar to bottom fixed wind turbines. For FOWT unfavorable combinations of wind and wave (wind-wave misalignment) and oscillation effects enabled by the additional dynamics of the station keeping system (e.g. ringing) are additionally critical [DNVGL RP 0286].

5.4.5 RINA and BV

For stiffened panels, buckling checks at BV are carried out with NI 615 "Bending Assessment of Plate Structures" while RINA is carried out in accordance with the Rules for the Classification of Floating Offshore Units at Fixed Locations and Mobile Offshore Drilling Units. The buckling of tubular members is to be checked according to recognized codes or standards. Furthermore, Limit design in fixed platform structural components is carried out using an ISO Standard or other recognized standard by verified methods.

BV NI 572 provides guidance notes for classification and certification of offshore wind turbines which structural strength assessment included design ULS using safety factors that are determined independently in the Guide. However, buckling for tubular members is checked according to a recognized standard.

6. BENCHMARK STUDY

Many approaches and numerical simulation methods for ultimate strength analysis of stiffened plate structures have been presented in the literature including closed-form equations, fast-running Smith's Method progressive collapse codes, and finite element analysis (FEA). These approaches are usually supported by validation examples from various experimental investigations on plates, panels, and large grillages. Often, the methods are tied together so that FEA is used to generate load-shortening curves for fast-running codes which can in turn be run to generate closed-form equations. Paik and Kim (2002) presented a benchmark study where formulas for combined axial loading, in-plane bending, and lateral pressure were compared. The collapse modes of a stiffened plate were divided into six groups: overall collapse of the stiffened plate structures, yielding at the corners of the plating between stiffeners, yielding of the plate-stiffener combination at the mid-span, local buckling of the stiffener web, lateral-torsional buckling (tripping) of the stiffener and gross yielding. The ultimate strength was defined as the lowest value among the various ultimate strengths calculated for each of the collapse

modes, a procedure that is now well established and is followed today. The validity of the developed method was confirmed in a comparison between experimental, numerical and theoretical results. In the study by Paik et al. (2011), a number of fast-running/practical computation codes for the ULS analysis of welded stiffened plate structures were compared against finite element analyses (FEA) and experiments. The conclusions from the study, carried out in the early 2000s, were that the versions of the practical codes used in the study showed relatively large differences compared to the experimental results. Driven by the need for more practical, computationally efficient and relatively accurate codes for ultimate strength analysis of stiffened plate structures, these methods have been further developed by numerous scholars. A number of subsequent benchmark studies have demonstrated their reliability and good agreement with experimental results for some standard types of stiffened plate structures; see, e.g., Paik et al. (2005) and Paik (2020b).

Although several practical codes are available, such as the DNV-GL PULS, ALPS/ULSAP and ULTSTR codes, the FE method is extensively used because it is often assumed and expected that a properly built model in all its components and features can mimic the characteristics of a real structure. FE modeling is also required to properly establish assumptions in such codes as well as to conduct parametric studies and sensitivity studies on various factors that influence the ultimate strength, such as loading and boundary conditions, geometrical imperfections, residual stresses, temperature effects and aging caused by corrosion or the presence of a fatigue crack. However, there are sources of uncertainties related to physical characteristics, model assumptions and human errors by the analyst that affect the accuracy or inaccuracy of the FEA results. There are a vast number of publications in the literature that contribute to reducing these uncertainties; see, e.g., Smith and Dow (1981).

This chapter presents a brief introduction to the benchmark study carried out by the committee. All details regarding the reference experiment, measurements, numerical models, and results are presented in the Appendix.

6.1 Description of the benchmark study

The overall purpose of the benchmark study presented by the committee was, with reference to the results from a reference experiment on a stiffened steel plate structure, to compare different class rules and guidelines, the participant's skills and experiences, numerical approaches and simulation methods, in their "ability" to make trustworthy predictions of the buckling collapse and ultimate strength of stiffened plate structures subjected to compressive loads. The influences from uncertainties in the modeling procedure, solver, material properties, geometrical initial imperfections, residual stresses, assumptions made by the modeler/analyst, etc., are incorporated in the study and form the basis for discussions, conclusions and recommendations for stricter/well-defined guidelines for the ultimate strength analysis of stiffened plate structures.

Seventeen groups participated worldwide: 9 of the groups were members of the committee, and 8 accepted an invitation that was sent to a larger group of experts outside the committee. The participants were invited to submit results from both FEA and/ practical codes; all submitted results from FEA and only a few also submitted results from practical codes. A detailed presentation of the benchmark study, with emphasis on the description of the reference experiment and the FEAs, is presented in Ringsberg et al. (2021). Thus, this chapter presents a shorter summary of the reference experiment and the FEAs since more details are referred to Ringsberg et al. (2021). Unpublished results from the practical codes, including a comparison with the reference experiment and FEAs, are also presented together with a discussion on material properties, constitutive material modeling, modeling of geometric imperfections, failure mode and location.

Figure 27 presents the physical model in the reference experiment carried out on a large full-scale steel grillage representative of a typical ship structure in warships and as secondary structure in larger ships. Design and testing of the grillage were performed by the US Navy's Naval Surface Warfare Center, Carderock Division (NSWCCD). The grillage consisted of three full sections and two partial sections and was longitudinally stiffened by three identical stiffeners and a single large girder. The plating consisted of two plates of different thicknesses that were butt-welded in Section 3 according to Figure 27. The experiment was displacement-controlled with clamped longitudinal end conditions except for the one end where longitudinal loading was applied in the moving direction; tie-downs were mounted on the sides along the length of the model to prevent vertical motions.

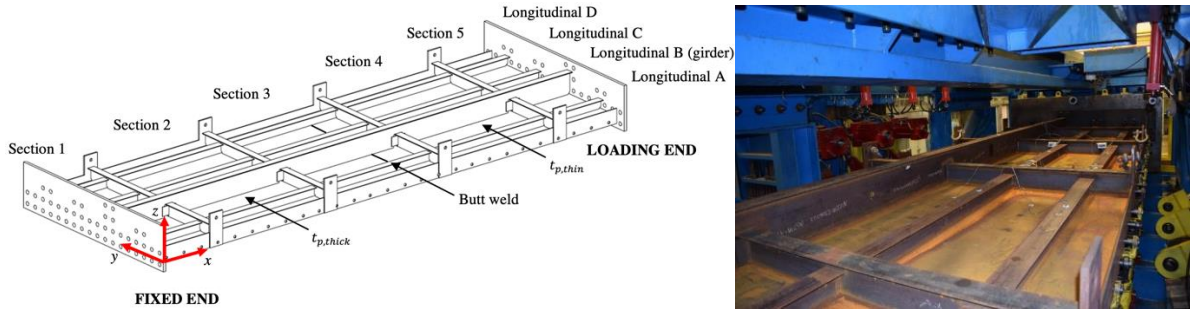

Figure 27: (Left) Geometry of the physical model (reference structure), and (right) a photograph of the experimental setup with the physical model installed in the testing machine.

Model, physical and human error-related uncertainties that affect the prediction of the ultimate strength capacity and failure mode characteristics of the stiffened steel plate structure, compared to the results from the experiment, were investigated by dividing the benchmark study into three phases; see Figure 28 for a schematic. The multiphase validation procedure was defined to reflect the amount of information available from the early design of a new stiffened plate structure with limited confirmed or measured data (Phase 1) to a very detailed design where the majority of the information that defines the structure has been thoroughly measured (Phase 3).

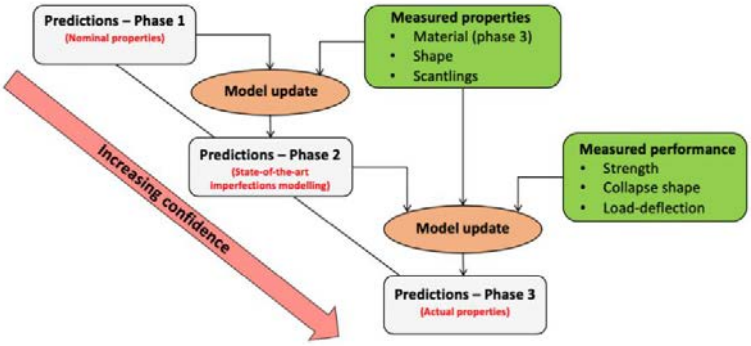

Figure 28: Schematic of the three phases of the benchmark study by multiphase validation of the reference structure.

6.2 Description of the three phases

The benchmark study was carried out as a blind study whereby participants did not have access to the test results from the experiment prior to the study. Results were not shared or discussed amongst participants prior to submission to the study coordinators. This ensured that each participating group exhibited their best performance, making use of their own best practices and

preferred reference literature to design and build numerical models that should replicate the physical model test of the reference stiffened plate structure. The participants received the same information, instructions, data and files needed to carry out the modeling and analyses for each phase; all files can be found as public research data in Nahshon et al. (2021). To meet the objective of the study, the phases were carried out in sequential order, i.e., only the information and data needed to accomplish the purpose of each phase were made available. When a participant had completed a phase, the results and the technical report were submitted to the coordinators of the benchmark study, access was granted to the next phase, and more information and data were made available. Note that a participant was not allowed to revise or update the results from a former phase. Insights of errors from assumptions or modeling issues that led to a revision of the methodology or models between the phases were documented in the technical report from each phase. Hence, it was possible to trace and analyze human error-related uncertainties. In the following, a brief overview of each phase is presented (see Table 2).

Table 2: Overview of the three phases and what was considered (green cells) in each phase.

Phase	Measured imperfections	Actual thickness	Actual material	Measured distortions	Measured thickness	Stress-strain data	Residual stress
1							
2-1							
2-2							
2-3							
3-1							
3-2							
3-3							

6.2.1 Phase 1 – nominal properties

The participants predicted and assessed the ultimate strength capacity of the reference structure based on its nominal properties. Printed 2D drawings and a 3D CAD file of the nominal geometry were shared together with a file that presented the nominal data and material selections for the different parts of the structure. A description of how the experiment was carried out was provided, including information on loading and boundary conditions. In this phase, it was stressed that each participant should clearly express their assumptions on how geometric imperfections were considered in the model and which reference, class rule or guideline was followed.

6.2.2 Phase 2 – nominal properties, actual properties, and measured geometrical imperfections

The information shared in Phase 1 was complemented with new information from thorough laser scanning/tracking of the geometry of the as-built reference structure as well as thick-ness measurements in some locations of different parts of the structure (referred to as the "actual thickness"). The participants were asked to repeat their analysis from Phase 1 considering the measured geometrical imperfections, distortions and deflections of the as-built reference model. Phases 2-3 included material information in the form of vendor-supplied material certification sheets that typify the level of information that can be expected at a shipyard. The phase was divided into three subtasks and reports to enable thorough assessment of each factor's influence on the results.

- Phase 2-1: nominal material properties, nominal thickness, and measured geometrical imperfections.
- Phase 2-2: nominal material properties, actual thickness, and measured geometrical imperfections.

- Phase 2-3: actual material properties, actual thickness, and measured geometrical imperfections.

6.2.3 Phase 3 – actual properties, measured properties, and residual stresses

In this final and third phase, the participants were provided with the remaining data available from measurements and testing including the exact thickness measurements made in many locations on the reference structure (referred to as the "measured thickness") and tensile test results, including full stress-strain curves, for all structural members. The participants were asked to repeat their analyses from the former phases but with revised/updated models based on the new data. This phase was also divided into three subtasks where the first two phases (Phases 3-1 and 3-2) were mandatory. The third subtask was optional, an add-on that included modeling of the residual stresses. The decision to make this phase optional was primarily due to the lack of residual stress measurements on the reference structure.

- Phase 3-1: actual material properties, measured thickness, and measured distortions and geometrical imperfections.
- Phase 3-2: material modeled according to stress-strain curves, measured thickness, and measured distortions and geometrical imperfections.
- Phase 3-3: material modeled according to stress-strain curves, measured thickness, measured distortions and geometrical imperfections, and (modeled) welding-induced residual stresses.

6.3 Concluding remarks

The present benchmark examined the ultimate limit state analysis of a realistic stiffened plate structure. Seventeen separate academic, industry, and government lab groups world-wide submitted FEA results, and a few results from fast-running codes, in three systematic phases, all conducted blindly to the experimental data. The various phases allowed the study organizers to isolate and discuss which data, modeling approaches and procedures have the greatest influence on the uncertainties in the prediction of the ultimate capacity level, failure mode and failure location of the reference structure. Overall, the objective of the study has been accomplished, and the statistics presented in Table A.6 (see the Appendix) show that the FEA results of Phases 3-2 and 3-3 are, on average, very close to the results from the test. If the level of accepted uncertainty of the ultimate capacity level would have been defined to be 5% prior to the start of the benchmark study, the majority of the participants' FE models for Phase 3-2 would be considered validated FE models (ID 2, 3, 5, 7, 8, 9, 10, 11, 12, 13, 15, 16, and 17). However, none of the FE models managed to predict the failure mode and location that occurred in the physical test. This is not surprising given the concurrent nature of failure in two adjacent sections described further in the Appendix.

As there was only a single reference experiment, it was not possible to quantify the uncertainties related to the experimental setup and the measurements carried out during the test. There was good agreement between the FEA results and test results with regard to the ultimate capacity level, but the expected failure mode and location were not well predicted by the FEA. The fast-running codes showed less good agreement for this benchmark study's structure: the ultimate capacity level was lower than the level predicted by the FEAs, and the failure mode and location were not well predicted compared to the test but in the same section as the FEAs. In the FEAs, prediction from ID 14 did identify failure that occurred in the adjacent section during Phase 3-3 despite the use of thicker plating in this region. Based on the documentation from the test of the reference structure and the analyses of all the results from the FEAs, it is difficult to conclude why the majority of the FE models and the fast-running codes could not

predict the correct failure mode and location. Possible reasons for this outcome include the inaccurate modeling of residual stresses, solver-specific and material modeling issues regarding the transition from elastic to inelastic behavior (e.g., see Schafer et al. (2010)), and the assumption that the test fixture provides perfectly rigid boundaries. In addition, there are measurement uncertainties related to material properties, imperfection levels etc. It is also likely that several failure modes are closely located and small variations in modeling assumptions may trigger different modes. The unsuccessful tracing of the force-displacement relationship at ultimate strength and in the post-collapse region for all participants is a strong indication that there are certain aspects of the tests that have not been sufficiently well captured. To address the statistical aspects of the benchmark, at least two more tests on a similar structure are needed to understand what cannot be captured by the majority of the FEA. Due to practical limitations, this could not be conducted in this research.

The summary of the results from all the FEAs from Phase 3-2 – where the FE models were based on the measured material data, geometrical imperfections, distortions, and thicknesses of the structural components – shows very good agreement with the results from the test on the reference structure with regard to the ultimate capacity level. The results of twelve of the seventeen FEAs were within 5% of the ultimate capacity level from the test. In total, the standard deviation of all the FEAs from Phase 3-2 was low. None of the FE models were able to predict the failure mode and location that occurred in the test. Hence, as mentioned above, it was concluded that at least two more tests on the same type of structure and experimental setup are needed to conclude if this uncertainty is related to the experiment or to the FE models' ability to mimic the experiment.

In addition to the FEAs, four participants used different fast-running computation codes to determine the ultimate strength capacity of the stiffened plate structure. A general introduction to these computation codes is given in Appendix Chapter A.2. It is well known that these computation codes are used in most cases in the design phase and can provide a reasonable estimation of the ultimate capacity of the structure. In contrast to commercial finite element software, these approaches are easy to use and have low computational time and effort in terms of data pre-processing, processing, and post-processing.

Comparing the results between the FEAs and the fast-running computation codes from Phase 1, the Smith method using the load-shortening curve from the IACS/CSR-H predicts a higher ultimate capacity. The ULTSTR code predicts a capacity value close to the FEAs, while ALPS/SPINE and ALPS/ULSAP predict a lower ultimate capacity value, see Figure A.14 for the other phases. Note that this comparison is only valid for a plate subjected only to compression. When dealing with an entire ship's cross-section where structural elements under vertical bending load are subjected to tension and compression, the comparison of the results between an FEA and a fast-running code may be different.

Fast-running codes have great potential to improve the accuracy of ultimate strength calculation of a structure by defining the load-shortening curve accurately as a function of failure mode and allowing to include residual stresses, geometrical imperfections or local loads (lateral pressure) as input. Today, the FE method remains one of the most reliable approaches for ultimate strength analysis. It is widely used by shipyards, design offices, and classification societies, to assess the ultimate strength of prototype ships and damaged structures. The present benchmark also indicated that the results from the fast-running codes were further off the test results for the current structure compared to the FEA.

All the participants followed recommended practices and guidelines in the design of their FE models. However, attention should be paid to the choice of element and mesh size related to

the physical dimensions of the structure and its members, geometrical imperfections, material models and failure modes. These are fundamental issues in ultimate limit state analysis by FEA.

Access to representative material data in the initial design/early prediction of a structure's ultimate capacity was discussed. The FEA that was based on nominal material data for the reference structures largely underestimated the ultimate capacity level of the structure. However, the actual material data, which defined the elastic modulus, yield strength, ultimate strength and elongation, were necessary for reasonably accurate prediction of the ultimate capacity, but did not allow precise tracing of the force-deformation curve at ultimate strength and post-collapse region. The access to specific stress-strain curves for each material did not alter the ultimate capacity level, failure mode or location between the FEAs.

The representations of the material in combination by the choice of constitutive material model (EP, BL or ML, see Table A.5) differed between the participants. These varieties were found to be the largest factor related to model uncertainty, and therefore, clearer recommendations and guidelines are needed to reduce the model uncertainty. It had less influence on the ultimate capacity level compared to the predictions made with respect to the failure modes and locations.

Modeling of geometrical imperfections and distortions affects the ultimate capacity level, failure mode and location of failure. The modeling approaches and procedures used by the participants varied moderately. The substitution of the assumed geometrical imperfections in Phase 1 to the measured imperfections in Phase 2-1 only have a minor influence on the results from the FEAs.

Welding-induced residual stresses were introduced in the FE models in Phase 3-3. The results from the FEAs showed that the nonlinear force-displacement curve from the test data was better replicated compared to when these residual stresses were disregarded in Phase 3-2. The introduction of these residual stresses also changed the failure mode and location between the two phases. Hence, residual stresses should be included to realistically reproduce the ultimate capacity level, failure mode and location of failure in FEA.

In retrospect, further efforts are needed to define what failure of a structural member means within FEA, which should be clarified better in existing recommendations and guidelines. Unlike closed-form criteria, neither FEA nor test data readily provide a determination of when "failure" occurs. Strict objective criteria would aide greatly in the comparison of FEA predictions of the ultimate strength.

7. CONCLUSIONS AND RECOMMENDATIONS

The committee presented a review of the published work relevant to the mandate and concluded an extensive benchmark exercise with researchers inside and outside the committee. Here we will summarize key findings by the committee and present recommendations for the community to further improve understanding of ultimate strength of ship and offshore structures.

7.1 Conclusions

Chapter 2 focuses on the aspects that are fundamental to ultimate strength prediction to include modeling methodologies and associated uncertainties. The determination of the ultimate strength of ship and offshore structure is still highly affected by aleatory and epistemic uncertainties. The quest for enhanced understanding of both is supported best by additional testing for data to support analysis of aleatory uncertainty and data for use in validation of predictive models. It is also important to establish methodologies enabling the ranking of uncertainties in computational modelling based on the sensitivity of the solution.

In the Finite Element context, the solid elements can be considered as more accurate than shell elements, but with a significant computational cost. Hence, shell models still represent a widely

accepted compromise, but we must be well aware of the influence of these idealizations to the ultimate strength, and highlights the importance of experimentation for additional realism.

The experimental work is still carried out in laboratory scale by using similarity rules especially at the hull girder, panel and component levels. Technologies like Digital Image Correlation are providing important advantages in the acquisition of data. Moreover, with the help of digital twins, we can keep up with the state of the structure (e.g. actual dimensions, distortions, damages) throughout the design, building and operational stages.

As the failure progresses in the structure, the coupling between non-linear geometry, material and load redistribution can be highly complex and occur very rapidly. In this context, even quasi-static tests may lead to sudden catastrophic failure. The rapid interactions are currently at the limits or beyond current experimental and computational capabilities with these limitations portrayed further in the Benchmark.

For ultimate strength analysis, reduced order models are commonly used to reduce the complexity of the problem in the design stage and accommodate limited information. In the last decade, there has been a continuous work in International Association of Classification Societies (IACS) to harmonize the rules for local buckling models. As a continuation, it has been decided that a harmonized buckling methodology should be further developed and implemented into CSR and all relevant Unified Requirements Strength of Ships (URS) resolutions (IACS 2019, 2015a d, 2017).

Lifecycle and degradation effects are addressed in Chapter 3 with a focus on carbon steel structural components and ship/hull form structures. Many of the studies involving Nonlinear FEA and reduced order models only considered the geometric imperfections induced by welding, as it has been suggested to be more influential to the strength capacity compared to the welding-induced residual stresses, though not welding defects.

Recent work considering inclusion of corrosion in strength modelling is addressed, along with other types of damage and material degradation, but this continues to be a developing and important area for research and practice. In particular, modeling of corrosion and other degradation remains important for further exploration. Increased availability of thickness measurements and other degradation measures in an open database would allow advanced data analytics such as machine learning to facilitate a better damage prognosis. This will have profound impact on developing optimized design/maintenance and full digital twin models. The recognition and incorporation of uncertainties has started early in offshore industry from design stage to maintenance and repair. This is realized by adoption of risk and reliability methods to make rational decisions. Over the last three years, continuous advancement in researching the effect life cycle and degradation can be seen, focusing on corrosion, marine fouling and the capability of updating prediction models based on in-service data collection.

Chapter 4 addresses ship-related structures and loads. For calculation of the wave loads, boundary element method, CFD, and its derivatives are mainly employed to predict linear/nonlinear variations of the effective ship forces/moments. The future trend is likely to require isogeometric analysis-based fluid-structure interaction coupling for ultimate strength of ships floating in waves. Moreover, the stochastic nature of the environment must be statistically integrated in these numerical simulations for a more realistic load prediction.

In addition, existing methods mainly consider material nonlinearity and large deformations for steel structures. Nevertheless, ultimate strength analysis of composite/aluminum hull is the future trend. Furthermore, recent numerical methods for ultimate strength of ship's structural elements are primarily based on FE simulation where stochastic optimization and uncertainty

quantifications is often disregarded, therefore more experimental-numerical comparison studies must be conducted towards future applications.

Lastly, the local buckling is mainly assessed as the most fundamental limit/failure state through nonlinear FE analysis and related formulas are developed. Global nonlinear analyses are more challenging and tend to require reduced order models, but newer formulations may be considered/pursued (e.g., particle-based methods, peridynamics). All in all, it is observed that ultimate strength of ships continues being a challenging problem that require a timely and focused research studies to be conducted in future by considering the main sections dedicated in the present chapter.

The literature review in Chapter 5 indicates that the research on the ultimate strength of offshore structures that operate in harsh environments such as extreme wind, thick ice, and excessive hydrostatic pressure has been very active. Major findings include:

- Rapid exploration of offshore wind energy, particularly in the typhoon- and hurricane-prone regions, demands much more study in the ultimate strength of wind turbine structures. Although both steel towers and wind turbine blades are thin-walled structures that are susceptible to buckling under extreme load, the identified prevailing failure modes are yielding driven buckling of steel towers where weld joints are present and the buckling driven collapse of composite rotor blades. There is a need for more study on the ultimate strength of offshore wind turbines in a large wind farm where flow interaction exists due to the wake effect.
- The studies on collapse pressure of flexible risers mostly focused on the effect of the geometric imperfections, while the studies on the effect of material stress hardening and residual stress are relatively rare, especially in terms of experimental investigation.
- New or improved reinforcements of tubular joints have been proposed in recent years. The focus has been placed on global & local behaviors of tubular structures, especially under accidental load cases. In the meantime, considerable research efforts have been made to improve the accuracy of simplified analytical models or beam finite element formulation aiming at developing more efficient methods to be used at a design phase. It is expected that these works will facilitate efficient structural optimization toward a safer and stronger design of offshore structures.
- Regarding design rules and standards, general applications of ultimate strength design for offshore structures in class society can be divided into ship-shaped or other types of installations. For the ship-shaped installation, almost every class society applies the same procedure as the HCSR or Unified Requirements Strength of Ships (URS). Meanwhile, for other types of installations, the use of recognized standards (ISO, API, NORSOK, etc.) is common by following acceptance procedures or safety factors that are determined independently in each class society.

Their ultimate strength design is still a remaining challenge when offshore structures scale up continuously and are approaching and surpassing their seemingly impossible physical size limit. Disruptive technologies may be necessary to considerably improve the ultimate strength of offshore structures with much larger sizes and under more extreme loads in harsher environments.

The benchmark study described in Chapter 6 and the Appendix examined the ultimate limit state analysis of a realistic stiffened plate structure. Seventeen separate academic, industry, and government lab groups worldwide submitted FEA results, and a few results from fast-running codes, in three systematic phases, all conducted blindly to the experimental data. Overall, the

objective of the study has been accomplished, and the statistics presented in Table A.6 (see the Appendix) show that the FEA results of Phases 3-2 and 3-3 are, on average very close to the results from the test. If the level of accepted uncertainty of the ultimate capacity level would have been defined to be 5% prior to the start of the benchmark study, the majority of the participants' FE models for Phase 3-2 would be considered validated FE models. However, none of the FE models managed to predict the failure mode and location that occurred in the physical test. This is not surprising given the concurrent nature of failure in two adjacent sections.

As there was only a single reference experiment, it was not possible to quantify the uncertainties related to the experimental setup and the measurements carried out during the test. There was good agreement between the FEA results and test results with regard to the ultimate capacity level, but the expected failure mode and location were not well predicted by the FEA. The fast-running codes showed less good agreement for this benchmark study's structure: the ultimate capacity level was conservatively lower than the level predicted by the FEAs, and the failure mode and location were not well predicted compared to the test but in the same section as the FEAs.

All the participants followed recommended practices and guidelines in the design of their FE models. However, attention should be paid to the choice of element and mesh size related to the physical dimensions of the structure and its members, geometrical imperfections, material models and failure modes.

Access to representative material data in the initial design/early prediction of a structure's ultimate capacity was discussed. The FEA that was based on nominal material data for the reference structures largely underestimated the ultimate capacity level of the structure. However, the actual material data, which defined the elastic modulus, yield strength, ultimate strength and elongation, were necessary for reasonably accurate prediction of the ultimate capacity, but did not allow precise tracing of the force-deformation curve at ultimate strength and post-collapse region. The access to specific stress-strain curves for each material did not alter the ultimate capacity level, failure mode or location between the FEAs.

Modeling of geometrical imperfections and distortions affects the ultimate capacity level, failure mode and location of failure. The modeling approaches and procedures used by the participants varied moderately. The substitution of the assumed geometrical imperfections in Phase 1 to the measured imperfections in Phase 2-1 only have a minor influence on the results from the FEAs.

Welding-induced residual stresses were introduced in the FE models in Phase 3-3. The results from the FEAs showed that the nonlinear force-displacement curve from the test data was better replicated compared to when these residual stresses were disregarded in Phase 3-2. The introduction of these residual stresses also changed the failure mode and location between the two phases. Hence, residual stresses should be included to realistically reproduce the ultimate capacity level, failure mode and location of failure in FEA.

7.2 Recommendations

The following recommendations can be given for the future work:

- When quantifying epistemic uncertanties in numerical modelling via experimental/numerical comparison, it is recommended to take into account more than just the ultimate strength value, but to consider in the validation also the failure modes and the overall collapse behavior.
- Numerical predictions should support multiple failure modes and their interactions, while giving precise predictions of collapse and post-collapse behaviour of the

structural members and assemblies involved. Especially in the compression zone, the structural elements should be modelled in a level allowing for a proper buckling/collapse shape to be developed.

- Shell elements currently represent a good modelling compromise, but as we look to the future, advances in computational power may lead to the development and use of larger scale models using solid elements.
- Significant literature showed that simplifications in the shape (e.g. due to imperfections and corrosion) leads to significant loss of accuracy at local scale, rather than global. In such cases, the recent experiments showed that in the ultimate strength assessment highly localised stresses can act as failure initiation points for overall collapse. For this reason, efforts should be devoted to expand our knowledge about the effect of real corrosion wastage, as well as initial imperfections, also on the experimental side.
- Further efforts are needed to define what failure of a structural member means within FEA, which should be clarified better in existing recommendations and guidelines. Unlike closed-form criteria, neither FEA nor test data readily provide a determination of when "failure" occurs. Strict objective criteria would aide greatly in the comparison of FEA predictions of the ultimate strength.
- Future research is needed to better predict/quantify the material degradation processes, especially when new materials are increasingly used for offshore construction; and to better incorporate the human element (from fabrication to operation) into the analysis.
- While numerical approaches are fast developing, large scale experiments on damaged structures and new repair methods are vital for model validation and providing physical evidence. Considering the cost and implementation efforts of such experiments, they will benefit from using more realistic damage features, realistic service conditions and advanced testing technique such as full-field imaging. In addition, more understanding into why structures behave in certain ways and critically scrutinizing the scope of applications for newly proposed methods/formulas will be beneficial for academics and industry.
- Many reduced order models are being proposed in the literature without a convenient means of comparison to other new or established models. The next committee should consider comparison of these models to determine their strenghs and weaknesses, preferably as part of a benchmark.
- Typically, academic communities aim for the most accurate solutions, while in engineering communities and in design, it is more common to be on the conservative side with a 'good enough' simplified solution (engineering accuracy). However, the application of Ultimate Strength procedures is normally associated with extended modelling and use of advanced analysis methods. The application of the Ultimate Strength principles in design is encouraged in order to increase structural safety. Ships and offshore structures are valuable assets to be operated for many years. The safety of these structures is of huge importance and safe design should not necessarily be limited by an assumption of excessive computational time and costs. A rational cost-benefit evaluation should be considered to compare the short-term costs of applying advanced design methods vs. the long-term costs and benefits to the investment. In addition, continued management and maintenance of the numerical models during the life cycle is recommended to inform Class approvals, operation, maintenance, repair, and life extension decision-making.

8. ACKNOWLEDGEMENTS

The Committee would like to acknowledge the work provided by Ken Nahshon.

REFERENCES

Aabo, C., Holm, J.S., Jensen, P.H. and Andersson, M. (2018) Annual Research and Innovation Agenda. In: NIELSEN, L. (ed.). Danish Wind Industry Association.

Abaqus (2021) Dassault Systèmes, Abaqus Software. https://www.3ds.com/products-services/simulia/products/abaqus/. [Accessed: 2021-10-11].

Abdussamie, N., Ojeda, R. & Daboos, M. (2018) ANFIS method for ultimate strength prediction of unstiffened plates with pitting corrosion. Ships and Offshore Structures, 13: 540-550.

Adamchak, J.C. (1984) An approximate method for estimating the collapse of a ship's hull in preliminary design. Ship Structure Symposium, Arlington, VA, USA.

ADINA (2021) ADINA Software. http://www.adina.com/. [Accessed: 2021-10-11].

Adiputra, R. and Utsunomiya, T. (2019) Stability based approach to design cold-water pipe (CWP) for ocean thermal energy conversion (OTEC). Applied Ocean Research 92: 1-15.

Ahn, J., Jeon, S., Jeong, Y., Cho, K. and Huh, J. (2018) Evaluation of residual compressive strength and behaviour of corrosion-damage carbon steel tubular members. Materials, 11: 1-20.

ALPS/SPINE (2019) Elastic-plastic large deflection analysis of plates and stiffened panels under combined biaxial compression/tension, biaxial in-plane bending, edge shear and lateral pressure loads. MAESTRO Marine LLC, Greensboro, MD, USA. (www.maestromarine.com).

ALPS/ULSAP (2019) Ultimate strength analysis of plates and stiffened panels under combined biaxial compression/tension, edge shear and lateral loads. MAESTRO Marine LLC, Greensboro, MD, USA. (www.maestromarine.com).

Ansys (2021) Ansys Software. https://www.ansys.com. [Accessed: 2021-10-11].

Anyfantis K.N. (2019) Preliminary design assessment of an alternative repair method for corroded shear panels in ship hull structures. Ocean Engineering 188(1): id 106323.

API (2014) Recommended Practice for planning, designing and constructing fixed offshore Platforms. American Petroleum Institute, API-PR 2A (22nd Ed), Washington DC, United States.

Ao, L., Wang, D., Wu, J. (2019) A Modified Formula for Predicting the Ultimate Strength of Stiffened Panels Under Longitudinal Compression, International Journal of Offshore and Polar Engineering, 29, 2, pp.228- 236.

ASTM A36/A36M-19 (2019) Standard specification for carbon structural steel, ASTM International, West Conshohocken, PA, USA. https://doi.org/10.1520/A0036_A0036M-19. [Accessed: 2021-10-11].

ASTM A992/A992M-20 (2020) Standard specification for structural steel shapes, ASTM International, West Conshohocken, PA, USA. https://doi.org/10.1520/A0992_A0992M-20. [Accessed: 2021-10-11].

ASTM E8/E8M-16ae1 (2016) Standard test methods for tension testing of metallic materials, ASTM International, West Conshohocken, PA, USA. https://doi.org/10.1520/E0008_E0008M-16AE01. [Accessed: 2021-10-11].

Babazadeh, A., Khedmati, M.R. (2018) Ultimate strength of cracked ship structural elements and systems A review, Engineering Failure Analysis, 89, pp.242-257, 2018.

Babazadeh, A., Khedmati, M.R. (2019) Semi-analytical simulation of plastic collapse mechanism of cracked continuous unstiffened plates used in ship structure under in-plane longitudinal compression, Thin-Walled Structures, 144, 106264, 2019.

Bajaj P., Hariharan A., Kini A., Kürnsteiner P., Raabe D. and Jägle E.A. (2020) Steels in additive manufacturing: A review of their microstructure and properties. Materials science & Engineering A 772, 138633.

Bitner-Gregersen, E.M., Vanem, E., Gramstad, O., Hørte, T., Aarnes, O.J., Reistad, M., Breivik, Ø., Magnusson, A.K., Natvig, B. (2018) Climate change and safe design of ship structures, Ocean Engineering, 149, pp.226-237.

Boopathi, R. and Ramesh M. (2020) Influence of eggshell nanoparticles and effect of alkalization on characterization of industrial hemp fibre reinforced epoxy composites, Journal of polymers and the environment, 28, 2178-2190.

Buchanan, C. and Gardner, L. (2019) Metal 3D printing in construction: A review of methods, research, applications, opportunities and challenges, Engineering Structures 180, 332-348.

Bruchman, D.D., Kihl, D.P. & Adamchak, J.C. (2000) Evaluation of the effects of construction tolerances on vessel strength, Ship Structures Committee Report SSC-411.

Cabos, C., Eisen, H., and Krömer, M. (2006) GL.ShipLoad: An Integrated Load Generation Tool for FE Analysis, COMPIT 2006, Delft

Cai, J., Jiang, X. and Lodewijks, G. (2017) Residual ultimate strength of offshore metallic pipelines with structural damage – a literature review, Ships and Offshore Structures, 12: 1037-1055.

Castaldo P., Gino D., La Mazza D., Bertagnoli G., Carbone V.I., Mancini G. (2018) Assessment of the partial safety factor related to resisting model uncertainties in 2D NLFEA of R.C. systems, Proceedings of Italian Concrete Days 2018.

Chen, B. and Guedes Soares, C. (2018a) A simplified model for the effect of weld-induced residual stresses on the axial ultimate strength of stiffened plates. Journal of Marine Science and Application, 17: 57-67.

Chen, H., Xu, Y., Hu, J. and Wang, X. (2019a) Optimisation of lightweight sub-stiffened panels with buckling analysis and imperfection sensitivity analysis. Proc IMechE Part G: Journal of Aerospace Engineering 233(15): 5507-5521.

Chen, T., Li, Z., Wang, X., Yuan, G., Liu, J. (2018b) Experimental study on ultimate bending performance of grouted connections in offshore wind turbine support structures. *Thin-Walled Structures* 132: 522-536.

Chen, X., Kitane, Y. and Itoh, Y. (2010) Mechanical properties of fillet weld joints by underwater wet welding in repairing corrosion-damaged offshore steel structures. Journal of Structural Engineering, 56A: 742-755.

Chen, X., Kitane, Y. and Itoh, Y. (2011) Evaluation of repair design on corrosion-damaged steel pipe piles using welded patch plates under compression. Journal of Structural Engineering 57A: 756-768.

Chen, X., Li, C., & Xu, J. (2015) Failure investigation on a coastal wind farm damaged by super typhoon: A forensic engineering study. Journal of Wind Engineering and Industrial Aerodynamics, 147, 132-142.

Chen, X., Li, C., & Tang, J. (2016a) Structural integrity of wind turbines impacted by tropical cyclones: A case study from China. Journal of Physics: Conference Series, 753.

Chen, X., & Xu, J. Z. (2016b) Structural failure analysis of wind turbines impacted by super typhoon Usagi. Engineering Failure Analysis, 60, 391-404.

Chen, X., Berring, P., Madsen, S. H., Branner, K., & Semenov, S. (2019b) Understanding progressive failure mechanisms of a wind turbine blade trailing edge section through subcomponent tests and nonlinear FE analysis. Composite Structures, 214, 422-438. https://doi.org/10.1016/j.compstruct.2019.02.024.

Chen, Y., Hu, Z.Z., Guo, Y., Wang, J., Dan, H., Liu, Q., Pan, Y. (2019c) Ultimate bearing capacity of CHS X-joints stiffened with external ring stiffeners and gusset plates subjected to brace compression, Engineering Structures, 181:76–88.

Chen, Z., Yu, C., Dong, P. (2019d) Rankine source method analysis for nonlinear hydroelastic responses of a container ship in regular oblique waves. Ocean Engineering, 187, p.106168.

Cheng, P., Huang, Y., Wan, D. C. (2019) A numerical model for fully coupled aero-hydrodynamic analysis of floating offshore wind turbine, Ocean Engineering 173: 183-196.

Choung, C., Lee, S. and Chang, D. (2019) Investigation on structural availability application in beam design: Buckling strength and structural deterioration due to corrosion. Ocean Engineering 184(1): 206-215.

Corak, M., Parunov, J., Soares, C.G. (2018) Structural reliability analysis of container ships under combined wave and whipping loads. Journal of Ship Research, 62(03), pp.115-133.

Cui, H.W., Yang, P. (2018a) Ultimate strength and failure characteristics research on steel box girders under cyclic-bending moments. Journal of Marine Science and Technology 23(4): 926-936.

Cui, H.W., Yang, P. (2018b) Ultimate strength assessment of hull girder under cyclic bending based on Smith's method. Journal of Ship Research, 62 (2), pp. 77-88.

Cui, J., Wang, D. and Ma, N. (2019a) Case studies on the probabilistic characteristics of ultimate strength of stiffened panels with uniform and non-uniform localized corrosion subjected to uniaxial and biaxial thrust, International Journal of Naval Architecture and Ocean Engineering, 11, Issue 1, pp.97-118.

Cui, J., Wang, D. (2019b) Ultimate Strength of Bilge Panels in Container Ships under Combined Axial Compression, Bending and Lateral Pressure, Proceedings of the 29th International Ocean and Polar Engineering Conference, pp.4839-4847.

Cui, J., Wang, D., Ma, N. (2019c) Key influencing factors in ultimate strength analysis for large container ships International Journal of Offshore and Polar Engineering, 29 (1), pp. 58-96.

Cui J. and Wang D. (2020) An experimental and numerical investigation on ultimate strength of stiffened plates with opening and perforation corrosion, Ocean Engineering, 205, 2020

Czujko, J., Bayatfar, A., Smith, M., Xu, M.C., Wang, D., Lutzen, M., Saad-Eldeen, S. Yanagihara, D. Notaro, G. Qian, X., Park, J.S., Broekhuijsen, J., Benson, S., Pahos, S.J., Boulares, J. (2018) Committee III. 2: Fatigue and Fracture, Proceedings of the 20th International Ship and Offshore Structures Congress (ISSC 2018), CRC Press.

de Borst, R. (1991) Simulation of strain localisation: A reappraisal of the Cosserat Continuum, Engineering Computations, Volume 8, Issue 4, pp. 317-332. DOI: 10.1108/eb023842.

de Borst, R., Sluys, L., Mulhaus, H. and Pamin, J. (1993) Fundamental issues in finite element analyses of localisation of deformation, Engineering Computations, Volume 10, Issue 2, 1993, pp. 99-121. DOI: 10.1108/eb023897.

Dinesh S., Elanchezhian C., Vijayaramnath B., Sathiyanarayanan K. and SyedAfiridi S. (2020) Experimental investigation of natural and synthetic hybrid composite for marine application. Materials Today: Proceedings, 22, 322-329.

Ding A., Wang J., Ni A. and Li S. (2019a) Assessment on the ageing of sandwich composites with vinylester-based composite faces and PVC foam core in various harsh environments. Composite Structures 213, 71-81.

Ding, S., Zhou, L., Zhong, C., Cao, J., Yin, Q., Zhang, J. (2019b) A Structural Analysis Procedure Combining Linear and Nonlinear FE Methods for Polar Ship, 29th International Ocean and Polar Engineering Conference, 16-21 June, Honolulu, Hawaii, USA.

DNVGL (2018) Buckling Class Guideline DNVGL-CG-0128, Edition January 2018

DNVGL (2020) Recommended practice—DNVGL-RP-C208. Edition: September 2019, amended January 2020. DNV GL AS, Høvik, Norway.

Do, Q. T., Muttaqie, T., Park, S. H., Shin, H. K., Cho, S. R. (2018) Ultimate strength of intact and dented steel stringer-stiffened cylinders under hydrostatic pressure. Thin-Walled Structures 132: 442-460.

Dowling, P.J., Chatterjee, S., Frieze, P. and Moolani, F.M. (1973) Experimental and predicted collapse behaviour of rectangular steel box girders, International Conference on Steel Box Girder Bridges. (1973) London.

Elanchezhian C., Vijaya Ramnath B., Ramakrishnan G., Sripada Raghavendra K.N., Muralidharan M. and Kishore V. (2019) Review on metal matrix composites for marine applications. Materials Today: Proceedings 5, 1211-1218.

Erofeev V., Grebenshchikova O. and Troyanovskaya I. (2019) Hydrogen impact on the origin and propagation of welded cold cracks in low-alloy steels at low temperatures. Materials Today: Proceedings 19, 1891-1894.

Evans, J.H. (1975) Ship Structural Design Concepts, Cornell Maritime Press, Centreville, MD, USA.

Faisal, M., Noh, S.H., Kawsar, M.R.U., Youssef, S.A.M., Seo, J.K., Ha, Y.C. and Paik, J.K. (2017) Rapid hull collapse strength calculations of double hull oil tankers after collisions, Ships and Offshore Structures, 12:5, 624-639, DOI: 10.1080/17445302.2016.1192747.

Feng, L., He, J., Hu, L., Shi, H., Yu, C., Wang, S. and Yang, S. (2020a) A parametric study on effects of pitting corrosion on steel plate's ultimate strength. Applied Ocean Research 95: 102026.

Feng, L., Li, D., Shi, H., Zhang, Q. and Wang, S. (2020b) A study on the ultimate strength of ship plate with coupled corrosion and crack damage. Ocean Engineering 200: 106950.

Fernando, U. S. (2015) Challenges and solutions in developing ultra-high pressure flexibles for ultra-deep water applications. In Proceedings of the MCE Deepwater Development, 24-26 March, London, UK.

Fiore V., Sanfilippo C. and Calabrese L. (2019) Influence of sodium bicarbonate treatment on the aging resistance of natural fiber reinforced polymer composites under marine environment. Polymer Testing 80, 106100.

Fletcher, C.A.J. (1984) Computational Galerkin method, Springer-Verlag, New York, NY, USA.

Fujikubo, M. (2019) Digital Twin for Ship Structures - Research Project in Japan, the Proceedings of the 14th International Symposium on Practical Design of Ships and other Floating Structures, September 22nd – 26th 2019, Yokohama, Japan, Paper A-1.

Gaiotti, M., Ravina, E., Rizzo, C.M., and Ungaro, A. (2018) Testing and simulation of a bolted and bonded joint between steel deck and composite side shell plating of a naval vessel, Engineering structures 172

Gan, N., Yao, X.L., Liu, L.T., Xiao, W., Wang, X.L. (2019) Research on overall damage characteristics of a hull girder under explosion bubble collapse. Ocean Engineering, 188, p.106315.

Gao Y.H., Liu S.Z., Hu X.B., Ren Q.Q., Li Y., Dravid V.P. and Wang C.X. (2019) A novel low cost 2000 MPa grade ultra-high strength steel with balanced strength and toughness, Materials Science & Engineering A 759, 298-302.

Guo, B., Gramstad, O., Vanem, E., Bitner-Gregersen, E. (2019) Study on the Effect of Climate Change on Ship Responses Based on Nonlinear Simulations. Journal of Offshore Mechanics and Arctic Engineering, 141(4), 041605.

Garbatov, Y., Parunov, J., Kodvanj, J., Saad-Eldeen, S., Guedes Soares, C. (2016) Experimental assessment of tensile strength of corroded steel specimen subjected to sandblast and sandpaper cleaning. Mar Struct. 49(1):18–30.

Garbatov, Y., Ås, S.K., Branner, K., Choi, B.K., den Besten, J.H., Dong, P., Lillemäe, I., Lindstrom, P., Lourenço de Souza, M., Parmentier, G., Quéméner, Y., Rizzo, C.M., Rörup, J., Vhanmane, S., Villavicencio, R., Wang, F. and Yuan, Y. (2018) Committee III. 2: Fatigue and Fracture, Proceedings of the 20th International Ship and Offshore Structures Congress (ISSC 2018), CRC Press, pp. 441-547.

Garbatov, Y., Sisci, F. and Ventura, M. (2018) Risk-based framework for ship and structural design accounting for maintenance planning. Ocean Engineering 166(1): 12-25.

Georgiadis, D. and Samuelides, M. (2019) A methodology for the reassessment of hull-girder ultimate strength of a VLCC tanker based on corrosion model updating. Ships and Offshore Structures, 14: 270-280.

Goa Da-wei and Shi Gui-jie (2018) Reliability of hull girder ultimate strength of steel ships, 4th International Conference on Advanced Engineering and Technology (4th ICAET), IOP Conf. Series: Material Science and Engineering 317, 012036

Gong, C., Frangopol, D.M. and Cheng, M. (2019) Risk-based life-cycle optimal dry-docking inspection of corroding ship hull tankers. Engineering Structures 195(1): 559-567.

Gordo, J.M. and Guedes Soares, C. (2004) Experimental Evaluation of the Ultimate Bending Moment of a Box Girder, Marine Systems and Offshore Technology. Vol. 1 No. 1 (2004): pp. 33–46.

Gordo, J.M. and Guedes Soares, C. (2015) Experimental Evaluation of the Ultimate Bending Moment of a Slender Thin-walled Box Girder, Journal of Offshore Mechanics and Arctic Engineering. Vol. 137 No. 2 (2015): 021604. DOI 10.1115/1.4029536

Hagenbeek M. (2020) Composite ship section passes load test, SWZ Maritime 12: 31

Harshini D., ul Haq A., Buddi T., Ajay Kumar K. and Anitha Lakshmi A. (2019) Comparative study on mechanical behavior of ASS 316L for low and high temperature applications. Materials Today: Proceeding 19, 767-771.

Hosseini Far A.R., Mousavi Anijdan S.H. and Abbasi S.M. (2019) The effect of increasing Cu and Ni on a significant enhancement of mechanical properties of high strength low alloy, low carbon steels of HSLA-100 type. Materials Science & Engineering A 746, 384-393.

Hu, K., Yang, P., Xia, T. and Peng, Z. (2018) Residual ultimate strength of large opening box girder with crack damage under torsion and bending loads. Ocean Engineering 162(1): 274-289.

Huang, X., Yan, X., Ong, M.C., Huang, Y. (2018) The Effect of Fatigue Loading Spectrum on Crack Propagation in a Ship Detail. In International Conference on Offshore Mechanics and Arctic Engineering (Vol. 51333, p. V11BT12A032). American Society of Mechanical Engineers, OMAE2018-77152.

Hughes, O.F. & Paik, J.K. (2013) Ship structural analysis and design. The Society of Naval Architects and Marine Engineers, Alexandria, VA, USA.

Hulkkonen, T., Manderbacka and Sugimoto, K. (2019) Digital Twin for Monitoring Remaining Fatigue Life of Critical Hull Structures, Tullamore, Ireland, 25-27 March 2019, Conference on Computer Applications and Information Technology in the Maritime Industries 2019, pp. 415-427.

Hulkkonen, T., Shin, H.C., Yi, N.H., Jang D.H. and Hang, T.G. (2017) Enabling a paradigm shift in ship structural design with a 3D approach, International Conference on Computer Applications in Shipbuilding 2017, 26-28 September 2017, Singapore.

Hussan, M., Rahman, M. S., Sharmin, F., Kim, D., Do, J. (2018) Multiple tuned mass damper for multi-mode vibration reduction of offshore wind turbine under seismic excitation. *Ocean Engineering* 160: 449-460.

IACS (2015a) International Association of Classification Societies – IACS Unified Requirements Strength UR-S11, Longitudinal Strength Standard

IACS (2015b) International Association of Classification Societies – IACS Unified Requirements Strength UR-S11A, Longitudinal Strength Standard for Container Ships

IACS (2015c) International Association of Classification Societies – IACS Unified Requirements Strength UR-S21, Evaluation of Scantlings of Hatch Covers and Hatch Coamings of Cargo Holds of Bulk Carriers, Ore Carriers and Combination Carriers

IACS (2015d) International Association of Classification Societies – IACS Unified Requirements Strength UR-S21A, Evaluation of Scantlings of Hatch Covers and Hatch Coamings and Closing Arrangements of Cargo Holds of Ships

IACS (2017) International Association of Classification Societies – IACS Unified Requirements Strength UR-S17, Longitudinal Strength of Hull Girder in Flooded Condition for Non-CSR Bulk Carriers

IACS (2018) International Association of Classification Societies – IACS Common Structural Rules for Bulk Carriers and Oil Tankers.

IACS (2019) International Association of Classification Societies. Common Structural Rules for Bulk Carriers and Oil Tankers, London, England

IACS (2020a) Common Structural Rules for Bulk Carriers and Oil Tankers. International Association of Classification Societies, London, UK. (http://www.iacs.org.uk).

IACS (2020b) Requirements concerning strength of ships. Unified Requirement S11; Longitudinal strength standard for container ships. International Association of Classification Societies, London, UK. (http://www.iacs.org.uk).

IACS (2021) International Association of Classification Societies – IACS Common Structural Rules for Bulk Carriers and Oil Tankers, Rule version date 1. January 2021, Effective date 1. July 2021.

Iijima, K. and Fujikubo, M. (2018) Hydro-elastoplastic behaviour of VLFS under extreme vertical bending moment by segmented beam approach, Marine Structures, Vol. 57, 2018, pp. 1-17, 10.1016/j.marstruc.2017.09.008.

Ilman, E.C., Wang, Y., Wharton, J.A. and Sobey, A.J. (2020) The impact of corrosion-stress interactions on the topological features and ultimate strength of large-scale steel structures. Thin-Walled Structures 157: 107104.

Ilman, E.C., Wang, Y., Wharton, J.A. and Sobey, A.J. (2022) A hybrid corrosion-structural model for simulating realistic corrosion topography of maritime structures. Thin-Walled Structures (in press).

Jesthi D.K. and Nayak R.K. (2019) Evaluation of mechanical properties and morphology of seawater aged carbon and glass fiber reinforced polymer hybrid composites. Composites Part B 174, 106980.

Jiao, J., Jiang, Y., Zhang, H., Li, C., Chen, C. (2019) Predictions of ship extreme hydroelastic load responses in harsh irregular waves and hull girder ultimate strength assessment. Applied Sciences, 9(2), p.240.

Jones, N., (1975) On the shakedown limit of a ship's hull girder. Journal of Ship Research, 19(02), pp.118-121.

Kai, Q., Renjun, Y., Mingen, C., and Haiyan, Zeng (2020) Failure mode shift of sandwich composite L-Joint for ship structures under tension load, Ocean Engineering, 214, 107863

Khargani, N. and Guedes Soares, C. (2018) Experimental and numerical study of hybrid steel-FRP balcony overhang of ships under shear and bending, Marine Structures, Vol. 60, Issue 1, 2018, pp. 15–33, 10.1016/j.marstruc.2018.03.003.

Kim, H., Daley, C. and Kim, H. (2018a) Evaluation of large structural grillages subjected to ice loads in experimental and numerical analysis, Marine Structures, Vol. 61, Issue 1, 2018, pp. 467–502, DOI: 10.1016/j.marstruc.2018.06.015

Kim, D.K., Lim, H.L., Yu, S.Y. (2018b) A technical review on ultimate strength prediction of stiffened panels in axial compression, Ocean Engineering, 170, pp.392-406.

Komoriyama, Y., Yanagihara, D. (2018a) A Simple Design Formula to Estimate the Ultimate Strength of Stiffened Panels under Bi-Axial Compression Mainly in Transverse Direction, Proceedings of the 37th International Conference on Ocean, Offshore and Arctic Engineering, OMAE2018-77747.

Komoriyama, Y., Tanaka, Y., Ando, T., Hashizume, Y., Tatsumi, A., Fujikubo, M. (2018b) Effects of Cumulative Buckling Deformation Formed by Cyclic Loading on Ultimate Strength of Stiffened Panel, Proceedings of the 37th International Conference on Ocean, Offshore and Arctic Engineering, OMAE2018-77855.

Kong, X., Zhou, H., Zheng, C., Pei, Z., Yuan, T., Wu, W. (2021) Research on the dynamic buckling of a typical deck grillage structure subjected to in-plane impact Load. Marine Structures, 78, p.103003.

Kõrgesaar, M., Reinaldo Goncalves, B., Romanoff, J. and Remes, H. (2016) Behaviour of orthotropic web-core steel sandwich panels under multi-axial tension, International Journal of Mechanical Sciences, Vol. 115-116, 2016, pp. 428–437.

Kõrgesaar, M., Romanoff, J. and Remes, H. (2017) Influence of material non-linearity on load carrying mechanism and strain path in stiffened panel, Procedia Structural Integrity, 2nd International Conference on Structural Integrity, ICSI 2017, 4-7 September 2017, Funchal, Madeira, Portugal. DOI: 10.1016/j.prostr.2017.07.050.

Kõrgesaar, M., Romanoff, J. and Palokangas P. (2018a) Experimental and numerical assessment of fracture initiation in laser-welded webcore sandwich panels, Eighth International Conference on, Thin-Walled Structures - ICTWS 2018, Lisbon, Portugal, July 24-27. Ref. b

Kõrgesaar, M., Romanoff, J., Remes, H. and Palokangas, P. (2018b) Experimental and Numerical Penetration Response of laser-welded stiffened panels, International Journal of Impact Engineering, Vol. 114, Issue 1, 2018, pp. 78-92. Ref. a

Lee, H.H. & Paik, J.K. (2020) Ultimate compressive strength computational modeling for stiffened plate panels with nonuniform thickness. Journal of Marine Science and Application 19: 658-673.

Li, C., Dong, S., Wang, T., Xu, W., Zhou, X. (2019a) Numerical Investigation on Ultimate Compressive Strength of Welded Stiffened Plates Built by Steel Grades of S235–S390. Applied Sciences 9, 2088.

Li, R., Yanagihara, D., Yoshikawa, T. (2018a) Residual Ultimate Strength of Simply Supported Corroded Plates with Initial Geometrical Imperfections under Uniaxial Compression, Proceedings of the 28th International Ocean and Polar Engineering Conference, pp.332-339, 2018.

Li, R. Yanagihara, D., Yoshikawa, T. (2019b) Axial compressive residual ultimate strength of circular tube after lateral collision, Int J Nav Arch Ocean 11(1):396-408.

Li, S., Benson, S.D. (2019c) A re-evaluation of the hull girder shakedown limit states. Ships and Offshore Structures, 14(sup1), pp.239-250.

Li, S., Hu, Z. and Benson, S. (2019d) An analytical method to predict the buckling and collapse behaviour of plates and stiffened panels under cyclic loading. Engineering Structures 199: 109627.

Li, S., Hu, Z. and Benson S. (2020) Progressive collapse analysis of ship hull girders subjected to extreme cyclic bending. Marine Structures 73: 102803.

Li, X., Jiang, X. L., Hopman, H. (2018b) A review on predicting critical collapse pressure of flexible risers for ultra-deep oil and gas production. Applied Ocean Research 80: 1-10.

Li, X. and Tang, W. (2019e) Structural risk analysis model of damaged membrane LNG carriers after grounding based on Bayesian belief networks. Ocean Engineering, 171, pp. 332-344. DOI: 10.1016/j.oceaneng.2018.10.047.

Liang, B. and Mahadevan, S. (2011) Error and uncertainty quantification and sensitivity analysis in mechanics computational models, International Journal for Uncertainty Quantification, 1 (2), 147-161

Liu, B., Wu, W., Guedes Soares, C. (2018) Ultimate strength analysis of a SWATH ship subjected to transverse loads. Marine Structures, 57, pp. 105-120.

Liu, Y., Frangopol, D.M. and Cheng, M. (2019) Risk-informed structural repair decision making for service life extension of aging naval ships. Marine Structures 64(1): 305-321.

Ljubinkovic, F., Martins, J.P., Gervasio, H., Silva, L.S. (2019) Ultimate load of cylindrically curved steel panels under pure shear, Thin-Walled Structures, 142, pp.171-188.

Ljubinkovic, F., Martins, J.P., Gervasio, H., Silva, L.S., Leitao, C. (2020). Experimental and numerical investigation on cylindrically curved steel panels under uniform compression, Thin-Walled Structures, 149, 106527.

LS-DYNA. (2021) LS-DYNA Software. https://www.lstc.com. [Accessed: 2021-10-11].

Ma, S., Liming F., Ma M. and Shan A. (2019a) Ultra-strong nickel aluminium bronze allows with ultrafine microstructures by continuous heavy hot rolling, Materials characterization, 158.

Ma, H., Yang, Y., He, Z., Zhang, Y. and Ji, F. (2019b) Experimental study on mechanical properties of steel under extreme cyclic loading considering pitting damage. Ocean Engineering 186(1): id 106091

Manco, T., Martins, J.P., Rigueiro, C and da Silva, L.S. (2018) Semi-analytical model for the prediction of the post-buckling behaviour of unstiffened cylindrically curved steel panels under uniaxial compression, Marine Structures, Vol. 59, Issue 1, 2018, pp. 387–400. DOI /10.1016/j.marstruc.2018.02.007.

Matsumoto, T., Shigemi, T., Kidogawa, M., Ishibashi, K., and Sugimoto K. (2016) Examination of effect of lateral loads on the hull girder ultimate strength of large container ships, OMAE (2016), pp. 1-8

Mestre Rodriguez C. (2018) The thickness effect in adhesive bonded joints, MSc. Thesis report Delft University of Technology.

Mestre Rodriguez C., Pavlovic M., Dragt R.C., and Schipperen J.H.A. (2019) The thickness effect in adhesively bonded joints; an experimental study, conference paper: Adhesion 2019

Moan, T. (2018) Life cycle structural integrity management of offshore structures, Structure and Infrastructure Engineering: Maintenance, Management, Life-Cycle Design and Performance, 14.

Mohd, M.H., Zalaya, M.A., Latheef, M., Choi, H.S., Rahman, M.a.A. & Kim, D.K. (2019) Ultimate bending capacity of aged fixed platform by considering the effect of marine fouling. Latin American Journal of Solids and Structures, 16: 1-12.

MSC Marc. (2021) MSC Marc Software. http://www.mscsoftware.com. [Accessed: 2021-10-11].

Murugan, N., Kaliveeran, V., Nagaraj, M.K. (2019) Effect of grooves on the static strength of tubular T joints of offshore jacket structures. Materials today: Proceedings, available online.

Nahshon K., Reynolds N., Shields M.D. (2018) Efficient uncertainty propagation for high-fidelity simulations with large parameter spaces: Application to stiffened plate buckling, Journal of Verification, Validation and Uncertainty Quantification, Vol. 3

Nahshon, K., Shilling, G., Ringsberg, J.W. & Darie, I. (2021) ISSC 2022 Committee III.1 – Ultimate Strength Benchmark Data. Mendeley Data, v1. http://dx.doi.org/10.17632/bsh4gmg8s5.1.

Nam, W., Hopperstad, O.S., Amdahl. J. (2018) Modelling of the ductile-brittle fracture transition in steel structures with large shell elements: A numerical study, Marine Structures, Vol. 61, Issue 1, 2018, pp. 40-59, DOI: 10.1016/j.marstruc.2018.07.003.

Narure, Y., Kim, M., Umezawa, R., Ishibashi, K., Koyama, H., Okada, T. and Kawamure, Y. (2019) Scantling Evaluations of Plates and Stiffeners Based on Elasto-plastic Analysis

under Axial Loads and Lateral Pressures the Proceedings of the 14th International Symposium on Practical Design of Ships and other Floating Structures, September 22nd – 26th 2019, Yokohama, Japan, Paper Th-1-A-1.

Nassiraei, H., Lotfollahi-Yaghin, M.A., Ahmadi, H. (2016) Static performance of doubler plate reinforced tubular T/Y-joints subjected to brace tension, Thin-Walled Struct., 108:138-152.

Oberkampf W.L., DeLand S.M., Rutherford B.M., Diegert K.V., Alvin K.F. (2002) Error and uncertainty in modeling and simulation, Reliability Engineering and System Safety 75, 333-357

Ok, D., Pu, Y. and Incecik, A. (2007) Computation of ultimate strength of locally corroded unstiffened plates under uniaxial compression. Marine Structures, 20: 100-114.

Ozdemir, M., Eggin, A., Yanagihara, D., Tanaka, S. and Yao, T. (2018) A new method to estimate ultimate strength of stiffened panels under longitudinal thrust based on analytical formulas, Marine Structures, Vol. 59, Issue 1, 2018, pp. 510–535. 10.1016/j.marstruc.2018.01.001.

Paik, J.K., Thayamballi, A.K., Lee, S.K. & Kang, S.J. (2001) A semi-analytical method for the elastic-plastic large deflection analysis of welded steel or aluminum plating under combined in-plane and lateral pressure loads, Thin-Walled Structures 39(2): 125-152.

Paik, J.K. & Kim, B.J. (2002) Ultimate strength formulations for stiffened plates under combined axial load, in-plane bending and lateral pressure: a benchmark study, Thin-Walled Structures 40(1): 45-83. https://doi.org/10.1016/S0263-8231(01)00043-X.

Paik, J.K. & Thayamballi, A.K. (2003a) Ultimate limit state design of steel-plated structures, John Wiley & Sons, Chichester, UK.

Paik, J.K., Thayamballi, A.K., Park, Y.I. & Hwang, J.S. (2003b) A time-dependent corrosion wastage model for seawater ballast tank structures of ships, Corrosion Science, 46: 471-486.

Paik, J.K. & Lee, M.S. (2005) A semi-analytical method for the elastic-plastic large deflection analysis of stiffened panels under combined biaxial compression/tension, biaxial in-plane bending, edge shear and lateral pressure loads, Thin-Walled Structures 43(2): 375-410.

Paik, J.K. and Hughes, O. (2010) Ultimate Strength of Ship Hulls, Chapter 16 in Ship Structural Analysis and Design; SNAME, 2010.

Paik, J.K., Kim, S.J., Kim, D.H., Kim, D.C., Frieze, P.A., Abbattista, M., Vallascas, M. & Hughes, O.F. (2011) Benchmark study on use of ALPS/ULSAP method to determine plate and stiffened plate ultimate strength, In: Soares CG, Fricke W, editors. Advances in Marine Structures. MARSTRUCT 2011: Proceedings of the 3rd International Conference on Marine Structures; 2011 March 12-15; Hamburg, Germany. Boca Raton: CRC Press-Taylor & Francis Group. p. 169-186.

Paik, J.K., Amlashi, H., Boon, B., Branner, K., Caridis, P., Das, P., Fujikubo, M., Huang, C.-H., Josefson, L., Kaeding, P., Kim, C.-W., Parmentier, G., Pasqualino, I.P., Rizzo, C.M, Vhanmane, S., Wang, X., and Yang, P. (2012) Committee III.1 Ultimate Strength, 18th International Ship and Offshore Structures Congress, Rostock, Germany

Paik, J.K. (2018) Ultimate limit state analysis and design of plated structures (2nd Edition). John Wiley & Sons, Chichester, UK.

Paik, J.K., , Dong Hun Lee , Sung Hwan Noh , Dae Kyeom Park & Jonas W. Ringsberg (2020a) Full-scale collapse testing of a steel stiffened plate structure under axial-compressive loading triggered by brittle fracture at cryogenic condition, Ships and Offshore Structures, DOI: 10.1080/17445302.2020.1787930, Volume 15, 2020 - Issue sup1: Papers from the 2019 International Conference on Ships and Offshore Structures

Paik, J.K. (2020b) Advanced structural safety studies with extreme conditions and accidents. Springer, Singapore.

Park, J.S., Paik, J.K., Seo, J.W. (2018) Numerical investigation and development of design formula for cylindrically curved plates on ships and offshore structures, Thin-Walled Structures, 132, pp.93-110.

Park, J.S., Seo, J.K. (2019) Development of design factor predicting the ultimate strength for wide spacing in container curved bilge structures, Journal of Marine Science and Technology, 24, pp.526-542.

Parunov, J., Rudan, S., Gledić, I., Primorac, B.B. (2018) Finite element study of residual ultimate strength of a double hull oil tanker with simplified collision damage and subjected to bi-axial bending. Ships and Offshore Structures 13(sup1): S25-S36.

Piscopo, V., Scamardella, A. (2018) Towards a unified formulation for the ultimate strength assessment of uncorroded and pitted platings under uniaxial compression, Ocean Engineering, 169, pp.70-86.

Putranto, T., Kõrgesaar, M., Jelovica, J., Tabri, K. and Naar, H. (2021) Ultimate strength assessment of stiffened panel under uni-axial compression with non-linear equivalent single layer approach", Marine Structures, Vol. 78, 2021, 103004, DOI: 10.1016/j.marstruc.2021.103004

Quinn, S., Wang, Y., MacDonald, A., Jogia, M., Thomsen, O. & Barton, J. (2019) Modernising composite materials regulations: Structural approval procedure for marine structures. https://eprints.soton.ac.uk/433348/

Raghava, G., Rao, A.G.M., Murthy, D.S.R. (1989) Behavior of Unstiffened and Stiffened Steel Tubular T-Joints. J. Offshore Mech. Arct. Eng. 111: 56–60.

Ranta, J., Polojarvi, A., Tuhkuri, J. (2018) Ice loads on inclined marine structures - Virtual experiments on ice failure process evolution. Marine Structures 57: 72-86.

Reinaldo Goncalves, B., Jelovica, J. and Romanoff, J. (2016) A homogenization method for geometric nonlinear analysis of sandwich structures with initial imperfections, International Journal of Solids and Structures, Vol. 87, Issue 1, 2016, pp. 194-205. DOI 10.1016/j.ijsolstr.2016.02.009

Ringsberg, J.W., Darie, I., Nahshon, K., Shilling, G., Vaz, M.A., Benson, S., Brubak, L., Feng, G., Fujikubo, M., Gaiotti, M., Hu, Z., Jang, B.S., Paik, J.K., Slagstad, M., Tabri, K., Wang, Y., Wiegard, B. & Yanagihara, D. (2021) The ISSC 2022 Committee III.1-Ultimate Strength benchmark study on the ultimate limit state analysis of a stiffened plate structure subjected to uniaxial compressive loads, Marine Structures, Vol. 79, 103026

Ringsberg, J.W., Li, Z., Johnson, E., Kuznecovs, A. and Shafieisabet, R. (2018) Reduction in ultimate strength capacity of corroded ships involved in collision accidents, Ships and Offshore Structures 13(sup1): S155-S166.

Riska, K. Bridges, R. (2019) Limit state design and methodologies in ice class rules for ships and standards for Arctic offshore structures, Marine Structures 63: 462-479.

Romanoff, J., Reinaldo Goncalves, B., Karttunen, A. and Romanoff, J. (2019) Potential of Homogenized and Non-Local Beam and Plate Theories in Ship Structural Design, Proceedings of the 14th International Conference on Practical Design of Ships and Other Floating Structures, September 22-26, 2019, PACIFICO Yokohama, Japan, Paper W3-A2.

Saad-Eldeen, S., Garbatov, Y., Guedes Soares, C. (2018) Structural capacity of plates and stiffened panels of different materials with opening, Ocean Engineering 167, 45–54.

Saad-Eldeen, S., Garbatov, Y., Guedes Soares, C. (2019) Buckling collapse tests of deteriorated steel plates with multiple circular openings. Ocean Engineering 172, 523-530.

Saad-Eldeen, S., Garbatov, Y., Guedes Soares, C. (2020) Experimental failure assessment of high tensile stiffened plates with openings. Engineering Structures 206, 110121.

Saleh M., Venkatesan P., Askarinejad S., and Katsivalis I. (2020) Material properties as a function of environmental and operational conditions, Public Qualify report D1.3.2 (Enabling Qualification of Hybrid Structures for Lightweight and Safe Maritime Transport | 2 Mers Seas Zeeën (interreg2seas.eu))

Schafer, B.W., Li, Z. & Moen, C.D. (1981) Computational modelling of cold-formed steel Thin-Walled Structures 48(10-11): 752-762. https://doi.org/10.1016/j.tws.2010.04.008.

Shen, Y., Greco, M., Faltinsen, O. M., Nygaard, I. (2018) Numerical and experimental investigations on mooring loads of a marine fish farm in waves and current. Journal of Fluids and Structures 79: 115-136.

Shi, G., Wang, D. (2012) Ultimate strength model experiment regarding a container ship's hull structures. Ships Offshore Struct. 7 (2), 165–174.

Shi, G.J., Gao, D.W. (2019a) Analysis of hull girder ultimate strength for cruise ship with multi-layer superstructures. Ships and Offshore Structures, 14 (7), pp. 698-708.

Shi, G.J., Gao, D.W., Zhou, H. (2019b) Analysis of hull girder ultimate strength and residual strength based on IACS CSR-H, Mathematical Problems in Engineering, p. 2098492.

Shi, G. and Gao, D. (2021) Model experiment of large superstructures' influence on hull girder ultimate strength for cruise ships", Ocean Engineering, Vol. 222 2021 108626, DOI: 10.1016/j.oceaneng.2021.10/626

Shi, X.H., Zhang, J., Soares, C.G. (2018) Numerical assessment of experiments on the ultimate strength of stiffened panels with pitting corrosion under compression, Thin-Walled Structures, 133, pp.52-70, 2018.

Shi, X.H., Zhang, J. and Guedes Soares, C. (2019c) Numerical assessment of experiments on the residual ultimate strength of stiffened plates with a crack. Ocean Engineering 171: 443-457.

Shiomitsu, D, Toh, K., Yanagihara, D. (2019) Tripping Buckling Strength of Ring-stiffener in Stiffened Cylindrical Shells under External Pressure. In proceedings of the 29th International Ocean and Polar Engineering Conference, (ISOPE2019), Honolulu, Hawaii, USA, 16-21 June 2019. (19TPC-0697).

Shiyekar, M.R., Kalani, M., Belkune, R.M. (1983) Stresses in Stiffened Tubular T Joint of an Offshore Structure. J. Energy Resour. Technol., 105: 177–183.

Smith, C.S. (1977) Influence of local compressive failure on ultimate longitudinal strength of a ship's hull, Proc. PRADS (1977) 73–79.

Smith, C.S. & Dow, R.S. (1981) Residual strength of damaged steel ships and offshore structures. Journal of Construction Steel Research 1(4): 2-15. https://doi.org/10.1016/0143-974X(81)90019-5.

Smith, C.S., Davidson, P. & Chapman, J. (1988) Strength and stiffness of ships' plating under in-plane compression and tension. Royal Institution of Naval Architects Transactions 130(1): 277-296.

Søreide, T., Amdahl, J., Eberg, E., Halmås, T., and Hellan, O. (1988) USFOS – a Computer Program for Progressive Collapse Analysis of Steel Offshore Structures. Theory Manual, SINTEF Report STF71 F88038

Srinivasa, A.R. and Reddy, J.N. (2017) An Overview of Theories of Continuum Mechanics with Nonlocal Elastic Response and a General Framework for Conservative and Dissipative Systems, Applied Mechanics Reviews, Volume 69, May 2017, pp. 030802-1-18. DOI: 10.1115/1.4036723.

Sugiyama T. (2004) Determination of partial factors for model uncertainties adopted in earthquake proof design code for highway arc bridges, 13th world conference on earthquake engineering, Vancouver Canada, August 1-6 2004, paper 338

Sumi, Y. (2018) Structural safety of ships developed by lessons learned from the T 100-year history of break-in-two accidents, Marine Structures, Vol. 64, Issue 1, 2019, pp. 481–491, DOI: 10.1016/j.marstruc.2018.12.003.

Tabri K, Naar H, Kõrgesaar M (2020) Ultimate strength of ship hull girder with grounding damage, Ships and Offshore Structures, 2020, Vol 15:sup1, S161-S175, DOI: 10.1080/17445302.2020.1827631

Takami, T., Matsui, S., Oka, M., Iijima, K. (2018) A numerical simulation method for predicting global and local hydroelastic response of a ship based on CFD and FEA coupling. Marine Structures, 59, pp.368-386.

Takami, T., Iijima, K. (2019) Numerical investigation into combined global and local hydroelastic response in a large container ship based on two-way coupled CFD and FEA. Journal of Marine Science and Technology (Japan), DOI: 10.1007/s00773-019-00668-7.

Takami, T., Komoriyama, Y., Ando, T., Ozeki, S., Iijima, K. (2020) Efficient FORM-based extreme value prediction of nonlinear ship loads with an application of reduced-order model for coupled CFD and FEA. Journal of Marine Science and Technology, 25(2), pp.327-345.

Tatsumi, A., Iijima, K. and Fujikubo, M. (2019) A Study on Progressive Collapse Analysis of a Hull Girder Using Smith's Method, the Proceedings of the 14th International Symposium on Practical Design of Ships and other Floating Structures, September 22nd – 26th 2019, Yokohama, Japan, Paper Th1-A-3.

Tatsumi, A. and Fujikubo, M. (2020) Ultimate strength of container ships subjected to combined hogging moment and bottom local loads part 1: Nonlinear finite element analysis, Marine Structures, Volume 69,

Tekgoz, M., Garbatov, Y. and Guedes Soares, C. (2018) Strength assessment of an intact and damaged container ship subjected to asymmetrical bending loadings. Marine Structures 58(1): 172-198.

Tekgoz, M., Garbatov, Y., Soares, C.G. (2020) Review of Ultimate Strength Assessment of Ageing and Damaged Ship Structures. Journal of Marine Science and Application, 19(4), pp.512-533.

Ueda, Y., Rashed, S.M.H., and Abdel-Nasser, Y. (1994) An improved ISUM rectangular plate element taking account of post-ultimate strength behaviour, Marine Structures 7 (2-5), pp.139-172

Van, T.V., Yang, P. (2017) Effect of corrosion on the ship hull of a double hull very large crude oil carrier. Journal of marine science and application, 16(3), pp.334-343.

Van, T.V., Yang, P. and Van, T.D. (2018) Effect of uncertain factors on the hull girder ultimate vertical bending moment of bulk carriers, Ocean Engineering, 148(1):161-168.

Vaz M.A., Cyrino J.C.R.R., Hernández I.D. Zegarra, V.D., Martinez, J.L., Liang, D.A. (2018) Experimental and numerical analyses of the ultimate compressive strength of perforated offshore tubular members. Mar Struct 58:1–17

Vu Van T, Yang P, Tuyen Doan Van T. (2018) Effect of uncertain factors on the hull girder ultimate vertical bending moment of bulk carriers. Ocean Engineering 148: 161–168

Wang, C., Wu, J. and Wang, D. (2018a) Numerical investigation of three-dimensional hull girder ultimate strength envelope for an ultra large container ship. Ocean Engineering 149(1): 23-37.

Wang, C. and Wang, D. (2019a) Bending and Torsional Ultimate Strength of Cross-Section of Container Ship – Model Test, the Proceedings of the 14th International Symposium on Practical Design of Ships and other Floating Structures, September 22nd – 26th 2019, Yokohama, Japan, Paper Th-1-A-2.

Wang C., Wu J., Wang D. (2019b) Experimental and numerical investigations on the ultimate longitudinal strength of an ultra large container ship, Ocean Engineering, 192, 106546

Wang H., Yu Y., Yu J., Xu W., Chen H., Wang Z. and Han M. (2019c) Effect of pitting defects on the buckling strength of thick-wall cylinder under axial compression, Construction and Building Materials, 224, 226-241.

Wang, Q., Qang, C., Wu, J. and Wang, D. (2020) Experimental and numerical investigations of the ultimate torsional strength of an ultra large container ship, Marine Structures, Vol. 70, Issue, 2020, 102695, DOI: 10.1016/j.marstruc.2019.102695.

Wang, R. & Shenoi, R.A. (2019d) Experimental and numerical study on ultimate strength of steel tubular members with pitting corrosion damage. Marine Structures, 64: 124-137.

Wang, Y., Downes, J., Wharton, J.A. and Shenoi, R.A. (2018b) Assessing the performance of elastic-plastic buckling and shell-solid combination in finite element analysis on plated structures with and without idealised corrosion defects. Thin-Walled Structures, 127: 17-30.

Wang, Y., Ilman, E.C., Sohan Roy, N., Sobey, A., Wharton, J.A. and Shenoi, R.A. (2019e) Implementation of in situ corrosion measurements in structural analysis considering the effect of surface stresses for marine applications. MASTRUCT 2019 Conference, Croatia, Dubrovnic.

Woloszyk, K., Kahsin, Garbatov, Y. (2018) Numerical assessment of ultimate strength of severe corroded stiffened plates. Engineering Structures 168 (2018), pp. 346-354.

Woloszyk, K. and Garbatov, Y. (2019) Structural Reliability Assessment of Corroded Tanker Ship Based on Experimentally Estimated Ultimate Strength. Polish Maritime Research, 26 (2), pp. 47-54. DOI: 10.2478/pomr-2019-0024.

Xia, T., Yang, P., Hu, K. and Cui, C. (2018) Combined effect of imperfections on ultimate strength of cracked plates under uniaxial compression, Ocean Engineering 150(1): 113-123.

Xu, M.C., Song, Z.J., Pan, J. (2017) Study on influence of nonlinear finite element method models on ultimate bending moment for hull girder. Thin-Walled Structures, 119, pp. 282-295.

Xu, M.C., Song, Z.J., Zhang, B.W., Pan, J. (2018a) Empirical formula for predicting ultimate strength of stiffened panel of ship structure under combined longitudinal compression and lateral loads, Ocean Engineering, 162, pp.161-175.

Xu, M.C., Zuo, Y.Q., Song, Z.J., Pan, J. (2018b) Study on the influence of temperature on the collapse behaviour of stiffened panels of ship, Proceedings of the 28th International Ocean and Polar Engineering Conference, pp.606-612, 2018.

Xu M, Guedes Soares C. (2020) Numerical study on the influence of experimental conditions on the collapse behaviour of stiffened panels, Ocean Engineering Vol. 220

Xu, M., Guedes Soares, C. (2021) Experimental evaluation of the ultimate strength of stiffened panels under longitudinal compression. Ocean Engineering.Vol.220, 2021, 108496.

Xu, S., Liu, B., Garbatov, Y., Wu, W. and Guedes Soares, C. (2019) Experimental and numerical analysis of ultimate strength of inland catamaran subjected to vertical bending moment. Ocean Engineering 188 (2019) 106320

Xu, W. H., Cheng, A. K., Ma, Y. X., Gao, X. F. (2018c) Flow-induced vibration (FIV) suppression of two tandem long flexible cylinders attached with helical strakes. *Ocean Engineering* 169: 49-69.

Yamada, Y. (2019) Dynamic collapse mechanism of global hull girder of container ships subjected to hogging moment. Journal of Offshore Mechanics and Arctic Engineering, 141(5), p.051605.

Yang, B., Wu, J., Guedes Soares, C. and Wang, D. (2018) Dynamic ultimate strength of outer bottom stiffened plates under in-plane compression and lateral pressure. Ocean Engineering 157(1): 44-53.

Yang, B., Guedes Soares, C. and Wang D. (2019) Dynamic ultimate compressive strength of simply supported rectangular plates under impact loading, Marine Structures, Vol. 66, Issue 1, 2019, pp. 258–271. DOI: 10.1016/j.marstruc.2019.05.001.

Yao, T., Brunner, E., Cho, S.R., Choo, Y.S., Czujko, J., Estefen, S.F., Gordo, J.M., Hess, P.E., Naar, H., Pu, Y., Rigo, P. and Wan, Z.Q. (2006) Committee III.1 Ultimate Strength, 16th International Ship and Offshore Structures Congress, Southampton, UK.

Yao, T., Astrup, A.C., Caridis, P., Chen, Y.N., Cho, S.-R., Dow, R.S., Niho, O. and Rigo, P. (2000) Special Task Committee VI.2 Ultimate Hull Girder Strength, 14th Interntional Ship and Offshore Structures Congress 2000, Nagasaki, Japan.

Yao T, Fujikubo M. (2016) Buckling and Ultimate Strength of Ship and Ship-Like Floating Structures. Elsevier. Retrieved from https://app.knovel.com/hotlink/toc/id:kpBUSSSLFD/buckling-ultimate-strength/buckling-ultimate-strength

Yeter, B., Garbatov, Y. and Guedes Soares, C. (2019) Ultimate strength assessment of jacket offshore wind turbine support structures subjected to progressive bending loading. Ships and Offshore Structures, 14: 165-175.

Youssef, S.A.M., Noh, S.H., Paik, J.K. (2017) A new method for assessing the safety of ships damaged by collisions, Ships and Offshore Structures, 12:6, 862-872, DOI: 10.1080/17445302.2017.1285679.

Yu C.L., Chen Y.T., Yang S., Liu Y., Lu G.C. (2018a) Ultimate strength characteristic and assessment of cracked stiffened panel under uniaxial compression, Ocean Engineering, 152, 6-16

Yu, Z and Amdahl, J. (2018b) A review of structural responses and design of offshore tubular structures subjected to ship impacts. Ocean Eng. 154:177–203.

Yu, Z. and Amdahl. J. Sha, Y. (2018c) Large inelastic deformation resistance of stiffened panels subjected to lateral loading, Marine Structures, Vol. 59, Issue 1, 2018, pp. 342–367. DOI: 10.1016/j.marstruc.2018.01.005.

Zeinoddini, M., Golpour, H., Khalili, H., Nikoo, H.M. and Ahmadi, I. (2017) Sensitivity analysis of selected random variables of existing offshore jacket structures in Persian Gulf. International Journal of Coastal & Offshore

Zhang, M., Liu, J. and Hu, Z. (2018) Experimental and numerical investigation of the responses of T scaled tanker side double-hull structures laterally punched by conical and knife edge indenters, Marine Structures, Vol. 61, Issue 1, 2018, pp. 62–84. DOI: 10.1016/j.marstruc.2018.04.006.

Zhang, L.M., Xue, H.X., Tang, W.Y. (2019a) Residual ultimate strength analysis of stiffened panels exposed to fire, Trends in the Analysis and Design of Marine Structures, pp.107-115.

Zhang, S. and Kahan, M. (2009) Buckling and ultimate capability of plates and stiffened panels in axial compression. Marine Structures, 22, pp.791-808.

Zhang, S., Villavicencio, R., Zhu, L., Pedersen, P.T. (2019b) Ship collision damage assessment and validation with experiments and numerical simulations. Marine Structures, 63, pp.239-256.

Zhang, X., Huang, L., Zhu, L., Tang, Y., Wang, A. (2017) Ultimate longitudinal strength of composite ship hulls. Curved and Layered Structures, 4 (1), pp. 158-166.

Zhou, L., Gao, J., Xu, S., Bai, X. (2018) A numerical method to simulate ice drift reversal for moored ships in level ice. Cold Regions Science and Technology, 152, pp.35-47.

Zhu, L., Liu, Q, Jones, No., Chen, M. (2018a) Experimental Study on the Deformation of Fully Clamped Pipes under Lateral Impact. Int J Impact Eng, 111: 94-105.

Zhu, L., Liu, Q, Jones, No., Chen, M. (2018b) Experimental Study on the Deformation of Fully Clamped Pipes under Lateral Impact. In proceedings of the ASME 37th International Conference on Ocean, Offshore and Arctic Engineering (OMAE2018), Madrid, Spain, 17-22 June 2018. (OMAE2018-78021).

APPENDIX: BENCHMARK

A.1 Description of the reference experiment

The reference ultimate strength testing experiment was performed utilizing a newly fabricated tee-stiffened plate steel structure (hereafter referred to as the "structure"). The structure was designed by the NSWCCD and fabricated by the US Army's Aberdeen Test Center in accordance with standard shipbuilding practices. Detailed surveys of the as-built structure were conducted prior to testing, including laser scanning/tracking, ultrasonic thickness measurements, and tensile tests of the material coupons. The test results consist of overall load and displacement measurements, strain gauge data used to determine the failure sequence, and video data. Residual stress measurements were not conducted due to practical limitations in conducting these measurements.

A.1.1 Description of the structure

The structure was fabricated from ASTM A36 (2019) steel plate and rolled steel shapes. The overall length of the structure was 7315 mm and the width was 2438 mm. The longitudinal frame spacing was 1829 mm such that the structure consisted of three full sections and two partial sections. Longitudinal stiffening consisted of three identical 124.6 mm depth tee shapes prepared from AISC W12×14 beams (Longitudinal A, C, D) and a single AISC W12×19 I-T longitudinal girder (longitudinal B), all spaced 610 mm center-on-center. Transverse stiffeners consisted of tee shapes with a depth of 177.8 mm prepared from AISC W10×17 I-T beams. All stiffeners fashioned from single beam to avoid any stiffener-to-stiffener welds and ensure consistent properties from one stiffener to the next. Furthermore, all material for a given beam size was from a single heat to minimize material variability. Stiffener intersections were fabricated using a slotted construction method that avoids collars, with the exception of the large girder, which uses conventional collar details where it intersects transverse stiffeners.

The plating consisted of two full-breadth strakes: 6.35 mm thick plating with a length of 3352 mm and 7.94 mm thick plating with a length of 3962 mm, joined in the middle section by a transverse butt weld that spans the width of the panel. The structure was outfitted with side plates, transverse frame cap plates, and heavy end plates. The side plates and cap plates were 9.53 mm thick except at the ends of the transverse stiffeners, where the plates were 19.05 mm thick. An array of holes was located on these pieces to facilitate the connection between the plate structure fixture and vertical tie-downs. The structure end plates were fabricated from a 38.10 mm plate with a matrix of bolt holes to connect the fixture loading to the reaction ends. All welding was performed using 70S-1 welding wire through a pulsed gas metal arc welding (GMAW-P) process and visually inspected at the time of construction. A summary of the nominal and actual properties of the stiffened plate structure and geometric imperfections is provided in Table A.1.

The properties of the structure in Table A.1 show that the magnitudes of the imperfections in the structure exceed typical tolerance levels given in codes, e.g., the maximum out-of-plane plate amplitude corresponds to $D_s/96$ (see Figure A.1 for local plate amplitudes: 6.4 mm corresponds to $0.07\beta^2 t_p$, which is in-between the slight ($0.025\beta^2 t_p$) and average ($0.1\beta^2 t_p$) levels defined by Smith *et al.* (1988)), the maximum side displacement corresponds to $D_f/219$, while typical magnitudes of the imperfections, implemented in buckling strength requirements (see IACS (2020a, 2020b)), are $D_s/200$ and $D_f/1000$ or $D_f/667$; D_f and D_s are the frame and stiffener spacings, respectively. The somewhat larger imperfections in the structure compared to IACS (2020a, 2020b) may be due to the high slenderness of the plates and stiffener webs. At one hand it is expected that the ultimate strength will be overpredicted if the smaller code-based

imperfections are used, on the other hand the actual imperfections shapes differ from the buckling eigenmodes and could thus increase the strength if they push the deformation response into a higher eigenmode.

Table A.1. Summary of the properties of the stiffened plate structure.

Symbol	Structural element	Nominal	Actual
$t_{p,thin}$	Thin plate thickness [mm]	6.35	6.45
$t_{p,thick}$	Thick side plate thickness [mm]	7.95	7.90
h_l	Longitudinal stiffener web height [mm]	124.61	118.85
$t_{w,l}$	Longitudinal stiffener web thickness [mm]	5.08	5.28
$b_{f,l}$	Longitudinal stiffener flange width [mm]	100.84	105.41
$t_{f,l}$	Longitudinal stiffener flange thickness [mm]	5.72	4.75
h_g	Girder height [mm]	308.76	295.61
$t_{w,g}$	Girder web thickness [mm]	5.97	5.84
$b_{f,g}$	Girder flange width [mm]	101.73	103.20
$t_{f,g}$	Girder flange thickness [mm]	8.89	8.81
h_T	Transverse stiffener height [mm]	177.80	169.88
$t_{w,T}$	Transverse stiffener web thickness [mm]	6.10	5.94
$b_{f,T}$	Transverse stiffener flange width [mm]	101.85	100.81
$t_{f,T}$	Transverse stiffener flange thickness [mm]	8.38	8.76
t_{SP}	Side plate thickness [mm]	9.53	9.83
	Maximum out of plane, plate [mm]		13.92
	Maximum side displacement, Longitudinal A [mm]		4.26
	Maximum tilt, Longitudinal A [degrees]		2.2
	Maximum side displacement, Longitudinal B [mm]		8.35
	Maximum tilt, Longitudinal B [degrees]		1.3
	Maximum side displacement, Longitudinal C [mm]		7.18
	Maximum tilt, Longitudinal C [degrees]		2.8
	Maximum side displacement, Longitudinal D [mm]		5.61
	Maximum tilt, Longitudinal D [degrees]		1.9

A.1.2 Material and geometric imperfection data

Tensile testing was conducted on various structural components to establish material properties. All tests were conducted following ASTM E8 (2016) utilizing a 50.8 mm gauge length. Coupons were extracted in the rolling and transverse directions of both the thickness plates as well as in the rolling direction for stiffener and girder elements. A total of 24 coupons were tested with three repeat tests for each configuration, and full stress-strain curves were collected through peak loading. The results, presented in Table A.4, indicate that the material yield strength is significantly greater than the yield strength of 250 MPa specified in ASTM A36 (2019) for all structural elements. Furthermore, the rolled shapes that were purchased met the specifications for both ASTM A36 (2019) and ASTM A992 (2020) with a higher minimum yield strength of 345 MPa.

Measurements for the initial shape and thickness were obtained prior to testing using a combination of laser tracking on the stiffener edges, laser scanning of the plating, and caliper and ultrasonic thickness measurements. Out-of-plane plate distortions were established using a

best-fit plane of the plate data as shown in Figure A.1. Stiffener measurements were used to establish the rotation (distortion, stiffener tilt) from the plate plane, an example of which is shown in Figure A.2. A summary of imperfection data is provided in Table A.1. It is evident that out-of-plane plate distortions are moderate in Section 2 and 3 and low in Section 4. A similar trend exists in the measurements of stiffener tilt. However, the cuts at x = 1500 mm (Section 2) and at x = 6000 mm (Section 4) in Figure A.3 shows that local out-of-plane plate distortions are of hungry horse type and have their highest amplitudes in Section 4.

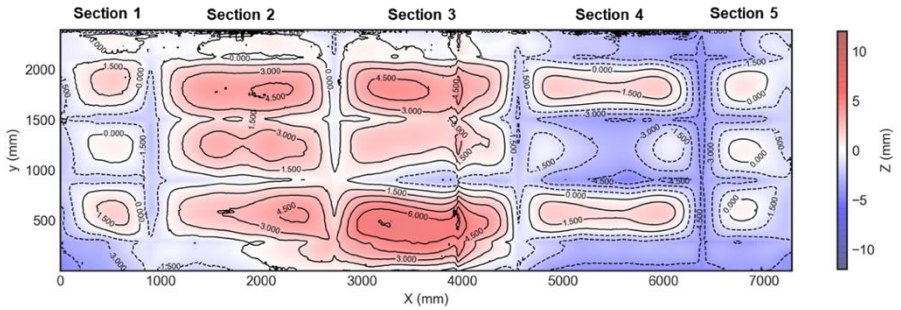

Figure A.1: Results from plate out-of-plane measurements of the plate; the coordinate system is referred to Figure 27 (z = 0 at the bottom of the plate).

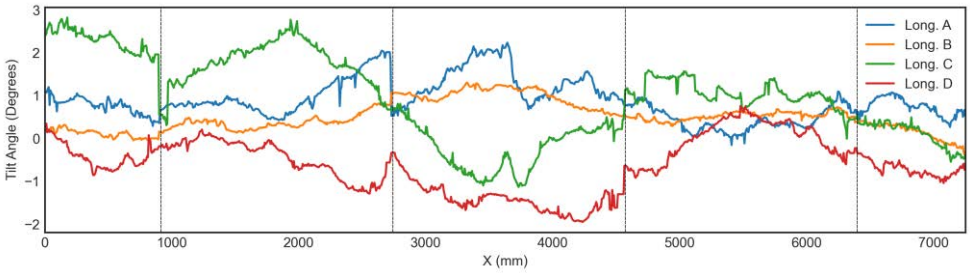

Figure A.2: Stiffener tilt example angle: vertical lines represent the locations of the transverse frames.

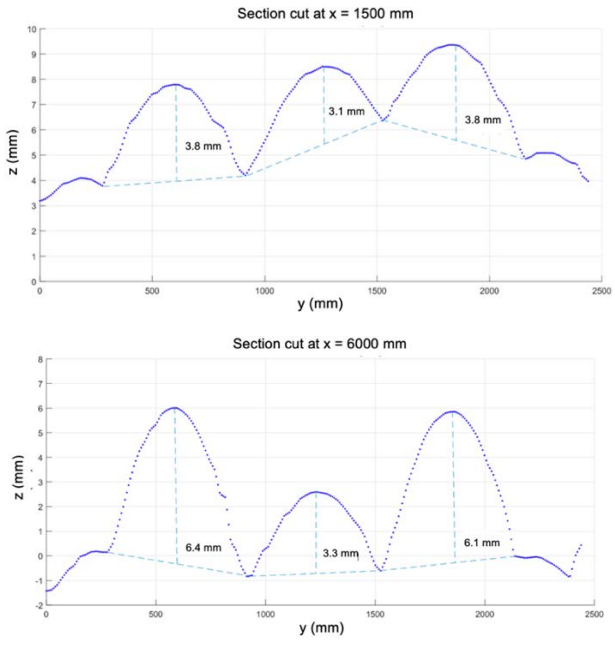

Figure A.3: Cuts at x = 1500 mm (Section 2) and at x = 6000 mm (Section 4) that present the local out-of-plane plate distortions which are of hungry horse type.

A.1.3 Test procedures, measurements and results

Structural testing was conducted using NSWCCD's Grillage Test Fixture (see Figure A.4). Longitudinal loads were applied through two rows of five 2.2 MN actuators located at one end of the fixture that are connected to a single heavy steel header onto which the plate structure is bolted. The structure was carefully shimmed prior to testing and strain gauges monitored to ensure that any eccentric loading was minimized, though loading eccentricity cannot be avoided when the neutral axis of the section shifts. Previous efforts have determined that the fixture compliance is 0.268 mm/MN, and the load-end shortening curves (hereafter referred to as force versus displacement curves) shown herein are corrected utilizing this value.

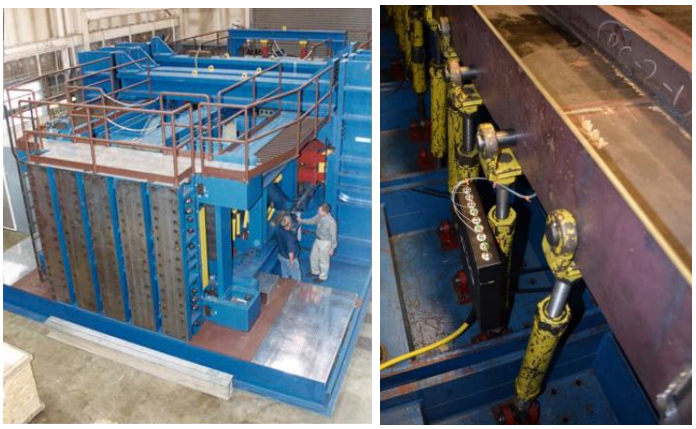

Figure A.4: (Left) Test fixture of the stiffened plate structure and (right) detailed view of the tie-downs and connection to the structure.

The boundary conditions were provided at the loading and fixed ends (see Figure 27). At these ends, all motion was fixed except for axial displacement at the loading end. Vertical motions along the long edges were restrained by a series of 27 tie-downs installed on each side of the structure at a spacing between 254 mm and 279.4 mm. The tie-towns, which consist of a 31.8 mm diameter threaded rod that is screwed into a 63.5 mm outer diameter cylinder, were hand-tightened prior to testing.

The test procedure was performed as follows. First, two low load-level compressive cycles are performed to capture the linear response of the structure, consisting of loading the structure to 1.1 MN (approximately 25% of the calculated anticipated peak load), unloading to zero load, and subsequently loading to 2.2 MN (approximately 50% of the calculated anticipated peak load) before again unloading the structure. After the completion of the compression cycles at 25% and 50% of the anticipated peak load, an ultimate strength collapse run was performed in which the structure was compressed well into the post-buckling range. The test was terminated once the structure dropped to 70% of the peak load.

A plot of the overall force-displacement behavior is shown in Figure A.5. The response for the two low load cycles of 25% and 50% is linear with no permanent set or change in structure compliance. The collapse run follows the same loading path as the low-load cycles with non-linearity observed in the overall load-shortening curve above 3.34 MN. The peak ultimate load achieved during collapse loading was 6.59 MN. Structure compression was halted at 4.68 MN of compression, and the structure returned to zero load.

The structure contains three full-length sections in which failure could occur. The primary failure zone occurred in Section 2, where the thicker plating was located, as seen in Figure 27. However, peak strength is observed in Section 3 and significant post-peak nonlinear response

occurs in Section 4. The closely spaced buckling modes suggest that minor differences in geometry, material properties, or residual stresses drive failure to Section 2 despite the thicker plating.

The dominant failure modes in Section 2 appear to be tripping of the girder and local flange buckling of the longitudinal stiffeners. The failure sequence during the collapse cycle in Section 2, obtained through a combination of video and strain gauge analysis, is as follows. First, the plating between the stiffeners starts to buckle downwards elastically, increasing compression in the longitudinal stiffener flanges during the increase in loading from approximately 0.9 to 4.5 MN. Tripping, or lateral-torsional buckling, of the longitudinal girder initiates at a load of approximately 4.5 MN. Finally, local flange buckling of the remaining stiffeners along with column-type buckling occurred, as seen in Figure A.6. A post-test view of the structure is shown in Figure A.7.

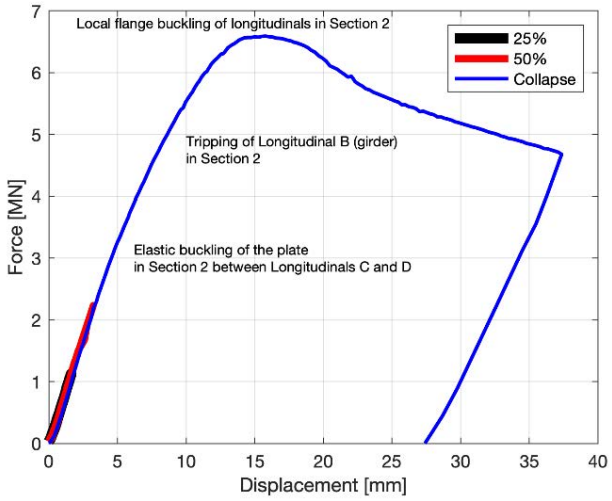

Figure A.5: Force-displacement curve of the stiffened plate structure.
The displacements are corrected for machine compliance.

Section 3, where the plate weld and thickness transition are located, behaves in a similar manner to Section 2. Analysis of strain gauge data indicates that peak load has been attained and that significant inelasticity is present and it is noted that several strain gauges failed due to excessive strains. In Section 4, where the plating is thin but distortions are noticeably lower (see Figure A.1 and A.2), plastic deformation is not visibly observed. The response of the stiffeners appears to be linear, though nonlinear behavior of the plating is observed.

Figure A.6: View of the final deformed structure shape in Section 2 illustrating the plate buckling, stiffener buckling, and girder tripping buckling modes.

Figure A.7: (Left) Views of the structure at a peak load of 6.59 MN and (right) at a load of 6.25 MN after reaching the peak load.

A.2 Finite element models and analyses

A.2.1 Geometry, boundary conditions and FE models

The participants of the benchmark study created their FE model using either 2D drawings or the 3D CAD file, both of which were provided by NSWCCD in Phase 1. The geometry of the FE model includes all the longitudinal stiffeners, the longitudinal girder, the transverse girders, transverse end caps, side plates and end plates. The dimensions of the stiffened plate structure are presented in Table A.1.

The end plates were included in the FE model by most participants. Six participants disregarded the end plates, and they were reproduced by applying fixed boundary conditions. Additionally, the scallop holes and collar plates in the longitudinal girder were treated differently in the FE model by the participants. Some participants included the scallop holes in the model while others ignored them. The geometry of the structure was modeled by all the participants by using either 4-noded or 8-noded shell elements (reduced or fully integrated) with five, seven or eleven integration points through the thickness. Figure A.8 shows an example of an FE model and the mesh density used for the benchmark study.

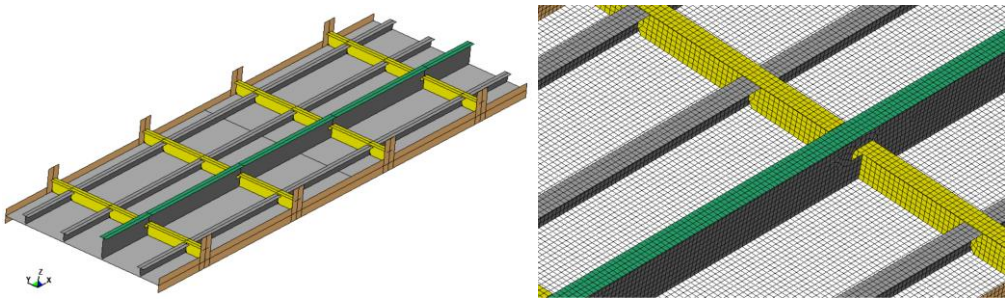

Figure A.8: (Left) Example of an FE model of the test structure and (right) close-up view of an example of the mesh density.

The recommended practice in DNV GL (2020) for obtaining the structural capacity by nonlinear FEA methods prescribes a mesh density of (minimum) 3 to 6 first order elements per expected half-buckling scenario to capture all the relevant buckling deformations and localized plastic collapse behavior in the structure. The mesh density of the reference structure corresponds to a mesh size between 50 and 100 mm. Half of the participants performed mesh sensitivity analyses to find the optimal element size. After the sensitivity test, each participant found an optimal mesh size between 12.5×12.5 mm and 50×50 mm, which fulfils the mesh size requirement given in recommended practices. The other half of the participants relied on their own knowledge and experience in this field and chose to use a mesh size between 25×25 mm and 56×70 mm for their analyses without performing any mesh sensitivity studies. Table A.2

presents a summary of the participants' different FE model definitions and parameters; the mesh size used by each participant can be found in Table A.2. The total DOFs in the FE models used in the benchmark study varied between 63,000 and 1,000,000.

Table A.2. Summary of the participants' FE model definitions and parameters.

ID	FE software	Solver	Solution control	Solution method*	Type of shell element	No. of integrations points on element plane	No. of integration points through element thickness	Mesh size [mm]	Number of DOF
1	Abaqus 2018	Implicit	Static	Modified Riks method	S4R	1	5	25×25	358745
2	LS-DYNA R712	Implicit	Static	Nonlinear static	Type 16	4	5	25×25	335814
3	ADINA-AUI 9.4.2	Implicit	Static	Iterative incremental scheme	Plate A, 4 node	4	6	56×70	100506
4	Abaqus 6.13-6	Implicit	Static	Modified Riks method	S4R and S3	1	5	30×30	265512
5	Abaqus 6.14-2	Implicit	Static	Modified Riks method	S4R	1	5	25×25	338142
6	LS-DYNA R712	Explicit	Dynamic	Dynamic explicit	Type 2	1	7	40×40	135156
7	Abaqus 6.14	Implicit	Static	Modified Riks method	S4R	1	11	50×50	123144
8	Abaqus 6.16-1	Implicit	Static	Modified Riks method	S4R and S3	1	5	12.5×12.5	1026305
9	MSC Marc 2017	Implicit	Static	Static arc length method	Type 75	4	11	30×30	116000
10	Abaqus 6.11-1	Explicit	Dynamic	Dynamic explicit	S4R	1	5	30×30	245994
11	Abaqus 2017	Implicit	Static	Modified Riks method	S4R	1	5	25×25	308269
12	LS-DYNA R10	Explicit	Dynamic	Dynamic explicit	Type 16	4	5	50×50	130934
13	MSC Marc 2017	Implicit	Static	Static arc length method	Type 75	4	5	20×20	474382
14	Abaqus 2017	Implicit	Static	Modified Riks method	S4R	1	5	40×40	135000
15	Ansys 18.2	Implicit	Static	Riks method	Type 181	1	5	40×40	107103
16	Abaqus 6.12	Implicit	Static	Modified Riks method	S4R	1	5	25.4×30.5	63360
17	Abaqus 2016	Implicit	Dynamic	Implicit dynamic with quasi-static settings	S8R	2	5	30×30	645000

* See Abaqus (2021) for the "Modified Riks method".

The applied boundary conditions in the FE model need to closely represent the reference experiment. All participants used the same boundary conditions as those described in Section A.1.3 in their models. The motion and rotation of both structure ends are fixed except for axial displacement at the loading end. The vertical displacement was constrained at the side plates to simulate the 27 tie-downs installed on each side of the structure. An axial displacement (longitudinal compression) was incrementally applied on the loading end (displacement control) to the point of post collapse of the structure. It should be noted that the two initial compressive load cycles performed in the physical experiment to capture the linear response of the structure (see Figure A.5) were not included in the FEA by the participants. The physical experiment was carried out at a slow loading rate so that dynamic effects were not important and buckling was well controlled; therefore, the majority of the FEAs were carried out as static analyses.

A.2.2 Initial geometric imperfections

Phase 1 of the benchmark study started without any information regarding geometric imperfections. Most of the participants, however, modeled initial imperfections in their FE models using different assumptions and procedures. In accordance with the recommendations given by

classification societies or in the literature, most of the FEAs were performed with initial deflection shapes based on eigenmodes associated with the applied loads. The amplitude of the imperfections used in the analyses varies considerably between participants. The initial geometrical imperfections were applied on the plates, the longitudinal stiffeners and the longitudinal girder. No initial imperfections were applied to the transverse frames. The maximum imperfection amplitudes on the different structural members are presented in Table A.3. In Phase 2-1, the initial geometrical imperfections of the structure obtained by laser scanning were provided to all the participants. The measurement data were included in the FE model by all the participants in Phases 2 and 3 and are shown in Figures A.1 and A.2.

From Table A.2, it can be noted that the plate amplitude assumed by the participants vary from zero to $D_s/87$, but more than 2/3 of the participants used approximately $D_s/200$ (i.e., 3 mm). For the stiffeners and girders, the amplitude varies from 0 to $0.05\times D_f$. Half of the participants adopted a value of approximately $0.001\times D_f$ (i.e., 1.8 mm) or $0.0015\times D_f$ (i.e., 2.7 mm). It is noted that scaling of one eigenmode to a desired level for the plate or the stiffer/girder may have yielded a small or large level for the amplitude of the other component, e.g., for ID 4 and 12. It is also noted that the assumed imperfection levels are generally significantly smaller than the actual values measured, see Table A.1.

Table A.3. Summary of the amplitude of the geometric imperfections applied in Phase 1 and the guidance/approach used in the model.

ID	Max. imperfection amplitude for the plate applied in Phase I [mm]	Max. imperfection amplitude for the stiffener/girder applied in Phase I [mm]	Guidance/approach used in the model
1	3.05	1.82	Harmonic sinusoidal imperfections
2	3.05	4.57	Harmonic sinusoidal imperfections
3	3.20	1.80	Imperfections applied following the suggestions in the standards
4	3.05	7.32	Imperfections based on the 1st eigen buckling mode
5	1.73	2.74	Imperfections according to Smith *et al.* (1988) and DNV GL (2020)
6	0.00	0.00	No local imperfections in Phase I
7	3.05	1.82	Harmonic sinusoidal imperfections
8	0.00	0.00	No local imperfections in Phase I
9	3.05	1.82	Lateral initial deflection of the local and overall buckling mode in the plate
10	0.00	0.00	No local imperfections in Phase I
11	7.00	2.00	Imperfections according to Smith *et al.* (1992)
12	3.00	9.10	Harmonic sinusoidal imperfections
13	3.65	1.83	Maximum initial deflection based on the measurement of a real ship
14	3.05	2.70	Harmonic sinusoidal imperfections
15	3.05	2.74	Harmonic sinusoidal imperfections
16	4.88	2.45	Imperfections applied according to Paik *et al.* (2012) and eigen mode analysis
17	3.66	5.54	Harmonic imperfections according to Benson *et al.* (2009)

A.2.3 Welding-induced residual stresses

Typically, in ship and offshore structures, the welding-induced residual stresses are either ignored or implicitly assumed when assessing the ultimate strength capacity, except in reduced

order models. This topic was not addressed at the outset of the benchmark study, and all FEAs were free of welding-induced residual stresses. After completion of Phase 3-2, however, the mismatch of the slope of the force-displacement between the FEA and the reference experiment was relatively large. Therefore, it was decided to investigate the effect of welding-induced residual stresses in Phase 3-3. These additional FEAs were essential to validate the experimental load-displacement curve from the NSWCCD reference experiment. Welding-induced residual stresses were included by the participants by using one of the following two approaches:

- assuming a uniform tensile region in the heat-affected zone (HAZ) of all the fillet welds and a matching opposing compression zone in the remainder of the plate.
- pre-stressing the structure through a thermal analysis in the HAZ and using the results as an initial condition for the collapse analysis.

A.2.4 Constitutive material models

The material data made available to the participants in the different phases is presented in Table A.4. "Nominal material" refers to material data as specified in ASTM A36 (2019), "Actual material" refers to the material specification provided by the supplier of the material of the reference structure, and "Measured material" refers to tensile testing undertaken of the materials used in fabrication. "Measured material" data included full stress-strain curves for each structural member.

The material was represented by different constitutive material models for each phase. These ranged from elastic-perfectly plastic, bilinear stress-strain curves with tangential module E_T, or multilinear stress-strain curves. Table A.5 presents a summary of the constitutive material models used by each participant in each phase. Measured material data provided to participants during Phase 3-2 consisted of raw engineering stress-strain curves. FE software packages most typically require that data must be given by the true stress-strain curve instead of the engineering stress-strain curve and this step was left to participants and is a source of potential analyst error. An example of the measured engineering stress-strain curve for the structure plate is shown in Figure A.9 along with the corresponding true stress-strain curve. The true stress-strain curve was calculated based on engineering stress-strain data. An additional source of differences in material modeling is the manner in which participants accounted for either a yield plateau (Plate A, stiffeners, girder) or lack of a clearly defined yield point (Plate B). An example for yield plateau of longitudinal B (girder web) is presented in Figure A.9 illustrating the need for simplifying assumptions regarding details of the yield plateau region. For the materials that showed a yield plateau, almost all participants consistently used the stress at which 0.2% plastic strain occurs as the plateau yield stress. In addition, as the provided stress-strain curves contained high-density data, most participants simplified the curve in their FE models with a multilinear (ML) stress-strain curve (see Table A.5). It should be noted that in Phase 3-2, all participants but one used more or less exactly the same definition of the plateau yield stress, plateau length and ML model after the plateau according to Figure A.9. The single participant used a bilinear model after the plateau instead of an ML model, which resulted in a lower ultimate capacity load compared to the other FEAs. Since the physical experiment was performed on the reference structure at low speed, strain-rate effects were considered negligible, i.e., they were disregarded in the analyses.

Table A.4. Material properties used in the benchmark study; see the text for details.

Material	Structural member	Young's modulus [GPa]	Yield strength [MPa]	Ultimate strength [MPa]	Elongation [%]
Nominal material (Phases 1, 2-1 and 2-2)	W12×14	200	250	400	20
	W12×19 – web	200	250	400	20
	W12×19 – flange	200	250	400	20
	Thick plate	200	250	400	20
	Thin plate	200	250	400	20
	Frames (W10×17)	200	250	400	20
	Side plate	200	250	400	20
Actual material (Phases 2-3 and 3-1)	W12×14 – web and flange	200	383	474	21
	W12×19 – web	200	399	478	27
	W12×19 – flange	200	399	478	27
	Thick plate	200	352	476	33
	Thin plate	200	326	453	33
	Frames (W10×17)	200	401	509	25
	Side plate	200	345	(n.a.)	(n.a.)
Measured material (Phases 3-2 and 3-3)	W12×14 – web and flange	215	394	464	35
	W12×19 – web	211	387	466	35
	W12×19 – flange	195	379	466	36
	Thick plate, rolling direction	220	339	461	37
	Thick plate, transverse direction	220	333	456	35
	Thin plate, rolling direction	222	316	459	35
	Thin plate, transverse direction	218	334	465	34
	Frames (W10×17)	(n.a.)	(n.a.)	(n.a.)	(n.a.)
	Side plate	243*	343	487	37

* This is a value estimated by the majority of the participants from the provided data, but it is unrealistically high. The majority used this value, but some participants reduced it to 210 GPa. A comparison of the results between participants showed that either choice of this value for the side plate did not influence the results from this benchmark study.

Table A.5. Summary of the participants' choice of constitutive material in each phase: EP = elastic-perfectly plastic; BL = bilinear stress-strain curve with tangential modulus ET; ML = multilinear stress-strain curve.

ID	Phase 1	Phase 2-1	Phase-2-2	Phase 2-3	Phase 3-1	Phase 3-2	Phase 3-3
1	ML	ML	ML	ML	ML	ML	ML
2	BL	BL	BL	BL	BL	ML	ML
3	BL	BL	BL	BL	BL	ML	(n.a.)
4	ML	ML	ML	ML	ML	ML	(n.a.)
5	BL	ML	ML	ML	ML	ML	ML
6	ML	ML	ML	ML	ML	ML	ML
7	BL	BL	BL	BL	BL	ML	(n.a.)
8	BL	BL	BL	BL	BL	ML	ML
9	BL	BL	BL	BL	BL	ML	(n.a.)
10	EP	EP	EP	EP	EP	ML	(n.a.)
11	EP	EP	EP	EP	EP	ML	(n.a.)
12	BL	BL	BL	BL	BL	ML	ML
13	EP	EP	EP	EP	EP	ML	ML
14	ML	ML	ML	ML	ML	ML	ML
15	EP	EP	EP	EP	EP	ML	ML
16	BL	BL	BL	BL	ML	ML	ML
17	EP	ML	ML	ML	ML	ML	ML

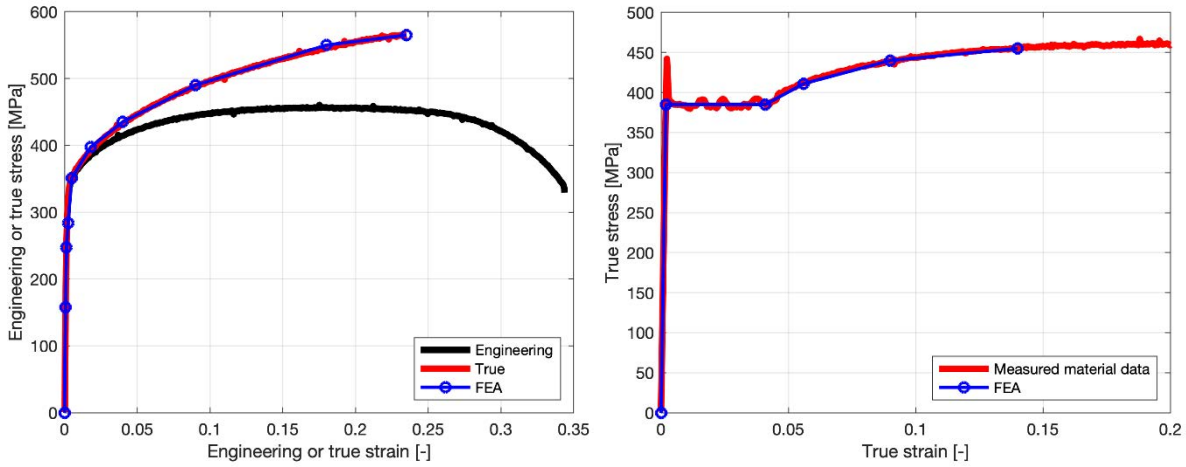

Figure A.9: (Left) Example of the stress-strain curve for Plate A (5/16): engineering, true and FEA stress-strain curves, and (right) example of modeling the yield plateau of longitudinal B (girder web).

A.2.5 Solver and solution control

The FE software programs used by the participants to perform the ultimate strength assessment according to the benchmark study include Abaqus (2021), ADINA (2021), Ansys (2021), LS-DYNA (2021) and MSC Marc (2021); see Table A.2. All the details of these commercial programs can be found in the corresponding references. The tests were conducted at a low speed; therefore, the dynamic effects in the FEA should be ignored. The most common FE method used by the participants was a nonlinear implicit solver. Fourteen participants used an implicit equation solver for their FE analyses (see Table A.2). Three participants used an explicit FE solver as implemented in the commercial programs Abaqus and LS-DYNA.

A.3 Fast-running/practical computation codes for the ULS analysis

Four fast-running/practical computation codes were used for comparison against the FEA and the test results: Smith's method described in IACS (2019), ALPS/SPINE (2019), ALPS/ULSAP (2019), and the ULTSTR code developed by Adamchak (1984). The input parameters to the codes and the models were in accordance with the procedure and description presented earlier.

A.3.1 Smith's method in IACS (2019): Phase 1

The incremental iterative method described in IACS (2019) in Pt1, Ch5, App2 is an analytical method where the ultimate strength of a ship structure is calculated between two adjacent frames. It was applied to calculate the ultimate capacity of the reference structure in Phase 1. In Smith's method, an interframe collapse is assumed, and the transverse sections are assumed to remain plane. In a calculation, the transverse section is divided into units (i.e., parts) of the structure so-called "elements" (stiffener element, stiffened plate element and hard corner element) whose structural behavior is calculated independently and expressed by load-end shortening curves. With these curves, the bending moment acting on the structure is calculated in an iterative procedure where the curvature is incremented, and the neutral axis is updated according to the stress distribution in the structure. In this benchmark study, no iteration was necessary because the applied load was a compressive load.

The part of the reference structure where the cross-section had the thinnest plate thickness was chosen for the determination of the ultimate capacity since it was assumed/expected to happen there. The material was modelled as elastic-perfectly plastic with properties according to Table

A.4. The cross-section was divided into six elements and the load-end shortening curves were determined for each element. The curve for the entire cross-section was obtained by a summation of each element's contribution to the resultant curve by consideration of their respective cross-section areas.

A.3.2 ALPS/SPINE and ALPS/ULSAP: Phases 1 to 3-3

The incremental Galerkin method (IGM) developed by Paik *et al.* (2001) and Paik and Lee (2005a) is a semi-analytical method for computing the elastic-plastic large-deflection behavior of steel or aluminum plates and stiffened panels up to their ULS. This method is designed to accommodate the geometric nonlinearity associated with buckling via an analytical procedure, whereas a numerical procedure accounts for the material nonlinearity associated with plasticity (Paik 2018). The method is unique in its use to analytically formulate the incremental forms of nonlinear governing differential equations for elastic large-deflection plate theory, although local stiffener web buckling or tripping of stiffeners is not dealt with. After solving these incremental governing differential equations using the Galerkin approach (Fletcher 1984), a set of easily solved linear first-order simultaneous equations for the unknowns is obtained, which facilitates a reduction in the computational effort.

It is normally difficult, but not impossible, to formulate the nonlinear governing differential equations to represent both geometric and material nonlinearities for plates and stiffened panels. A major source of difficulty is that an analytical treatment of plasticity which increases with the applied load is quite cumbersome. An easier alternative is to deal with the progress of the plasticity numerically. The benefits of this method are to provide excellent solution accuracy with great savings in computational effort and to handle in the analysis the combined loading for all potential load components, including biaxial compression or tension, biaxial in-plane bending, edge shear, and lateral pressure loads. The effects of initial imperfections in the form of initial deflection and welding-induced residual stresses are also considered. Details of the IGM theory and applied examples are presented in Paik (2018). The ALPS/ULSAP code calculates the ultimate strength of plate and stiffened panels together with the definition of collapse modes, which are grouped into six types: Mode I – overall collapse of plating and stiffeners as a unit; Mode II – plate collapse without distinct failure of stiffener; Mode III – beam-column collapse; Mode IV – collapse by local web buckling of stiffener; Mode V – collapse by lateral-torsional buckling of stiffener; and Mode VI – gross yielding, as originally categorized by Paik and Thayamballi (2003a) and Paik (2018). The ALPS/SPINE code analyses the elastic-plastic large deflection responses of plates and stiffened panels until the ultimate strength is reached. The codes have been used to analyze the majority of the phases of the benchmark study; they have been validated against tests presented in several other studies, e.g., Hughes and Paik (2013), Lee and Paik (2020), and Paik (2018).

One bay section of the physical test structure between the transverse frames was considered and all of the four edges were modelled as simply supported, kept straight while allowing to move in the plane. The material was modelled as elastic-perfectly plastic with properties according to Table A.4, i.e., the strain-hardening effect was not considered. The section model had two versions: one with the thinner plate (Section 4) and one with the thicker plate (Section 2). Initial deflections and residual stresses were represented as described in Paik (2018) for the phase analyses that allowed for these factors. It should be noted that the ALPS/SPINE code allows for different dimensions of support members at different locations, while the ALPS/ULSAP code assumes that all of the longitudinal stiffeners have the same dimensions with equal spacing between them. A benefit of ALPS/ULSAP and ALPS/SPINE is that panel collapse modes can be identified similar to nonlinear FEA.

A.3.3 The ULTSTR code: Phases 1 and 3-1

The ULTSTR code is a Naval Surface Warfare Carderock Division developed tool for performing structural analysis of ship cross-sections. ULTSTR discretizes a cross-section into various structural elements such as gross panel, curved plate, and hard corner elements and incrementally increases either the curvature or the displacement. Every structural member type has a prescribed load-end shortening behavior based on the inputs provided and includes a stable linear regime, a plateau regime and an unloading regime. Gross panels, the primary element used to describe stiffened plating, can consist of either a single plate-beam combination or a number of plate-beam combinations to represent either a single or multiple stiffeners. ULTSTR considers inelastic flexural column buckling, lateral torsional (tripping) buckling, and overall grillage buckling. Plate buckling is incorporated using the effective width concept. Initial distortions and residual stresses can be included in a semi-empirical manner through modification of coefficients associated with the capacity of structural members. See Adamchak (1984), Bruchman *et al.* (2000) and Evans (1974) for further details.

The ULTSTR analyses were performed for Phases 1 and 3-1 using the latest 2012 version of the ULTSTR code. Individual gross panels were created for each plate-beam set and hard corner elements used for the side plates. ULTSTR is based on the assumption of interframe buckling and as such a load-end shortening curve cannot be readily generated for the entire grillage. Therefore, only frame-to-frame displacements and strains in the collapse bay are calculated but re-calculated to peak load values valid for all bays of the structure.

Similar to the ALPS/SPINE and ULSAP/ULSAP models, one section of the physical model between the transverse frames was modelled in ULTSTR, and with two versions corresponding to thin and thick plating in Sections 2 and 4, respectively. The grillage was discretized using four gross panel elements, representing the stiffener and attached plating for longitudinal stiffeners, and hard corner elements to represent the side plates. The material was modelled as elastic-perfectly plastic with properties according to Table A.4, i.e., the strain-hardening effect was not considered.

A.4 Results

A.4.1 Force versus displacement curve, failure mode and location of failure

Figure A.10 presents the force-displacement curves for selected phases together with the bar diagrams of the ultimate capacity; see Ringsberg *et al.* (2021) for the complete set of results for all phases. Overall, the numerical (FEA) predictions show relatively low scatter between the participants up to the ultimate load for each of the phases; note that analysis of the post-buckling behavior and residual strength were not incorporated in the current study. Differences between the participants' models and results are discussed in more detail later in this section.

The Phase 1 ultimate capacity predictions using nominal material values and geometry uniformly underestimated values from the reference experiment. This was an expected outcome as use of nominal material properties introduces conservatism relative to the actual tensile and ultimate strength properties of the material. This underestimation is satisfactory or even desirable in the case of an initial design and maintaining a margin of safety from the perspective of a class rules and guidelines.

Analysis of the results successive phases shows that the largest change in the ultimate capacity is between Phase 2-2 and Phase 2-3. The difference between these phases is due to the introduction of the "actual material" properties instead of the "nominal material" properties. The FE models used in all phases except Phase 3-3 could not fully capture the nonlinear behavior seen in the test data curve even when the peak predicted strength was close to the experimental value. By introducing welding-induced residual stresses in the FE models in Phase 3-3, a better

match between the FEA and test data curves is obtained. Nevertheless, all predictions underestimated the displacement and slightly underestimated the ultimate capacity compared to the test result. This indicates that the compliance and strength of the reference structure was greater than in the submitted predictions.

The results in Figure A.10 show that the force-displacement curves predicted by the participants in Phase 1 were generally softer than the test curve, but they were closer to the test curve in Phase 2-1 to 3-1. The access to true (measured) stress-strain data (Phase 3-2) and inclusion of welding-induced residual stresses (Phase 3-3) in the FE models gave less agreement with test curve. In all phases one or two participants had a substantially stiffer force-displacement curve than the majority of the participants. It is also interesting to observe that the participants that actually predicted a relatively good match of the stiffness behavior before Phase 3-2 when the true (measured) stress-strain data became available.

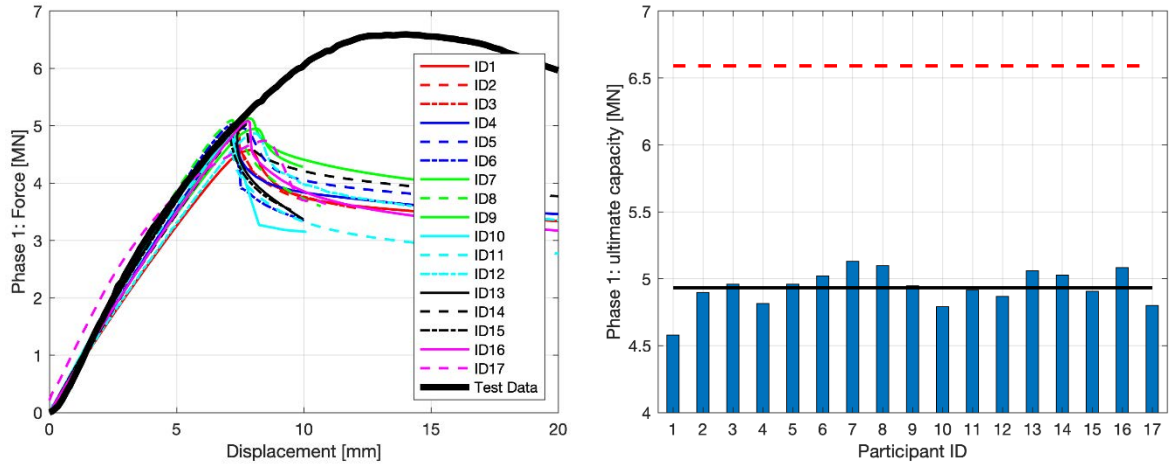

Figure A.10 (a) Phase 1.

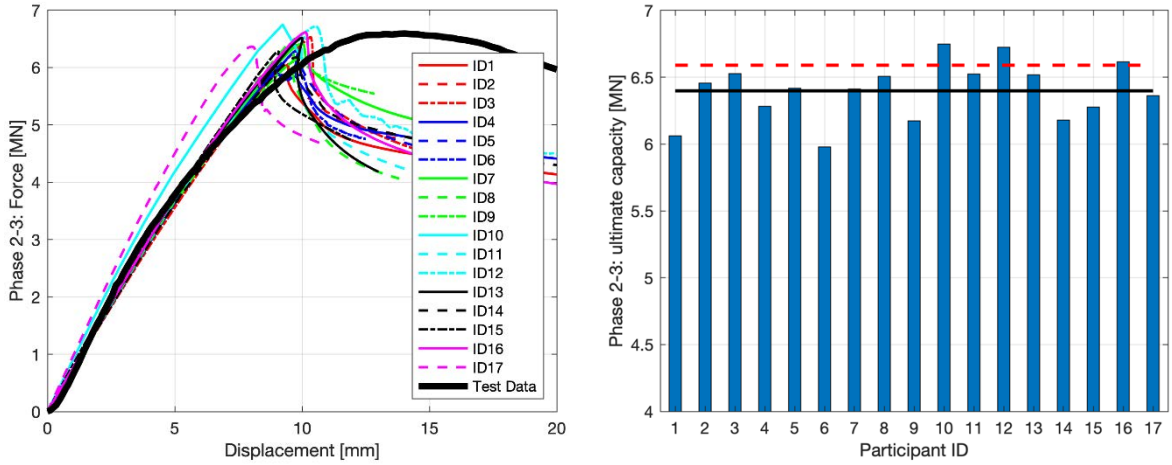

Figure A.10 (b) Phase 2-3.

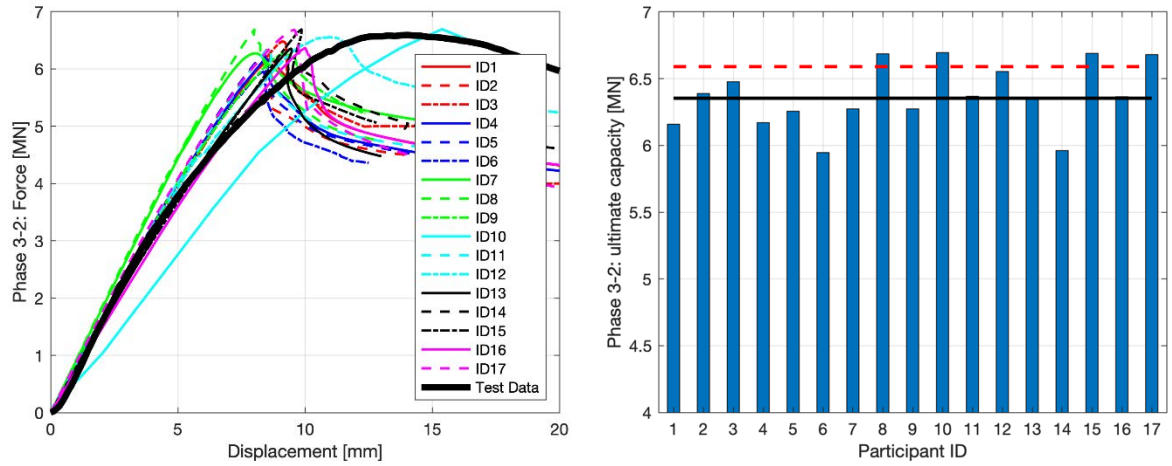

Figure A.10 (c) Phase 3-2.

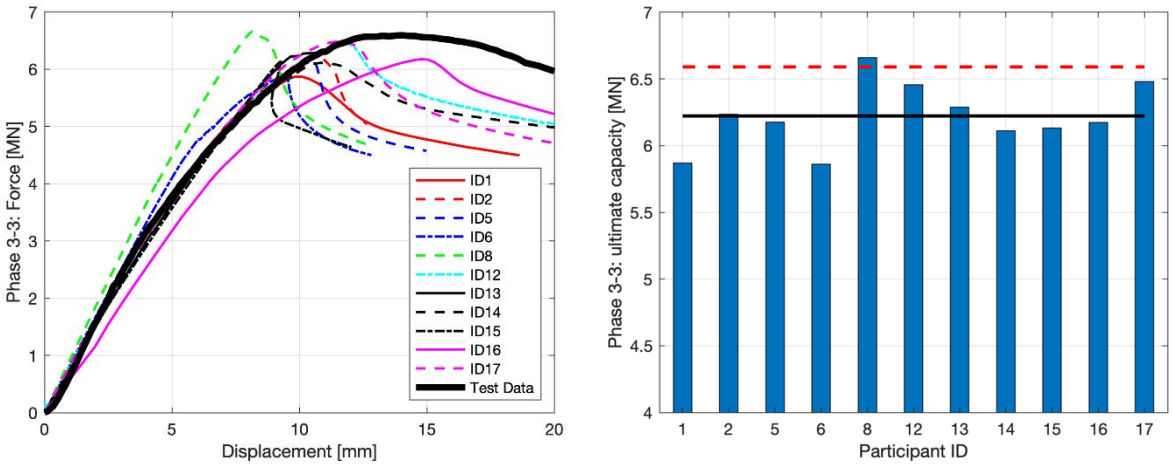

Figure A.10 (d) Phase 3-3.

Figure A.10 (a)-(d): Force-displacement curves and bar plots of the ultimate capacity for Phase 1, Phase 2-3, Phase 3-2 and Phase 3-3. The solid line in the bar plots is the mean value from the FEA results, and the dashed line is the ultimate capacity from the reference experiment.

The failure modes at the ultimate strength and corresponding locations predicted in Phases 1, 2-3, 3-2 and 3-3 are presented in Figure A.11. Figure A.12 presents two examples from Phases 2-3 and 3-3 from ID2 of the equivalent plastic strain distribution in Section 4 directly after the maximum load capacity is reached. The change in the failure modes and corresponding locations for the phases and for each participant are shown, and there is no consensus between them. Figure A.11 shows that although the participant's analyses performed very well on average and had low scatter in the predicted ultimate capacity, the participants' assumptions, modeling approaches and procedures affected the prediction of the failure mode and its location to a larger extent. The primary region of failure of the reference structure was in Section 2 and was governed by tripping of the girder, though post-buckling response is also observed in Section 3. Note that none of the participants predicted the failure mode and location from the reference experiment.

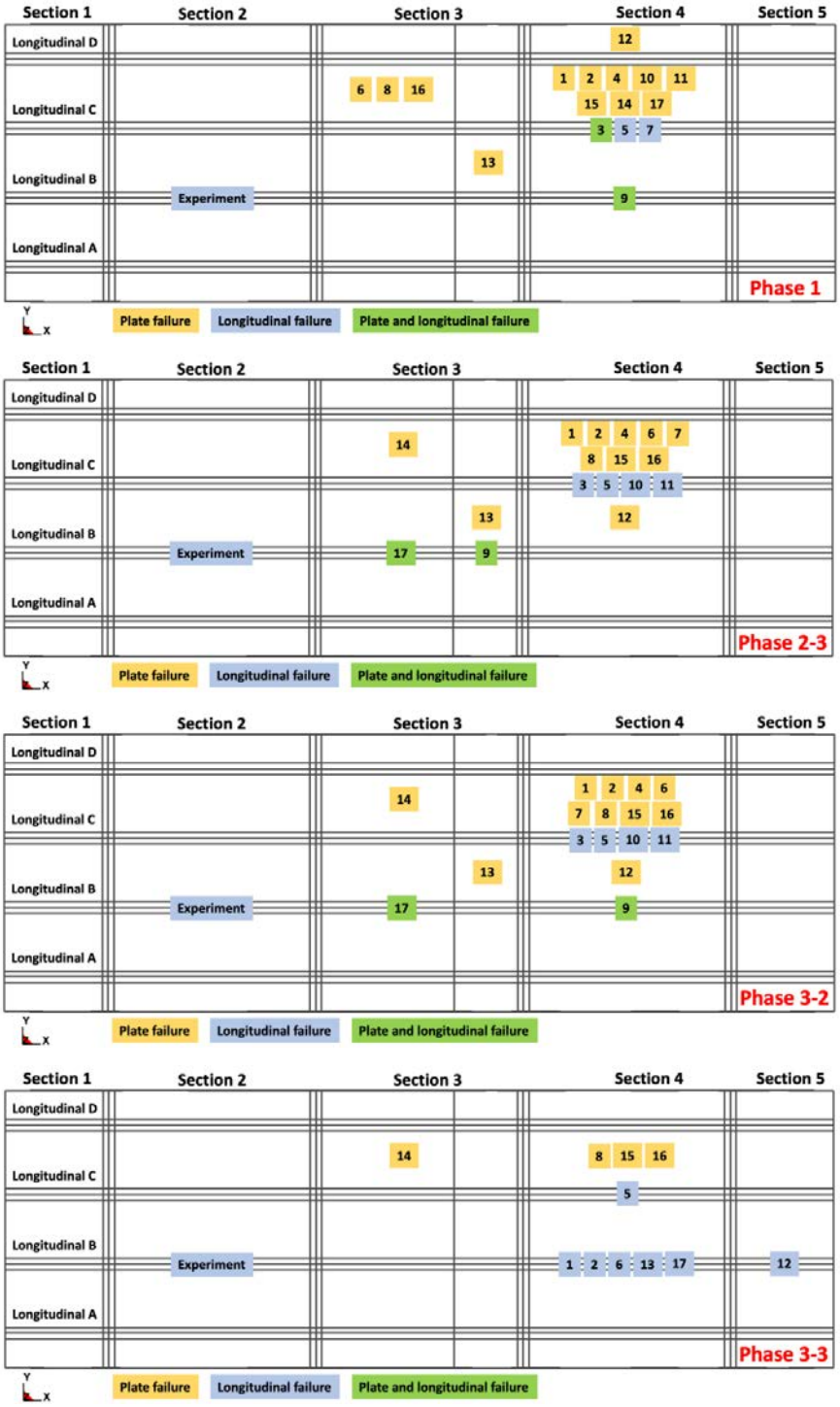

Figure A.11: Failure modes and locations (identifies the section and which part of the structure) for Phase 1, Phase 2-3, Phase 3-2 and Phase 3-3.

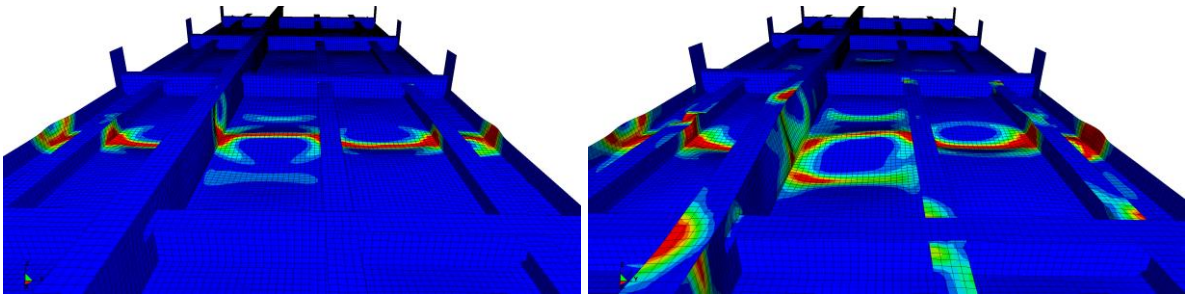

Figure A.12: Example of equivalent plastic strain in Section 4 directly after the maximum load capacity was reached (deformed FE models, scale factor: 2): (left) Phase 2-3 and (right) Phase 3-3 from ID 2 FEA.

A.4.2 Discussion on the FE models, modeling procedures and access to data

A statistical analysis of the FEA results is presented in Table A.6 in terms of the mean value and the standard deviation of the ultimate capacity; see Figure A.13 for the bar diagram. The results show that the mean values for Phases 1 to 2-2 are relatively far from the test results, while the results from Phases 2-3 to 3-3 show good agreement with the test result. The magnitudes of the standard deviations are generally low. It can be seen that for Phases 2-3 to 3-3, the test result is within one standard deviation for Phases 2-3, 3-1 and 3-2 and just outside for Phase 3-3. It was concluded that, despite the differences in the assumptions, modeling approaches and procedures, the participants of the benchmark study were able to satisfactorily predict the ultimate capacity of the reference structure. The following subchapters present more detailed discussions on the results related to the participants' assumptions and modeling approaches.

Table A.6. Statistical analysis of the results from the FEA of each phase: mean value and standard deviation of the ultimate capacity.

Source – ultimate capacity	**Mean value [MN]**	**Standard deviation [MN]**	**Deviation [%]**
Reference experiment	6.59	(n.a.)	(reference)
Phase 1	4.93	0.14	-33.6
Phase 2-1	4.87	0.12	-35.4
Phase 2-2	4.94	0.21	-33.5
Phase 2-3	6.40	0.22	-3.0
Phase 3-1	6.35	0.23	-3.7
Phase 3-2	6.37	0.24	-3.4
Phase 3-3	6.22	0.24	-5.9

A.4.3 Results from fast-running/practical computation codes

The CPU time for the three codes was very short compared to the FEA, and thus their computations are very efficient. Figure A.14 presents a summary of the results from the four codes. The Smith method was only used to calculate the ultimate capacity while the other codes also indicated the failure mode. For all analysed phases, the ALPS/SPINE code indicated plate buckling of the thin plate in Section 4 as the collapse mode (as ALPS/SPINE does not deal with local stiffener web buckling or tripping of stiffeners) while the ALPS/ULSAP code indicated failure of longitudinal B by tripping in Section 4. The ULTSTR code predicted plate failure of the thin plate in Section 4 for Phase 1 but failure of longitudinal B by tripping in Section 4 for Phase 3-3. It should be noted that these were the expected failure modes and locations based on former studies in e.g. Lee and Paik (2020).

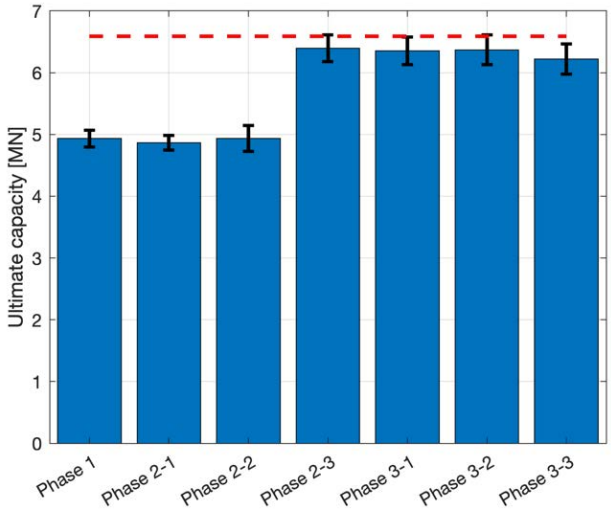

Figure A.13: Bar diagram presenting the mean value and the standard deviation of the ultimate capacity for each phase. The dashed line represents the ultimate capacity from the reference experiment.

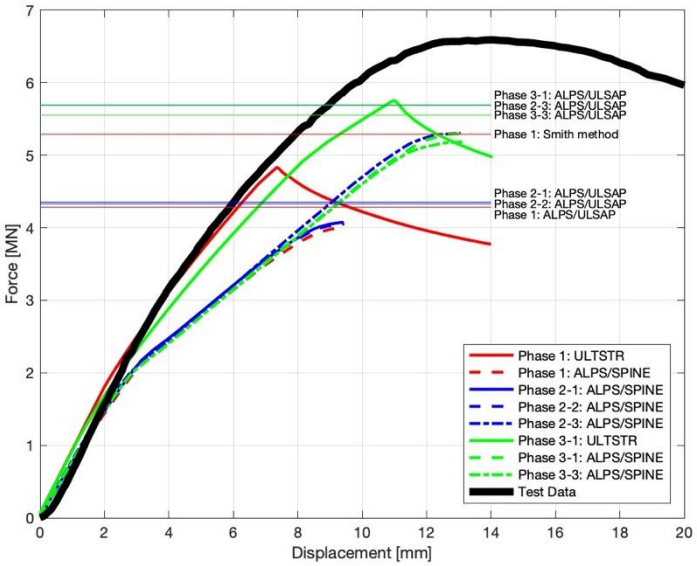

Figure A.14: Results from analyses using the Smith method, the codes ALPS/SPINE, ALPS/ULSAP and ULTSTR.

The ultimate capacity from the Phase 1 FEA showed a mean value of 4.93 MN (see Table A.6). The Smith method predicts a higher value, the ULTSTR code predicts a value close to the Phase 1 FEA result while ALPS/SPINE and ALPS/ULSAP predict a lower value. Similar to the observations made from the FEA results for Phases 2-1 and 2-2, the results from the ALPS/SPINE and ALPS/ULSAP codes do not change that much compared to Phase 1.

The codes ALPS/SPINE, ALPS/ULSAP and ULTSTR follow the same trend as the FEAs where the results from Phase 2-3 to Phase 3-3 change significantly compared to the former phases. It verifies the importance also for these codes of having access to representative material data for the material in the structure, thicknesses of the structural members, measured distortions, geometrical imperfections and inclusion of welding-induced residual stresses. It should be noted that the ultimate capacity predicted by the practical codes was relatively far off from the test result of the current reference experiment, and that the FEA seems to be more

accurate with regards to the level of the ultimate capacity. Neither the FEAs, nor these codes, could predict the failure mode that occurred in the test.

A.4.4 FE models and modeling procedures (Phase 1 and 2-1)

The FE models and results from Phase 1 served as a basis for the participants' basic assumptions, modeling approaches and procedures. All participants used the same boundary conditions and nominal material data in the FE model, but the choice of the constitutive material model differed (see Table A.5).

A detailed analysis and comparison of all the participant's results from Phase 1 did not result in an identification of or correlation between any of the sources in Table A.2 that pinpointed why an ultimate capacity value that was too low or too high was predicted compared with the mean value from all the participants' results. An analysis of the results shows that the different FE model definitions, with or without modeling the scallop holes and collar plates in the longitudinal girder, were not the reason for the different failure modes and locations.

The geometric imperfections that were assumed and modeled in Phase 1 are presented in Table A.3. By comparing Tables A.2 and A.3, IDs with similar definitions in Table A.2 but with different geometric imperfections in Table A.3 were identified, such as IDs 1, 4, 5 and 16. Since the results from these IDs show different ultimate capacities, failure modes and locations, it was expected that the difference in how the geometric imperfections were modeled was the major factor behind for the differences in the results. However, the results from Phase 2-1, where all the participants used the same measured imperfections, ruled out geometric imperfections as the most important factor; the high plate slenderness of the reference structure suppressed the influence of the geometric imperfections. This conclusion is further strengthened by the observation that the IDs 1, 3, 7 and 9 used the same imperfection levels, but got very different results. The results for the majority of the participants (except for IDs 3, 6, 7 and 12-14) did not change significantly compared to the Phase 1 results. It is noted that ID 12, who used the largest stiffener/girder imperfection in Phase 1, got a substantial increase of the ultimate capacity in Phase 2-1, while ID 4, who had the next but largest stiffener/girder imperfection (same plate imperfection) did not experience a similar increase. The statistics in Table A.6 also show that the mean value of the ultimate capacity and the standard deviation for Phase 2-1 are just slightly lower than those for Phase 1. However, the failure mode and location for some of the IDs changed between Phases 1 and 2-1, where the majority of them were predicted to occur in Section 4 in the reference structure; see Ringsberg *et al.* (2021) for more details.

A comparison and analysis of the various constitutive material models (which included how the participants interpreted the material properties) used by the participants were performed. The choice of the material model for the nominal material in Phases 1 and 2-1 had a very large influence on the results. The trend is that participants who used a multilinear (ML) material model presented a lower ultimate capacity than the participants who use a bilinear (BL) or elastic-plastic (EP) material model. The difference between ML and BL results indicate that the finite post yield stiffness may be important compared to models using a yield plateau. This affirms that despite relatively clear rules and guidelines from various references, the variety of constitutive material models used in Phases 1 and 2-1 together with how the participants handled the provided material properties in those models had the largest influence on the scatter in the results.

A.4.5 Access to material data, thickness measurements and measured distortions

The importance of having access to representative material data for the material in the structure subject to analysis is clearly seen by the FEA results from Phases 1 (nominal material data), 2-3 (actual material data) and 3-2 (measured stress-strain curves). In this benchmark study, the

use of nominal data gave a misleading ultimate capacity for the reference structure compared to the test data, while the use of actual material data gave a much better prediction. The access to the stress-strain curves of the material did not affect the ultimate capacity level (see Table A.6). With regard to the failure mode and location, Figure A.11 shows that they do not change to a large extent between Phases 2-2 and 3-2, and the changes that are observed are related to the other factors introduced in Phases 2-3 and 3-1, i.e., the measured thickness and distortion.

It should be highlighted that access to representative material data is important as well as how these data are used to represent the material in the FE model with a constitutive material model. The choice of constitutive material model was identified as the model uncertainty that had the largest influence on the predicted ultimate capacity levels and its standard deviation. It also remains unclear what the importance of assumptions regarding the presence of a yield plateau has on FEA results. For some of the material coupons, the 0.2% yield strength is nearly 8% below the peak stress prior to a yield plateau.

One of the differences between Phases 2-3 and 3-1 is that measured thicknesses and distortions were added to the FE models in Phase 3-1. The possibility of a more accurate representation of these factors in the FE models did not result in a major change in the ultimate capacity (see Table A.6). Hence, for the reference structure in this benchmark study, the measured thicknesses and distortions (stiffener tilt angle) had a low influence on the overall results and the model uncertainty.

A.4.6 Geometrical imperfections and welding-induced residual stresses

Table A.3 presents the guideline/approach the participants used to model and include geometrical imperfections in their FE models for Phase 1. In the Phase 2-1 FE models, the only change in the FE models compared with Phase 1 is that all the participants used the measured geometrical imperfections. Figure A.15 presents the relative change (with Phase 1 as the reference) in ultimate capacity for Phase 2-1 based on the Phase 1 level. For the majority of the participants, the change was minor. This was presented in Table A.6 and Figure A.13, in which the ultimate capacity level and its standard deviation were slightly reduced; there were some changes in the predicted failure modes and locations (see Figure A.11). Overall, this indicates that if the goal of the FEA is to predict the ultimate capacity level, any of the guidelines/approaches presented in Table A.3 can be used. However, the present study cannot provide a clear conclusion which of the guidelines/approaches presented in Table A.3 as regards imperfections levels that shall be used. With regard to the failure mode and location, the results from this benchmark study cannot be used to make any recommendations or draw conclusions based on the FEA and test results.

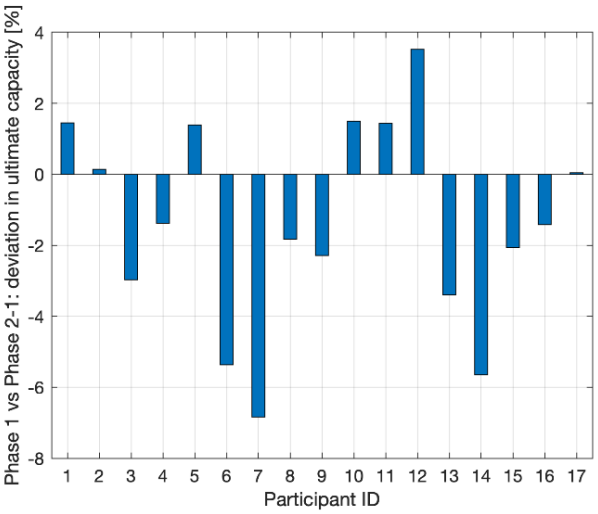

Figure A.15: Change in the ultimate capacity (%) for Phase 2-1 based on the level calculated for Phase 1.

The force-displacement curves from the Phase 3-2 FEA did not capture the nonlinear characteristics from the test data curve, i.e., the larger displacement at ultimate strength and more gradual change in the stiffness (see Figure A.10). In Phase 3-3, the majority of the participants included welding-induced residual stresses in their FE models. Table A.7 presents a summary of the residual stress level (longitudinal direction of the weld along longitudinals A to D) in the heat-affected zone (HAZ) and its width.

The results from the Phase 3-3 FEA show that the introduction of residual stresses in the FE models gives better agreement with the nonlinear test data force-displacement curve. Figure A.16 presents the relative change (with Phase 3-2 as the reference) in ultimate capacity for Phase 3-3 based on the Phase 3-2 level. Note that the peak load of the ultimate capacity level is reduced on average by 2.2% compared to the Phase 3-2 results. Figure A.11 shows that the majority of the participants predicted a different failure mode and location compared with Phase 3-2. Hence, it appears to be beneficial and it is recommended to introduce welding-induced residual stresses in an FE model according to a guideline or recommended practice even if their absolute levels or distributions have not been quantified by measurements.

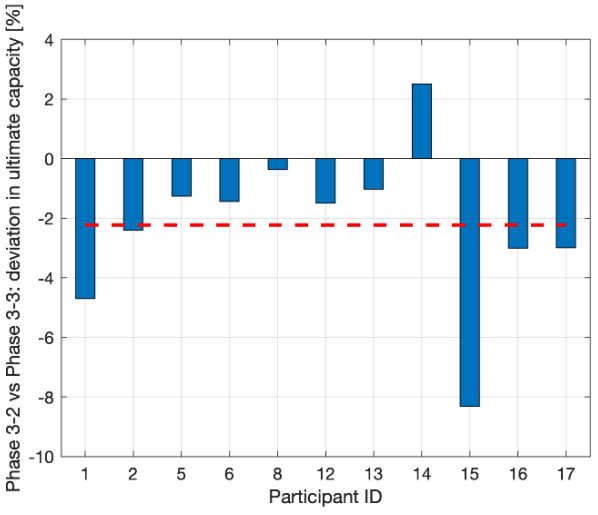

Figure A.16: Change in the ultimate capacity (%) for Phase 3-3 based on the level calculated for Phase 3-2. The dashed line represents the mean value.

Table A.7. Representation of welding-induced residual stresses in the FE models: HAZ residual stress level as percentage (%) of the yield stress and assumed width of the HAZ in the FE model (note: in the plate, it refers to both sides of a longitudinal).

	Longitudinals A, C and D			**Longitudinal B (girder)**		
ID	**Tensile residual stress [% of σ_y]**	**HAZ width in the plate [mm]**	**HAZ width in the longitudinal [mm]**	**Tensile residual stress [% of σ_y]**	**HAZ width in the plate [mm]**	**HAZ width in the longitudinal [mm]**
1	68	60	50	68	60	50
2	70	100	50	70	100	50
5	100	100	24	100	100	43
6	100	80	40	100	80	80
8	100	34	12	100	82	50
12	50	50	25	50	100	60
13	100*/80**	41		100*/80**	41	
14	20	80	20	80	80	80
15	100	34		100	34	
16	30	69	24	30	69	51
17	75	50	50	75	50	50

*thin plate; **thick plate